The petrogenesis of the Nelshoogte pluton: The youngest and most compositionally variable TTG pluton in the Barberton Granite-Greenstone Terrain

by

Risa Matsumura

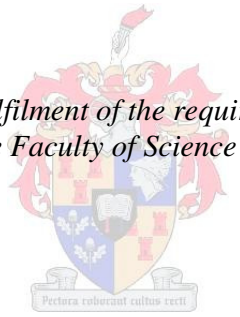

Thesis presented in fulfilment of the requirements for the degree of Master of Science in the Faculty of Science at Stellenbosch University

Supervisor: Prof Gary Stevens
Co-supervisor: Prof J. D. Clemens

April 2014

Declaration

By submitting this thesis electronically, I declare that the entirety of the work contained therein is my own, original work, that I am the sole author thereof (save to the extent explicitly otherwise stated), that reproduction and publication thereof by Stellenbosch University will not infringe any third party rights and that I have not previously in its entirety or in part submitted it for obtaining any qualification.

April 2014

Abstract

The compositions of tonalite-trondhjemite-granodiorite (TTG)-series rocks from the Barberton Granite-Greenstone Terrain (BGGT) of Southern Africa vary in terms of major element concentrations (leuco-trondhjemites to tonalites), trace elements (e.g. Sr, Rb, REE) and degree of HREE depletion [$(La/Yb)_N$ ~ 0.50 - 121]. These geochemical parameters have been interpreted to have significance for the geodynamic processes that produced TTG magmas, particularly the depth of the source. In the Nelshoogte pluton, trondhjemite emplacement occurred prior to and during (D2)-tectonism, and hornblende-bearing tonalites/granodiorites occur as intrusive plugs within the trondhjemite. The geochemical range portrayed by the ca. 3230 Ma Nelshoogte pluton covers almost the whole range portrayed by all the TTG rocks of the BGGT, formed in the time interval 3550 to 3230 Ma. U-Pb zircon dating reveals no significant differences in apparent ages between the trondhjemites and tonalites of the Nelshoogte pluton; all lie between ca. 3240 and 3220 Ma.

A/CNK- and Ti-maficity correlations within the Nelshoogte pluton show behaviour typical of I-type granitic rocks, confirming the metamafic character of the source and the involvement of a peritectic garnet and clinopyroxene component in the magmas. The REE and trace-element patterns resemble those of both ca. 3450 Ma TTG plutons and other ~ 3230 Ma TTG plutons in the BGGT. This suggests that these different generations of TTG magmas were generated from similar sources and by similar processes. The geochemical details are consistent with a metamafic source which underwent melting at high pressure. This TTG source was fundamentally different from the more potassic source/s that produced the younger 3100 Ma granites. Additionally, high Zr/Sm and low Nb/Ta ratios in the Barberton TTG rocks suggest that the Nelshoogte pluton originated as a group of chemically distinct magmas, in a similar way to other ~ 3200 Ma TTGs. The protoliths of ~ 3450 Ma plutons and ~ 3200 Ma plutons might typically be rutile-bearing eclogite and/or 10 to 30 % garnet bearing amphibolite.

The geochemical features of the Barberton TTGs suggest similar source compositions, but different pressures of partial melting. For the ca. 3230 Ma plutons, the rocks of the Badplaas pluton and the Nelshoogte trondhjemites/tonalites correspond to the high-pressure magmas, as reflected by high Sr content, as well as high Sr/Y and $(La/Yb)_N$ ratios. In contrast, the Kaap Valley TTGs and Nelshoogte granodiorites reflect the melting of a similar source at moderate pressure. Furthermore, the Hf isotope data; εHf_t (+ 0.1 to + 1.9) and T_{DM} model

ages (3330 - 3230 Ma), suggest that the source rocks are ~ 20 to 100 Myr older than the pluton.

Opsomming

Die samestellings van tonaliet-trondhjemiet-granodioriet (TTG)-reeks gesteentes vanaf die Baberton Graniet-Groensteen terrien (BGGT) van Suiderlike Afrika verskil in terme van hoofelement konsentrasies (leuko-trondhjemiete tot tonaliete), spoorelemente (bv. Sr, Rb en seldsameaarde-elemente(SAE)) en ook van swaar seldsameaarde-element (SSAE) uitputting [$(La/Yb)_N$ ~ 0.50 - 121]. Deur interpritasie is daar vasgestel dat hierdie geochemiese beperkings betekenis dra vir die geodinamiese prosesse wat TTG magmas produseer het, en veral vir die diepte van die bron. In die Nelshoogte pluton het trondhjemiet inplasing voor en gedurende (D2)-tektonisme voorgekom en horingblende-draende tonaliet/granodioriet kom voor as intrusiewe proppe binne-in die trondhjemiet. Die geochemiese reeks wat uitgebeeld is deur die ~ 3230 Ma Nelshoogte pluton ondersteun byna die hele reeks wat uitgebeeld is deur al die TTG gesteentes van die BBGT wat gevorm het gedurende die tydsinterval 3550 tot 3230 Ma. U-Pb sirkoon datering openbaar geen merkwaardige verskille in ouderdomme tussen die trondhjemiete en tonaliete van die Nelshoogte pluton nie. Al die ouderdomme lê tussen 3240 en 3220 Ma.

A/CNK- en Ti-mafisiteit korrelasies binne die Nelshoogte pluton toon die tipiese gedrag van I-tipe granitiese gesteentes, en bevestig sodoende die metamafiese karakter van die bron, asook die betrokkenheid van ‘n peritektiese granaat en klinopirokseen component in die magmas. Die seldsameaarde-element en spoorelement patroone lyk soos dié van albei ~ 3450 Ma plutons en ander ~ 3230 Ma TTG plutons in die BGGT. Dit stel voor dat hierdie verskillende generasies van TTG magmas genereer was vanaf soortgelyke bronne en ook deur soortgelyke prosesse. Die geochemiese besonderhede stem ooreen met ‘n metamafiese bron wat smelting teen hoë druk ondergaan het. Hierdie TTG bron het fondamenteel verskil van die meer kalium-ryke bron/ne wat die jonger 3100 Ma graniete prodiseer het. In ‘n eenderse manier as ander ~ 3200 Ma TTG gesteentes, stel hoë Zr/Sm en lae Nb/Ta verhoudings in die Baberton TTG gesteentes verder voor dat die Nelshoogte pluton ontstaan het as ‘n groep chemies verskillende magmas. Die protoliete van ~ 3450 Ma plutons en ~ 3200 Ma plutons mag dalk tipies rutiel-draende eklogiet en/of 10 tot 30% granaat draende amfiboliet wees.

Die geochemiese aspekte van die Baberton TTGs stel eenderse bron komposisies, maar verskillende drukke van gedeeltelike smelting voor. Vir die ~ 3230 Ma plutons stem die gesteentes van die Badplaas pluton en die Nelshoogte trondhjemiete/tonaliete ooreen met die

hoë druk magmas, soos weerspieël deur hoe Sr inhoud, sowel as hoe Sr/Y en $(La/Yb)_N$ verhoudinge. In kontras weerspiel die Kaap Valley TTGs en Nelshoogte granodioriet die smelting van 'n eenderse bron teen matige druk. Verder stel die Hf isotoop data; εHf_t (+ 0.1 to + 1.9) en T_{DM} model ouderdomme (3330 - 3230 Ma) voor dat die bron gesteentes ~ 20 to 100 Mjr ouer is as die pluton.

Acknowledgements

I would thank to Professor Gary Stevens and Professor John Clemens for supervising in many ways, Vittoria Morena Salermo, Romain Lainé and Sébastian Nahan for helping to collect samples, Richard Belcher for offering some thin sections, Madelaine Frazenburg for teaching how to use SEM, Esmé Spicer and Herschel Achilles for XRF analyses, Riana Rossouw for LA-ICP-MS analyses, Fundisile Nkumenge for teaching me how to separate zircons, Professor Dirk Frei for Pb-U zircon analysis, Professor Axel Gerdes and Dr Federico Farina for Hf-Lu analysis, Professor Alex Kisters, Dr Martin Klausen, Professor Ian Buick for giving some suggestions, the SARCHI Chair in Experimental Petrology for an MSc Bursary, and other staff members (Loxie Conradie and George Olivier) and Gary's research group members (Cynthia, Jeanne, Angelique, Kathryn, Priscilla, Cristiano, Federico, Byron, Luhan, Corné, Gautier, Cedric and Fabiana) in many ways. Also I would like to thank my parents, my host families (especially for Adams family; aunti Evelyn), my friends (Mirei and Carlo) and my husband (Mukasa) for letting us stay away from 'skollies'. Lastly, I thank my kids (Takeru and Akito) for giving me tough time but also a lot of smiles.

Table of contents

List of figures

List of tables

Chapter 1

Introduction

The TTG (tonalite–trondhjemite–granodiorite) rock association consists of sodic granitoids that appear to have formed the fundamental building blocks of the Archaean cratons, yet are almost completely absent from the post-Archaean record. Much of what we know about the growth of the Archaean felsic crust has been the result of studies of TTG rocks. Thus, understanding TTG genesis constitutes a route to understanding the processes involved in the development of Earth's earliest preserved continental crust (Martin, 1994; Foley et al., 2002; Martin et al., 2005; Condie, 2005; Smithies et al., 2009).

TTG magmas appear to have formed through partial melting of hydrous metabasaltic rocks (i.e. greenstones, amphibolites and eclogites) under a variety of fluid conditions, in a variety of tectonic settings (e.g. Martin, 1987; Rapp and Watson, 1995; Winther, 1996; Condie, 2005), and at a variety of depths, as implied by the range of mineral assemblages implied in the possible protoliths by the geochemistry of the TTG rocks. It is, however, debated whether melting occurred under eclogite-facies (e.g., Rapp et al., 2003) or high-pressure amphibolite- to granulite-facies conditions (e.g., Foley et al., 2002). The two tectonic scenarios invoked are (1) melting of oceanic crust in a subducting slab (Martin, 1986; Drummond and Defant, 1990), or (2) shallower melting within oceanic plateaux or tectonically thickened island arc crust (Smithies, 2000; Condie, 2005; Van Kranendonk, 2010; Hoffmann et al., 2011a). The petrogenesis of TTGs that are interpreted to be products of partial melting of the subducted slab, has been extensively studied by experiments (e.g., Rapp et al., 1991; Rapp and Watson, 1995; Schmidt et al., 2004; Klemme et al., 2005; Xiong et al., 2005; Laurie and Stevens, 2012).

Some aspects of TTG chemistry appear to have considerable potential for deciphering the environment of partial melting that gave rise to the magmas. In particular, the high Sr/Ca ratio and HREE-depleted character of the high-Al TTGs, combined with their distinct negative HFSE anomalies (including Nb, Ta and Ti) and common positive Pb anomaly, imply that the magmas arose through the melting of metabasaltic rocks at pressures in excess of plagioclase stability and with rutile and a considerable proportion of garnet in the residuum.

Melting of such eclogitic assemblages would produce the low Nb/Ta and high Zr/Sm ratios of 'average' Archaean TTG rocks, from a source with initially subchondritic Nb/Ta (Rapp et al., 2003).

Barberton TTGs have variable compositions in terms of major elements (leuco-trondhjemite to tonalite), trace elements (e.g. Sr) and degree of HREE depletion [$(La/Yb)_N$]. This, coupled with a switch from TTG to more granitic magmatism, has been interpreted to have significance for the ~ 3550 to 3100 Ma geodynamic processes that produced the TTG magmas that intruded at ca. 3500, 3450, and 3200 Ma, and the laterally extensive, sheet-like potassic granites intruded between 3140 and 3100 Ma (Fig. 1). The ~ 3500 Ma plutons are trondhjemitic and have moderate Sr/Y and $(La/Yb)_N$. The ~ 3450 Ma plutons are trondhjemitic with high Sr/Y and $(La/Yb)_N$ ratios. The ~ 3200 Ma plutons are trondhjemitic to tonalitic and include rocks with both lower and higher Sr/Y and $(La/Yb)_N$ characteristics (Yearron, 2003; Clemens et al., 2006). The ~ 3100 Ma granites are potassic and are characterised by lower Sr/Y (Moyen, 2011). Moyen et al. (2006) suggested that the older trondhjemites represent slab melts with on-going and steepening subduction, while the ~ 3200 Ma plutons represent a transition from this regime to lower pressure melting, as a consequence of slab break-off and asthenospheric upwelling.

Previous geochemical studies indicate that the Nelshoogte pluton shows as much major-element geochemical variation as occurs within all Barberton TTGs (Yearron, 2003; Clemens et al., 2006). This variation has been interpreted to reflect a variety of processes, including melting of metamafic source rocks at different pressures (Moyen and Stevens, 2006). This would appear to be consistent with the suggestion by Kisters et al. (2010) that the Badplaas domain of the BGGT was assembled over some 60 Myr, between ca. 3290 and 3230 Ma, and that the timing and duration of plutonism, together with the structural and compositional heterogeneity of the Badplaas domain imply that the domain represents part of a convergence-related magmatic arc. Furthermore, the whole-rock Sr-Nd isotope data (Barton et al., 1983; Kröner et al., 1996; Yearron, 2003; Sanchez-Garrido, 2012) indicate the source rock for ~ 3200 Ma plutons in the BGGT. The source rock was possibly derived from either pre-existing rocks of the Onverwacht Group (Hamilton et al., 1979; Kröner et al., 1996) or its high-grade equivalents in the Swaziland Ancient Gneiss Complex (Kröner et al., 1993; Kröner and Tegtmeyer, 1994) or even the Fig Tree Group (Toulkeridis et al., 1999; Sanchez-Garrido, 2006). Because the isotopic ratios of ca. 3230 –3210 Ma plutons indicate that crust

is consistent with origin from an enriched mantle source or from part of the Onverwacht crust. Consequently, the Nelshoogte pluton may present an opportunity to examine the full spectrum of TTG magma-forming processes during Archaean collision.

This thesis aims to investigate the petrogenesis of the Nelshoogte pluton by testing the hypotheses, outlined above, which interpret magma compositions to be primarily controlled by source composition and the P-T conditions of partial melting. In addition, this work will also consider potential magma modification processes within the pluton, such as magma mixing and fractional crystallization. The pluton is an ideal candidate for such a detailed study because it is a well-defined pluton that is round-shaped and clearly separated from other plutons by later potassic/mafic intrusions and displays a considerable compositional range. The results of petrogenetic models will be tested using the existing knowledgebase on the geodynamic evolution of the region. Key questions that the study will seek to address are:

(1) Over what time period was the Nelshoogte pluton emplaced? Kisters et al. (2010) suggested that the adjacent 3290 - 3230 Ma Badplaas domain was constructed over 60 Myr. Also, for the Nelshoogte pluton, various ages have been obtained. Older age determinations (zircon U-Pb age) are 3220 ± 40 Ma (Oosthyzen, 1970) and 3236 ± 1 Ma for the main trondhjemitic phase (De Ronde and Kamo, 2000) and an age of 3225 ± 2 Ma for a late-tectonic tonalitic phase (Belcher et al., 2005). How long these Nelshoogte TTGs age period was? Was the Nelshoogte pluton also assembled over such a long time? How is the relationship among ~ 3200 Ma plutons as the youngest plutons in the BGGT? Zircon U-Pb ages will be determined for as many different phases of the Nelshoogte pluton as possible in order to constrain the time period of pluton construction. Additionally, these dates will allow the age relationship of Nelshoogte plutonism relative to D2 deformation that is partitioned into domains alternating prevailing folding and shearing deformation, to be better established (Carmignani et al., 1979; Simpson, 1999; Carosi & Oggiano, 2002; Carosi et al., 2004).

(2) How was the geochemical diversity generated within the granitoid rocks of the BGGT, and to what degree is this a reasonable model for the origin geochemical diversity within the Nelshoogte pluton? In the BGGT, older plutons are trondhjemitic and younger plutons have both trondhjemitic and tonalitic character (Yearron, 2003; Clemens et al., 2006). The older trondhjemites have been interpreted to have formed by higher-pressure of partial melting of a mafic source (Moyen and Stevens, 2006). The ~ 3200 Ma plutons display a considerable

compositional range, and have been interpreted to belong to both high- and medium-pressure groups. Thus, the compositions for the younger plutons suggest different process to those that formed the older plutons, with previous studies inferring slab-break off to have been important in allowing a transition from higher-pressure to lower-pressure melting. Does this interpretation fit with the time period over which the Nelshoogte pluton was assembled and does it fit with the geochemical details of the Nelshoogte rocks?

(3) Are the source rocks for TTG magmas oceanic crust or arc volcanic rocks (greenstone belt rocks)? There are two possible tectonic scenarios for the formation of TTG rocks. Firstly, that they formed by partial melting of Archaean hydrated basaltic crust, at high pressures, in subduction zones. In this case, enrichment in Na, Sr and LREE in these basalts was not the result of crustal assimilation but was inherited from a mantle source that was less depleted than modern MORB sources and enriched in recycled crustal components (Smithies, 2000; Rapp et al., 2003; Condie, 2005; Smithies et al., 2009). Secondly, that these rocks formed by partial melting of island-arc crust at lower pressures (Kamber et al., 2005; Foley, 2008; Van Kranendonk, 2010). Note that, as discussed by Moyen (2012), pressure in this setting needs to be high enough to stabilize rutile and a considerable fraction of garnet in the residuum because such pressures are extremely unlikely to be achieved within the crust, especially in an Archaean crust for which the higher heat flux from the mantle would result in a weaker crust unable to support a great thickness (England and Bickle, 1984; Rey and Houseman, 2006). The geochemical features for the pressure of partial melting and Lu-Hf isotope ratios in zircon will be used in this study to provide information on the age of the crust that partially melted to form the Nelshoogte pluton.

In this study the questions posed above are addressed using three different types of data. Firstly, whole-rock major- and trace- element data are used to construct chemical variation diagrams that are useful in constraining the nature of the magma sources (e.g. source rock type, pressure of melting), as well as processes such as magma batch evolution through processes such as mixing, partial melting or crystal fractionation. Secondly, zircon separates obtained for each trondhjemite/tonalite allow for U-Pb ages to be used to determine the magmatic age of each rock, thereby constraining the range of crystallization age for the pluton. Thirdly, Lu-Hf isotope ratios, determined on the same zircon populations, allow the age of the source of the TTGs to be constrained.

In combination with the basic field observations, petrographic descriptions and mineral chemical information, these three datasets allow the petrogenetic model for the Nelshoogte pluton to be expanded for other plutons in the BGGT and tested using the existing knowledgebase on the geodynamic evolution of the proto-Kaapvaal craton at 3300 to 3200 Ma. This should contribute to an understanding of why this is the last significant TTG pluton to form and why, following 3200 Ma, crustal magmatic processes switched to producing more potassic calc-alkaline felsic magmas.

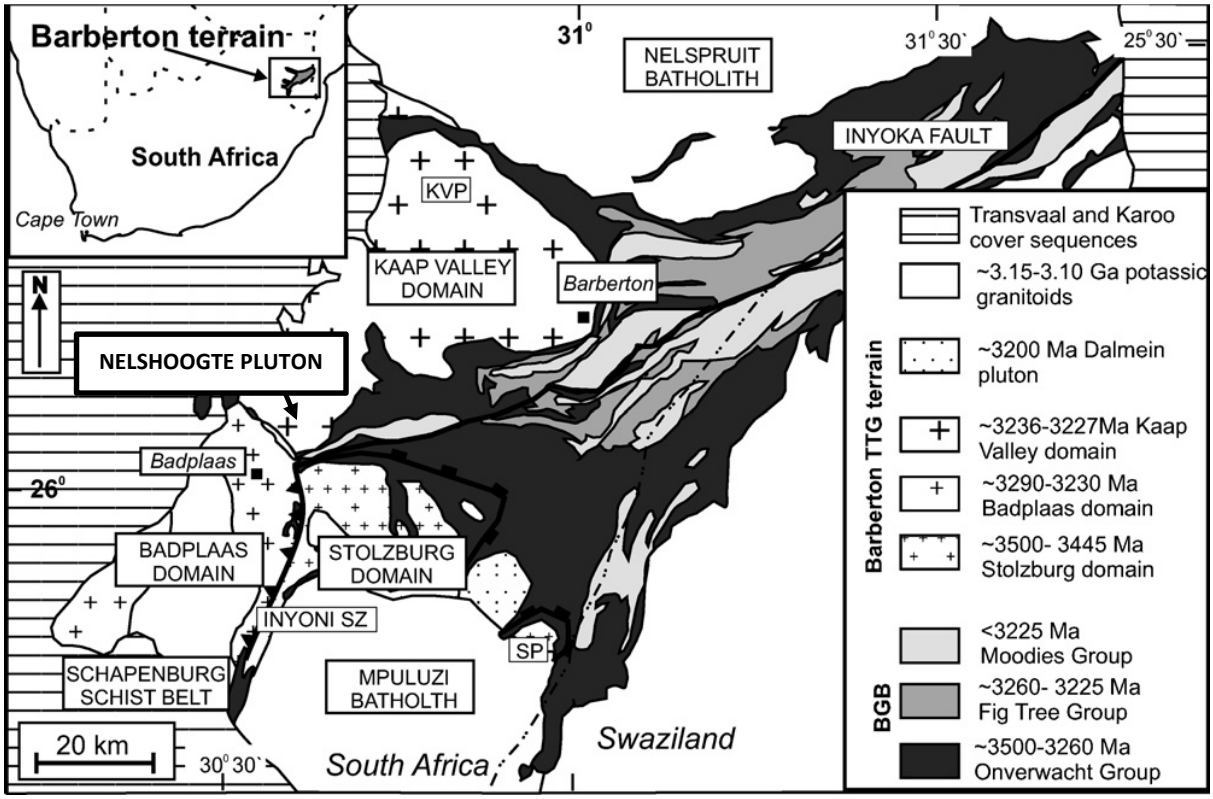

Fig. 1. Simplified geological map of the Barberton granitoid-greenstone terrain (modified from Kisters et al., 2010) KVP, Kaap Valley Pluton; SP, Steynsdorp Pluton. The Inyoni shear zone is marked by black line and teeth (pointing to the upper plate); the trace of the southern extensional detachment at the base of the greenstone belt is marked by solid black line (blocks on upper plate). The ca. 3450 Ma plutons in the south, are separated from the former by the Komati fault, leading to the identification of a distinct "Stolzburg domain" (Kisters et al., 2003; Diener et al., 2005; Moyen et al., 2006) corresponding to the amphibolite-facies portion of the Songimvelo terrane. The main structure is the Inyoni–Inyoka fault system, separating the western (Kaap Valley block) from the eastern domain (Steynsdorp and Songimvelo blocks, including Stolzburg terrane). Note that the "Onverwacht Group", on both

sides of the Inyoka fault, actually corresponds to rocks with different stratigraphy and with contrasting ages: 3300 – 3250 Ma to the west, and 3550 – 3300 Ma in the east. (Viljoen and Viljoen, 1969a; Anhaeusser et al., 1981,1983; de Wit et al., 1992; de Ronde and de Wit, 1994; Lowe, 1994; Lowe and Byerly, 1999, 2007; Lowe et al., 1999; de Ronde and Kamo, 2000).

Chapter 2

Geological setting

The Early to Mid Archaean granite-greenstone terrain of the Barberton Mountain Land, South Africa, forms an early part of the Kaapvaal Craton (shield) and represents one of the best preserved and oldest, pre-3000 Ma, granite-greenstone terrains (Heubeck and Lowe, 1999) See Fig.1. The greenstone belt is dated at ca. 3550 to 3220 Ma. The sequence comprises mafic volcanic rocks, layered ultramafic complexes, and felsic volcaniclastic rocks of the Onverwacht Group, tectonically overlain by and infolded with argillaceous and coarse-clastic sediments of the Fig Tree and Moodies Groups. Surrounding the belt are a large number of both Na-rich and K-rich granitoid plutons. The Na-rich TTG plutons are the oldest granitoids in the field area, and vary in age from ca. 3509 to 3227 Ma (Kamo and Davis, 1994). Subsequent more potassic magmatism came in the form of a granodiorite pluton (the Kaap Valley pluton) at ca. 3227 Ma (Armstrong et al., 1990) and voluminous monzogranite-granodiorite batholiths (Nelspruit, Salisbury Kop, Pigg's Peak, Heerenveen and Mpuluzi batholiths), with an associated syenite-granite complex (Boesmanskop pluton and Keens Zyn Doorns syenite), at ca. 3107 Ma (Kamo and Davis, 1994).

The 3550 – 3500 Ma TTGs, represented by the Steynsdorp pluton (Anhaeusser and Robb, 1983; Kröner et al., 1996), have a pervasive solid-state gneissosity and occur mostly as banded gneisses. The protolith of these gneisses was tonalitic (Kisters and Anhaeusser, 1995; Kröner et al., 1996). The ca. 3450 Ma (syn-D1; earlier deformation event) TTGs are represented by a number of intrusive bodies in the Stolzburg terrane, located to the south of the main part of the BGB (Barberton Greenstone Belt) (Viljoen and Viljoen, 1969; Anhaeusser and Robb, 1980, 1983; Kisters et al., 2003; Moyen et al., 2006). The two most prominent and best-defined intrusions are the Stolzburg and Theespruit plutons. Together with the smaller Doornhoek pluton, these intruded the supracrustal rocks of the belt.

The 3290 - 3210 Ma plutons (syn-D2 and D3) occur along the northern and southwestern margins of the Barberton Greenstone Belt (BGB) (Viljoen and Viljoen, 1969d; Anhaeusser and Robb, 1980; Robb and Anhaeusser, 1983). In the south, the Badplaas domain is comprised of the 3290 – 3230 Ma Badplaas gneisses (Poujol et al., 2003; Kisters et al., 2010),

the 3290 - 3240 Ma Rooihoogte gneisses (Kisters et al., 2010) and west of the 3100 Ma Heerenveen batholith. The plutons in the Badplaas domain are composed of two main suites. The one is an older, coarse-grained leuco-trondhjemitic component that underwent solid-state deformation. The other one is a younger, multiphase intrusive into the Elandsfontein gneisses and made up a variety of typically finer-grained trondhjemites. In its eastern parts, the Badplaas pluton shows intrusive contacts with the gneissose rocks of the Batavia pluton. In proximity to the Inyoni shear zone, most of these intrusions are syntectonic: the Batavia pluton, of coarse-grained, leucocratic, porphyritic trondhjemite, is syntectonic in the central part of the Inyoni Shear Zone (Anhaeusser et al., 1981; Kisters et al., 2010; Nédélec et al., 2012). The eastern contact of the Badplaas pluton is characterized by the progressive strain increase and transposition of the gneissose banding into the steep E-dipping banded gneisses of the Inyoni shear zone. The Rooihoogte pluton refers to the westernmost parts of the Badplaas domain, underlain by one main and a number of volumetrically minor varieties of trondhjemitic gneisses. The most widespread phase of the Rooihoogte pluton is a homogeneous, coarse- to medium-grained, grey trondhjemite with a well-developed solid-state gneissosity (Kisters et al., 2010). The Kaap Valley domain is comprised of the largely trondhjemitic Nelshoogte pluton and 3226 Ma tonalitic Kaap Valley pluton (Armstrong et al., 1990) that form large ovoid TTG bodies along the northwestern flank of the greenstone belt (Robb et al., 1986; Yearron, 2003) (Fig. 1).

2.1. Geochemical arguments for TTG magma generation at high pressures

TTGs encompass a degree of geochemical diversity that can potentially be related to differences in melting depth of geochemically similar sources. The mineralogical model for amphibolite partial melting suggests that TTGs formed at $P >$ 15 kbar and T between 900 ºC and 1100 ºC (Moyen and Stevens, 2006), corresponding to low (15 ºC/km) geothermal gradients that are likely to be attained only in subduction zones (Moyen, 2011; Moyen and Martin, 2012). The major-element composition of the TTGs, in general, is explained by fluid-absent partial melting of plagioclase-amphibole assemblages (Rushmer, 1991; Rapp and Watson, 1995; Vielzeuf and Schmidt, 2001; Moyen and Stevens, 2006); i.e., partial melting during which water was supplied by the breakdown of hydrous phases (either amphibole, or sometimes epidote), or plagioclase + quartz; melting at pressure above plagioclase stability (Laurie and Stevens, 2012). While the role of plagioclase accounts for the sodic nature of the

melts, the presence of mafic peritectic phases in the residuum keeps the melt leucocratic, by locking up the Fe and Mg in the residuum to very high temperatures (>1100 ◦C). Trace element characteristics are largely due to the presence of garnet in the residuum (either as a pre-existing phase, or as a peritectic product), implying melting at pressures above 10–12 kbar. In the case of high pressure type TTGs in particular, their Na_2O-rich character has been interpreted to reflect a metabasaltic source; their high HREE contents have been interpreted to reflect a high abundance of garnet in the residuum, which is consistent with a formation pressure above 2.0 GPa; their negative Nb anomaly is interpreted to reflect rutile in the residuum, which supports a similarly high pressure in the source (see Moyen and Stevens (2006) for a review on the about listed indicators); and their high Ni and Cr contents, as well as high Mg#s are interpreted to reflect interaction with the mantle wedge during magma ascent (Martin and Moyen, 2002).

These implications on trace element abundances for the mineralogy of the residuum represent the pressure of melting of the source rock of individual plutons in the BGGT, because the Barberton TTGs show variable trace element compositions (e.g. Sr/Y and La/Yb ratios). They suggest ~ 3500 Ma plutons were generated by low pressure (shallow source), ~ 3450 Ma plutons were by high pressure (deep source) and ~ 3200 Ma plutons were by both high and low pressure (Moyen and Stevens, 2007).

2.2. The ages of rocks that possibly formed in association with subduction zones

The emplacement of large volumes of TTG magmas in Barberton has been linked with major episodes of terrane accretion at ~ 3445 and ~ 3230 Ma (D1 and D2 respectively) (De Ronde and De Wit, 1994; De Ronde and Kamo, 2000). De Ronde and De Wit (1994) was the first to attribute each episode to an arc-trench environment, that the earliest, well-recognized tectonothermal events (3490–3450 Ma) represent mid-ocean ridge-like processes. These were followed by two periods of arc-related and trench-related processes, separated by ~160 Myr; the first (3445–3416 Ma) recording an intra-oceanic suprasubduction-like environment and the second, (3260–3225 Ma) intra-arc and interarc-like processes, culminating in arc amalgamation. Accretion-like convergent processes dominated between 3230 Ma and 3080 Ma, overlapping with the assembly of the Kaapvaal craton. They have the coeval nature of TTG magmatism and dacitic volcanism in the greenstone sequences. Structural and chemical

data imply that the hydrated ophiolitic rocks of the Barberton greenstone belt are allochthonous and were thrust over similar simatic rocks from which the felsic igneous rocks were syntectonically derived by partial melting. Such structural imbrication of simatic crust can be best incorporated in a model advocating Archaean intra-oceanic obduction associated with shallow-angle subduction, similar to that documented for the neotectonics of the Western Aleutians (De Wit et al., 1987).

For the first major episode (D1), Grosch et al. (2011) suggests that the 3460–3437 Ma Stolzburg TTG terrane and the proposed oceanic crust of the Hooggenoeg formation of the Songimvelo Block most likely developed in a supra-subduction zone setting; the Songimvelo Block is accreted onto older microcontinental terranes of the Steynsdorp Block and the Ancient Gneiss Complex, in an arc-continent collision zone, similar to that in Phanerozoic ophiolite terranes. This resulted in major uplift and erosion of the Hooggenoeg oceanic crust including the Buck Reef volcano-sedimentary complex during terrane accretion and possible obduction onto older proto-continental blocks of the Kaapvaal craton at or some time shortly after ca. 3432 Ma. Because the occurrence of both zircon overgrowths with Pb–Pb ages and new zircon growth ages of 3433 ± 8 Ma reported in ca. 3644 Ma banded gneisses in the northwestern Ancient Gneiss Complex have close proximity to the Phophoyane Shear Zone (Compston and Kroner, 1988; Kroner et al., 1989). The inherited zircon xenocrysts in the Steynsdorp trondhjemitic intrusion dated at ca. 3553 ± 4 Ma (Kroner et al., 1992, 1996) indicate a possible early intrusive connection between the Steynsdorp Block and the Ancient Gneiss Complex, prior to a major craton-scale tectonic accretion event with the Songimvelo Block of the BGB at ca. 3432 Ma.

For the second major episode (D2), Kisters et al. (2010) suggests that the timing and duration of plutonism (ca. 60Ma between ca. 3290 and 3230Ma and prior to the main collisional event in the granitoid-greenstone terrain at 3230 Ma), together with the structural and compositional heterogeneity of the Badplaas domain represents part of a convergence-related magmatic arc. This indicate that 3200 Ma plutons occurred in subduction zone, because continental crust is mainly added at convergent plate margins along magmatic arcs situated above subduction zones on the modern Earth (Reymer and Schubert, 1984; Arculus, 1994; Rudnick, 1995; Hamilton, 1995). These arcs typically record continuous magmatism over tens of millions of years, depending on the duration of convergence prior to collisional tectonics.

The D2 event and later metamorphic events (D3, D4) are likely related with subduction in Barberton. Kamo and Davis (1994), Dziggel et al. (2002) and Stevens et al. (2002) estimated U-Pb zircon age (ca 3230 Ma) for D2, and structural observations and U-Pb data from Lana et al. (2011) indicate that the D3 folding of the Moodies Group into the Malolotja synform was followed by the D4 extension and exhumation of the granitoid complex between 3228 ± 10 and 3205 ± 9 Ma.

2.3. Metamorphic evidence for subduction in Barberton

Moyen et al. (2006) reported garnet–albite-bearing mineral assemblages that record pressures of 1.2–1.5 GPa at temperatures of 600–650 ºC from supracrustal amphibolites from the Inyoni shear zone. These conditions point to apparent geothermal gradients of 12–15 ºC/km—similar to those found in recent subduction zones—that coincided with the main phase of terrane accretion in the structurally overlying BGB (De Wit et al., 1992). These high-pressure, low-temperature conditions represent metamorphic evidence for cold and strong lithosphere, as well as subduction-driven tectonic processes. The advective heat transfer associated with the intrusion of these synkinematic granitoids also contributes to the syn- to late-collisional heat budget of the collisional belt that acted to partially destroy the evidence for the earlier high-pressure, low-temperature metamorphism. In many respects, this is similar to high-pressure amphibolites from more recent subduction–collision belts that often occur as partially retrogressed boudins within migmatites.

The 3227 Ga Kaap Valley and 3236 Ma Nelshoogte plutons were exhumed shortly after emplacement in the northwestern margin of the greenstone belt. In addition, the 3228 Ma age for the extension in the eastern margin of the BGB coincides in time with the 3230-3227 Ma magmatism and exhumation of the southern TTG complex in the BGGT (Kisters et al., 2003). Lana et al. (2010, 2011) proposes that much of the eastern and western margins of the BGB record a syn- to post-Moodies shortening deformation that is related to the effects of vertical movements of the 3236 ± 1 Ma Nelshoogte, 3227 ± 1 Ma Kaap Valley and 3228 ± 10 Ma Malolotja granitoids. The granitoid emplacement and solid-state shearing (D4) in the Malolotja Inlier were contemporaneous with the solid-state exhumation of high-P low-T granitoids of the southern margin of the greenstone belt.

Taylor (2012) also supports these hypotheses of convergent plate boundary processes investigating 3100 Ma granulites from the Ancient Gneiss Complex, Swaziland, and explains that radiogenic heating of the orogenically thickened crust, and continued subduction-driven convergence along an active plate margin, led to protracted heating of these sediments and major mid- to lower crustal differentiation between ca. 3230 and 3070 Ma. The long-lived, coaxial nature of the NW-SE shortening, combined with protracted crustal melting and calc-alkaline granitoid magmatism in the southeastern domain of the Craton is, as a first approximation, reminiscent of an Andean-style accretionary margin. In such a setting, extended periods of subduction-convergence are punctuated by short regional orogenic events (terrane accretion), with strain concentrated into zones of mechanical and thermal weakness such as the back-arc and magmatic arc region (i.e. the Granodiorite-Monzonite-Syenite suite and Luboya-Kubuta migmatite zone).

Amphibolite-facies rocks of the Theespruit Formation record high-*P*, low-*T* peak metamorphic conditions of 7.4 ± 1.0 kbar and 560 ± 20 ℃ that were attained during the main phase of terrain accretion in the greenstone belt at 3230 Ma. In contrast, the greenstone sequence ca. 4 km to the north only records low greenschist-facies metamorphism, indicating that a metamorphic break of ca. 18 km exists between the high-grade terrain and the greenstone belt. The main phase of deformation in the Theespruit Formation was initiated under peak metamorphic conditions and continued during retrogression. Retrograde *P–T* estimates and mineral reactions indicate that retrogression involved near-isothermal decompression of ca. 4 kbar prior to cooling into the greenschist-facies, suggesting that the fabric in these rocks is an exhumation fabric that accommodated the juxtaposition of the high-grade terrain against the greenstone belt (Diener et al., 2005).

Moyen et al. (2006) and Nédélec et al. (2012) suggest that the genesis of large volumes of medium-pressure TTG magmas is likely formed at greater depth. The derived geothermal gradient of ca. 17–22 °C/km by thermobarometric estimates from the Inyoni Shear Zone migmatitic rocks cluster in the range 720–800 °C and 1.1–1.2 GPa for the melting reaction is consistent with either H_2O-present melting or fluid-absent partial melting involving the breakdown of hydrate minerals. Unmelted garnet-bearing amphibolites correspond to slightly lower conditions. The magmatic cumulates crystallized at ca. 0.6 GPa. The cumulate rocks provide evidence that the TTG parental magmas experienced fractional crystallization of a

large amount of amphibole before crystallizing as tonalite–trondhjemite plutons at slightly shallower depths (ca. 0.5 GPa).

Chapter 3

Rocks of the Nelshoogte pluton

The Nelshoogte and the Kaap Valley plutons are the youngest TTG intrusions in the BGGT, (dated at ca. 3236 and ca. 3226 Ma, respectively; Kamo and Davis, 1994; Armstrong et al., 1990), and are located at its western margins (Fig. 1). The Nelshoogte pluton, approximately 17 by 15 km is rounded in shape. To the north and east it is surrounded by the BGB. To the northwest and west it is overlain by the younger cover of the Transvaal Supergroup. To the south it is in contact with the composite Badplaas pluton. This contact is developed as an, at least, 1000m wide intrusive breccia and gneissose rafts of the Nelshoogte pluton are found within the mainly fine-grained leucocratic phase of the Badplaas pluton. The actual contact seems to be delineated by a NW-trending train of greenstone remnants that outline the semicircular southern margin of the Nelshoogte pluton (Figs. 1 and 2) (Kisters et al., 2003; Belcher et al., 2009; Kisters et al., 2010).

Also the dyke-like 3107 Ma (Kamo and Davis, 1994) Kees Zyn Doorns syenite that intruded close to this contact, although the position of the contact is poorly defined. Notably, the ENE-trending gneissosity of the Badplaas pluton trends at high angles to the pervasive ESE-trending gneissosity developed in the Nelshoogte pluton to the immediate north (Kisters et al., 2010). Also, there are many younger (post 3000 Ma) gabbroic to dioritic intrusions, especially near the contact with the BGB (Fig. 2), Figure 4(b) shows the contact between the gabbroic rock and trondhjemite near by the northern margin. Also there are migmatites and enclaves of gabbro in trondhjemite near by the contact with the BGB (Fig. 3cd). The northern margin, the contact between the pluton and the Kaap Valley pluton is not clear. It may be covered by those mafic intrusions.

The pluton mainly consists of trondhjemites that have variable developed gneissosities. The variation in gneissosity developed within the different phases and the syn- to late/post-tectonic emplacement suggest a protracted emplacement history (Belcher et al., 2009). The contact between the trondhjemite and tonalite/granodiorite is sharp, and Figure 3(f) shows the tonalitic vein is parallel to the foliation of the trondhjemite in the southeastern part. The tonalite is also brittle deformed. The trondhjemites were then intruded by tonalite

/granodiorite magmas. However, the TTGs in the northern part of the pluton are not foliated. It is common to find fine- to medium- grained, highly felsic, granite/trondhjemite sheets (10-30cm) (Fig. 4a) that are later intrusions of second-generation granite/trondhjemite. Figure 3(a) shows the sharp contact between tonalite and porphyritic trondhjemite intrusion (>1m). Also there are potassic granite veins that intruded to trondhjemite in the eastern to nourtheastern part of the pluton (Fig. 3e). The both of trondhjemites are foliated. The contact between amphibolite/greenstone (the BGB) and trondhjemite is also sharp (Fig. 4c). The trondhjemite forms brittle deformed fine-grained texture. The enclaves of gabbro in trondhjemite are found near the northern margin of the pluton (Figs. 3c and 3d). Foliation varies from 280 to 310º, dipping at 50 to 60º NE, in the centre of the pluton to 336 to 356º and 85º E near the northwest margin (Yearron, 2003). In northern part of the pluton, none of the rocks have well developed foliations.

Various U-Pb zircon ages have been obtained for the Nelshoogte pluton, suggesting a protracted pluton construction period between ca. 3236 and ca. 3225 Ma. Older age determinations include 3220 ± 40 Ma (Oosthyzen, 1970) and 3236 ± 1 Ma, recorded for the main trondhjemitic phase by De Ronde and Kamo (2000), and an age of 3225 ± 2 Ma by Belcher et al. (2005) for a late-tectonic tonalitic phase. The latter provides a lower age limit for the pluton and indicates an emplacement history spanning some 10 Myr.

The ages of ca. 3230 Ma for the Nelshoogte pluton (De Ronde and Kamo, 2000) indicate a pre- to syn (D2)-tectonic emplacement of the trondhjemites. Hornblende-bearing tonalites occur, as intrusive plugs (the shape is unknown), particularly along the eastern and northern margins of the Nelshoogte pluton. Belcher et al. (2005) interpreted the pluton as a large, composite sill complex emplaced along and into the basal detachment that forms the granitoid-greenstone contacts at the base of the BGB. The pluton was intruded, probably as a laccolith, during regional folding and shows lit-par-lit intrusive relationships as well as smaller-scale brecciation with the surrounding greenstone wall rocks. This suggests a relatively shallow level of emplacement. The domal map pattern reflects late-stage folding and steepening of the, initially flat-lying syn-emplacement fabrics.

Kisters et al. (2010) also suggest that trondhjemitic gneisses of the pluton are intrusive. The contact with the northern Badplaas pluton is developed as an intrusive breccia at least 1 km wide, and gneissose rafts of the Nelshoogte pluton are found within the mainly fine-grained

leucocratic phase of the Badplaas pluton. Kisters et al. (2003) explain that the 3227 Ma Kaap Valley and 3236 Ma Nelshoogte plutons were exhumed shortly after emplacement in the northwestern margin of the greenstone belt, because NE–SW stretching of mid-crustal basement rocks and non-coaxial, top-to-the-NE shearing along retrograde mylonites at upper crustal levels, suggests that it is consistent with an extensional orogenic collapse of the belt and the concomitant exhumation of deeper crustal levels. The extensional collapse is coeval with or shortly follows the main D2 collisional event in the BGB at ca. 3230–3220 Ma. Voluminous plutonism at ca. 3225 Ma along the northern margin of the belt is possibly related to the orogenic collapse and associated decompression melting of lower crustal rocks.

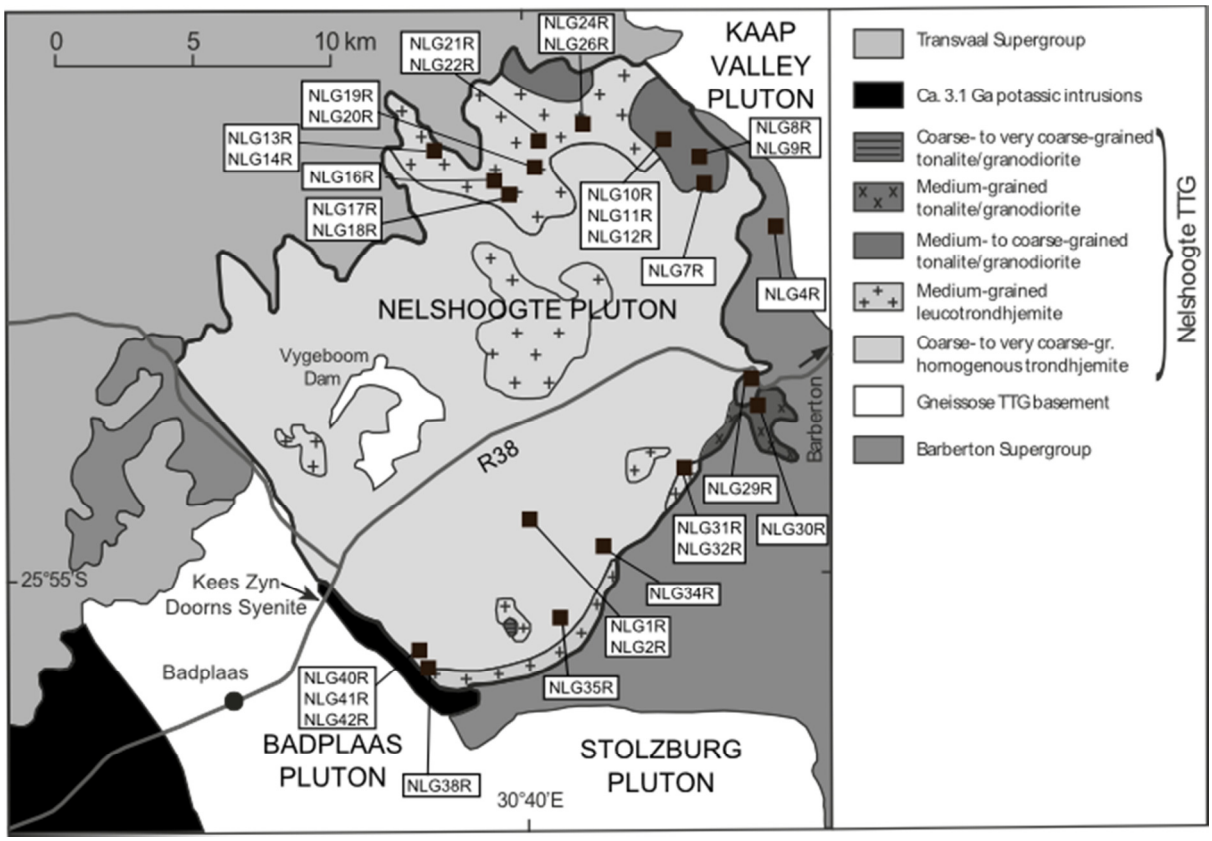

Fig. 2. Geological map of the Nelshoogte pluton (modified from Belcher et al., 2009), illustrating sample localities.

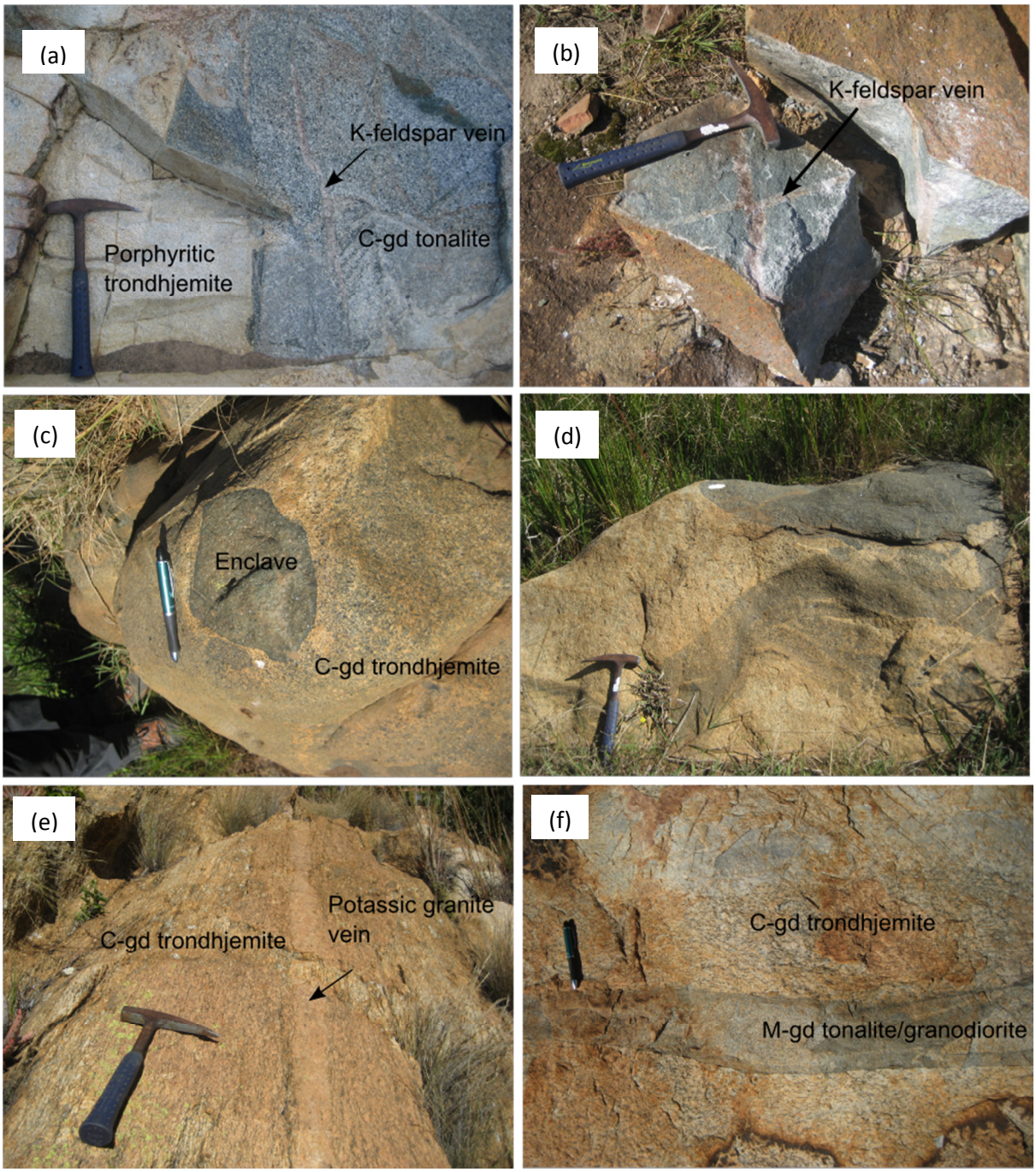

Fig. 3. (a) Fine-grained (F-gd) trondhjemite intrusion (NLG12R) and coarse-grained (C-gd) tonalite (NLG11R). (b) Cross-cutting K-feldspar vein in C-gd granodiorite (NLG13R). (c) Enclave of gabbro (NLG15R) and C-gd trondhjemite (NLG16R). (d) Migmatite (NLG15R and NLG16R). (e) Foliated C-gd trondhjemite (NLG31R) with porphyritic potassic granite vein (NLG32R). The vein is parallel to the foliation but it is not foliated. (f) Foliated C-gd trondhjemite (NLG34R) and medium-grained (M-gd) granodiorite vein. The vein is also brittle deformed and parallel to the foliation.

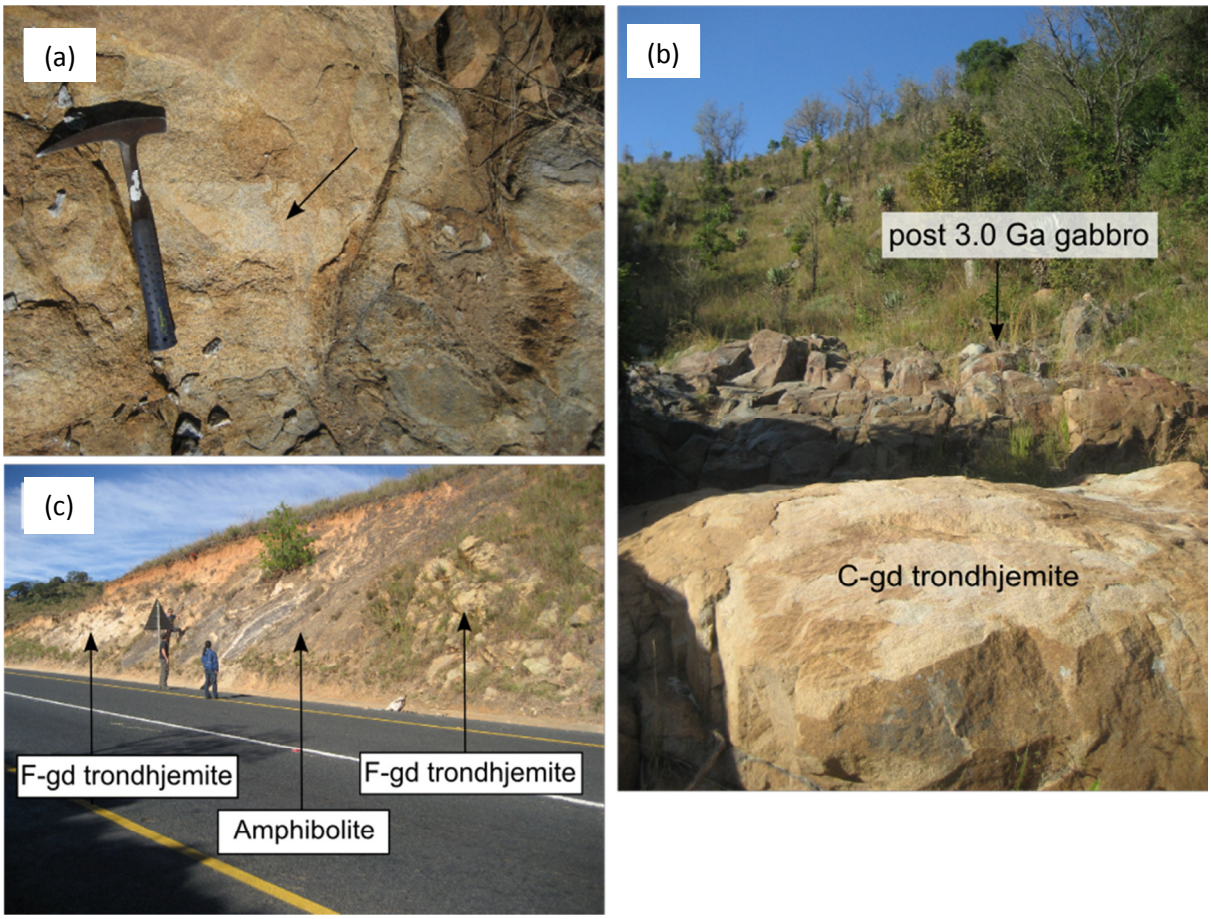

Fig. 4. (a) Foliated medium-grained trondhjemite (NLG41R) vein. (b) The contact between gabbro (NLG25R) and coarse-grained trondhjemite (NLG26R) (c) The sharp contact between fine-grained trondhjemite (NLG29R) and amphibolite (NLG28R) that is a raft of the Barberton greenstone belt rock within the Nelshoogte pluton in the eastern margin of the pluton. Both rocks are foliated.

Chapter 4

Analytical techniques

Mineral compositions and inclusions in zircon

Imaging of the samples and analysis of the phase compositions was accomplished using a Zeiss EVO® MA15 Scanning Electron Microscope at the Stellenbosch University. Quantitative analysis and backscatter images require 15 micrometer thickness (peacock blue colour) of carbon coating, a flat and polished surface. Samples were identified with backscattered electron (BSE) and/or Secondary electron images, and phase compositions were quantified by EDX analysis using an Oxford Instruments® X-Max 20mm2 detector and Oxford INCA software. Beam conditions during the quantitative analyses were 20 KV, with a working distance of 8.5 mm and approximately beam current of – 20nA. The counting time was 10 seconds live-time. Internal Astimex Scientific mineral standards were used for standardization and verification of the analyses. Pure Co were used periodically to correct for detector drift.

Major-element compositions

Whole-rock analyses were performed after crushing the rocks in a stainless steel jaw crusher, and powdering representative splits in either an agate or a tungsten carbide mill. The tungsten carbide mill showed detectable contamination of Co in, so this element is not reported.
Major-element compositions have been obtained by XRF analysis on La-free glass beads (Axios from PANalytical with a 2.4kWatt Rh X-ray Tube at the Stellenbosch University). The gas-flow proportional detector and scintillation detector, or a combination of the two, were used to cover the elements fluorine to uranium. Major elements (Na_2O, MgO, SiO_2, K_2O, CaO, TiO_2, MnO, P_2O_5, Al_2O_3, Cr_2O_3 and Fe_2O_3T) are analysed on a fused glass bead and trace elements (Cr, Ni, Zn, As, Ga, Co, V, Rb, Sr, Y, Zr, Nb, Ce, Nd, La, Th, U, Ba as well as S and Cl) are analysed on a powder briquette. A wide range of international (NIST®) and national (SARM®) standards is used in the calibration procedures and Quality Assurance (accuracy) for both major and trace element analyses. Detection limits for the elements quoted, depending on the matrix (combination of elements present), are approximately 0.5

ppm for trace elements on a pressed pellet and approximately 0.001 wt% for major elements on a fused bead. A local granitic sample "HG" is used as in-house secondary process control for Quality Control (precision) purposes.

Trace element compositions

Trace element compositions were obtained using Laser Ablation-Inductively Coupled Plasma-Mass Spectrometry (LA-ICP-MS) at the Stellenbosch University. Fusion disks used for XRF analysis were coarsely crushed and a chip of sample mounted along with 9 other samples in a 2.4cm round resin disk. The mount was mapped, and then polished for analysis. A New Wave 213nm laser ablation system connected to an Agilent 7500ce ICP-MS was used in the analysis fusion disks. Ablation was performed with 110 μm diameter ablation spots in He gas and mixed with argon after exiting the ablation cell, then passed through a mixing chamber before introduction into the ICP. Operating conditions for the laser were 10 Hz frequency and ~ 10.5 kJ energy. Trace elements were quantified using NIST 612 for calibration and ^{29}Si as internal standard, using standard – sample bracketing. Three replicate measurements were made on each sample. The calibration standard was run every 12 samples. A quality control standard was run in the beginning of the sequence as well as with the calibration standards throughout. BHVO 2G, a basaltic glass certified reference standard produced by USGS (Dr Steve Wilson, Denver, CO 80225), was used for this purpose. Data was processed using Glitter software, distributed by Access Macquarie Ltd., Macquarie University NSW 2109.

Sample preparation

Zircon separates were prepared from 1 to 2 kg rock samples that were crushed and pulverized at Stellenbosch University. Zircons were separated using a Frantz isodynamic separator and heavy liquids. Zircon concentrates were handpicked under a binocular microscope, mounted in epoxy, and then polished to half their thickness to expose internal structures.

CL images of zircon

Imaging of zircons was accomplished using a Leo® 1430VP Scanning Electron Microscope at the Stellenbosch University. Prior to imaging the samples were mounted on a stub with

double-sided carbon tape. The sample was then coated with a thin layer of gold in order to make the sample surface electrically conducting. The Cathodoluminescene (CL) images show the surface structure of material. Beam conditions during surface analysis were 20 KV and approximately 1.5 nA, with a working distance of 13 mm and a spot size of 500.

U-Pb analysis

All U–Pb age data obtained at the Stellenbosch University, were acquired by laser ablation - single collector - magnetic sectorfield - inductively coupled plasma - mass spectrometry (LA-SF-ICP-MS) employing a Thermo Finnigan Element2 mass spectrometer coupled to a NewWave UP213 laser ablation system. All age data presented here were obtained by single spot analyses with a spot diameter of 30 µm and a crater depth of approximately 15–20 µm. The methods employed for analysis and data processing are described in detail by Gerdes and Zeh (2006) and Frei and Gerdes (2009). For quality control, the Plešovice (Sláma et al. 2008) and M127 (Nasdala et al. 2008; Mattey 2010) zircon reference materials were analyzed, and the results were consistently in excellent agreement with the published ID-TIMS ages. Full analytical details and the results for all quality control materials analysed are reported in Table 1 in the electronic supplementary material. The calculation of concordia ages and plotting of concordia diagrams were performed using Isoplot/Ex 3.0 (Ludwig 2003).

Table 1. LA-SF-ICP-MS U-Th-Pb dating methodology CAF, Stellenbosch University

Laboratory & Sample Preparation	
Laboratory name	Central Analytical Facility, Stellenbosch University
Sample type / mineral	Detrital zircons
Sample preparation	Conventional mineral separation, 1 inch resin mount, 1 µm polish to finish
Imaging	CL, LEO 1430 VP, 10 nA, 15 mm working distance
Laser ablation system	
Make, Model & type	ESI/New Wave Research, UP213, Nd:YAG
Ablation cell & volume	Custom build low volume cell, volume ca.3 cm^3
Laser wavelength	213 nm
Pulse width	3 ns
Fluence	2.5 J/cm^{-2}
Repetition rate	10 Hz

Spot size	30 µm
Sampling mode / pattern	30 µm single spot analyses
Carrier gas	100% He, Ar make-up gas combined using a T-connector close to sample cell
Pre-ablation laser warm-up (background collection)	40 seconds
Ablation duration	20 seconds
Wash-out delay	30 seconds
Cell carrier gas flow	0.3 l/min He
ICP-MS Instrument	
Make, Model & type	Thermo Finnigan Element2 single collector HR-SF-ICP-MS
Sample introduction	Via conventional tubing
RF power	1100 W
Make-up gas flow	1.0 l/min Ar
Detection system	Single collector secondary electron multiplier
Masses measured	202, 204, 206, 207, 208, 232, 233, 235, 238
Integration time per peak	4 ms
Total integration time per reading	1 sec *(should represent the time resolution of the data)*
Sensitivity	20000 cps/ppm Pb
Dead time	6 ns
Data Processing	
Gas blank	40 second on-peak
Calibration strategy	GJ-1 used as primary reference material, Plešovice & M127 used as secondary reference material (Quality Control)
Reference Material info	M127 (Nasdala et al. 2008) Plešovice (Slama et al. 2008) GJ-1 (Jackson et al. 2004)
Data processing package used / Correction for LIEF	GLITTER *or* In-house spreadsheet data processing using intercept method for LIEF correction *or* IOLITE;VISUAL AGE
Mass discrimination	Standard-sample bracketing with $^{207}Pb/^{206}Pb$ and $^{206}Pb/^{238}U$ normalised to reference material GJ-1
Common-Pb correction, composition and uncertainty	204-method, Stacey & Kramers (1975) composition at the projected age of the mineral, 5% uncertainty assigned

Uncertainty level & propagation	Ages are quoted at 2 sigma absolute, propagation is by quadratic addition. Reproducibility and age uncertainty of reference material and common-Pb composition uncertainty are propagated.
Quality control / Validation	Plešovice: Wtd ave $^{206}Pb/^{238}U$ age = 338 ± 4 (2SD, MSWD = 0.2) M127: Wtd ave $^{206}Pb/^{238}U$ age = 560 ± 5 (2SD, MSWD = 0.8)
Other information	For detailed method description see Frei & Gerdes (2009)

Hf isotopes

Hafnium isotope measurements were performed with a Thermo-Finnigan Neptune multicollector ICP-MS at GUF coupled to the same laser as described in the U–Pb method (Resolution M- 50 193 nm ArF excimer laser). Laser spots with diameter of mostly 40 _m were drilled with repetition rate of 5.5 Hz and an energy density of 6 J/cm2 during 55 s of data acquisition. All data were adjusted relative to the JMC475 of $^{176}Hf/^{177}Hf$ ratio = 0.282160 and quoted uncertainties are quadratic additions of the within run precision of each analysis and the reproducibility of the JMC475 (2 SD = 0.0033%, n = 8). Accuracy and external reproducibility of the method was verified by repeated analyses of reference zircon GJ-1 and 91500, which yielded a $^{176}Hf/^{177}Hf$ of 0.282000 ± 0.000023 (2 SD, n = 13; supplementary material, Table 8) and of 0.282293 ± 0.000027 (n = 11), respectively. This is well within the range of solution mode data (Woodhead and Hergt, 2005; Gerdes and Zeh, 2006). For calculation of the epsilon Hf [εHft] the chondritic uniform reservoir (CHUR) was used as recommend by Bouvier et al. (2008; $^{176}Lu/^{177}Hf$ and $^{176}Hf/^{177}Hf$ of 0.0336 and 0.282785, respectively), and a decay constant of 1.867 × 10−11 (average of Scherer et al., 2001; Soderlund et al., 2004). Initial $^{176}Hf/^{177}Hft$ and εHft for all analyzed zircon domains were calculated using the apparent Pb–Pb ages obtained for the respective domains, and for all co-genetic zircon domains by using the intrusion ages of the respective granitoids (supplementary material, Table 8). Depleted mantle hafnium model ages (TDM) were calculated using values for the depleted mantle as suggested by Blichert-Toft and Puchtel (2010), with $^{176}Hf/^{177}Hf$ = 0.283294 and a $^{176}Lu/^{177}Hf$ of 0.03933, corresponding to a straight DM-evolution line with εHf_{today} = +18 and $\varepsilon Hf_{4.558Ga}$ = 0.0. TDM ages for all data were calculated by using the measured $^{176}Lu/^{177}Hf$ of each spot for the time since zircon crystallization, and a mean $^{176}Lu/^{177}Hf$ of 0.01 for the Palaeoproterozoic-Archaean crust [mean of average continental crust as suggested by Taylor and McLennan, 1985; Wedepohl, 1995; Zeh and Gerdes, 2012].

Chapter 5

Petrography

A total of 26 TTG and 4 potassic granite samples were collected from the Nelshoogte pluton. The list of sample no., rock type, textures and location are shown in Figure 2 and Appendix A.

5.1. Mineral assemblages

TTG samples are coarse- to fine-grained and classified as tonalite, granodiorite, trondhjemite and granite (Fig. 7). The mineral assemblages are shown in Table 1. Minerals are mainly plagioclase, quartz and biotite. Tonalite and granodiorite samples contain hornblende in addition to the minerals listed above. Hornblende-bearing tonalites and granodiorites were collected along the eastern and northern margins of the pluton.

Tonalite /Granodiorite

Tonalites and granodiorites have similar textures. Grains are inequigranular. Plagioclase forms subhedral to euhedral crystals, 1 to 4 mm long, with polysynthetic twinning and lobate to polygonal grain boundaries. Normal zoning is found in grains that are unaltered (Fig. 5a). Quartz forms as clusters of crystals, 0.5 to 4 mm long and exhibits undulose extinction. Biotite forms euhedral to subhedral platy crystals, 0.5 to 3 mm in length. Hornblende forms euhedral to subhedral diamond shaped crystals 0.5 to 2 mm in size. The accessory minerals are generally allanite, apatite, zircon, titanite, ilmenite and magnetite, and secondary minerals are epidote, chlorite and muscovite.

Trondhjemite/Granite

Trondhjemites and granites have similar mineral assemblages (Table 2). Grains are inequigranular. Plagioclase forms subhedral crystals, 1 to 4 mm long with polysynthetic twinning and polygonal grain boundaries. Quartz forms as clusters of crystals, 0.5 to 4 mm long and exhibits undulose extinction. Biotite forms euhedral to subhedral platy crystals, 0.5

to 3 mm in length, aligned parallel to the foliation. Microcline forms as interstitial crystals with crosshatched twinning. Myrmekite occurs as a replacement of K-feldspar (Fig. 5e). The accessory minerals are generally allanite, apatite, zircon, titanite, ilmenite and magnetite, and secondary minerals are epidote, chlorite and muscovite.

Table 2. Mineral assemblages for silicic minerals established by CIPW norm calculation using the major-element compositions. For biotite and hornblende, they were estimated by observation under microscope.

	Plagioclase	Quartz	Microcline	Biotite	Hornblende
Tonalite	60-65%	15-20%	5%	5-10%	5-10%
Granodiorite	50-55%	20-30%	5-10%	<5%	<5%
Trondhjemite	45-55%	20-40%	5-10%	<10%	<5%
Granite	45%	30-35%	15%	<5%	0%
Potassic granite	40-45%	25-35%	20-30%	<5%	0%

*Secondary minerals are epidote, chlorite and muscovite.

*Accessory minerals are apatite, allanite, ilmenite, magnetite, sphene and zircon.

5.2. Textures

There are variable textures such as granitic (Fig. 5a), porphyritic, foliated (Fig. 5c), xenomorphic-granular (Fig.5ef) hypidiomorphic-granular (Fig. 5d) textures in the Nelshoogte TTGs. Magmatic textures such as porphyritic and granitic textures are found from TTGs in northern part of the pluton. Deformation textures such as foliated and xenomorphic textures are found from TTGs in southern to southeastern part of the pluton.

Foliated texture

It is common to find foliated texture in trondhjemites from southern part, near the southwestern margin of the Nelshoogte pluton (Fig. 2). Recrystallized quartz forms elongate,

strongly undulose quartz-ribbon aggregates and biotite aggregates align parallel to the foliation (NLG34R) (Fig. 5c). Recrystallized plagioclase forms small (0.1 to 0.3 mm) crystals. Myrmekite occurs as intergrowth of quartz in plagioclase/K-feldspar.

Porphyritic texture

Quartz occurs as fine-grained groundmass mineral. Plagioclase occurs either as a fine-grained quartz-plagioclase groundmass or as phenocrysts. Zoning occurs in the phenocrysts of plagioclase. Biotie aggregates are round shaped and consist of small (0.1 to 0.5 mm) crystals. Myrmekite occurs as intergrowth of quartz in plagioclase (NLG12R) (Fig. 5b).

Xenomorphic granular texture

This texture was found in the rocks at a contact between greenstone and the pluton in the eastern margin of the pluton. Plagioclase here is inequigranular, and myrmekite occurs as intergrowth of quartz in plagioclase/K-feldspar in fine-grained trondhjemite (NLG29R) (Fig. 5e). Hornblende in medium-grained granodiorite (NLG30R) forms round shaped subhedral crystals that are larger than the crystals of the other minerals (Fig. 5f).

Granitic texture

Plagioclase, hornblende and biotite form euhedral to subhedral crystals. Hornblend forms diamond shaped crystals. Normal zoning occurs in plagioclase (NLG11R) (Fig. 5a).

Hypidiomorphic-granular texture

Very coarse phenocrysts of plagioclase are commonly found in the Nelshoogte TTGs. In Figure 5(d) (NLG35R, tonalite), saussuritized plagioclases with rim overgrowths (sieve texture?) are weakly cumulated with minor interstitial quartz representing glomeroporphyritic aggregate. Some hornblendes are found in the core of plagioclase crystals. Also synneusis of plagioclase crystals occurs.

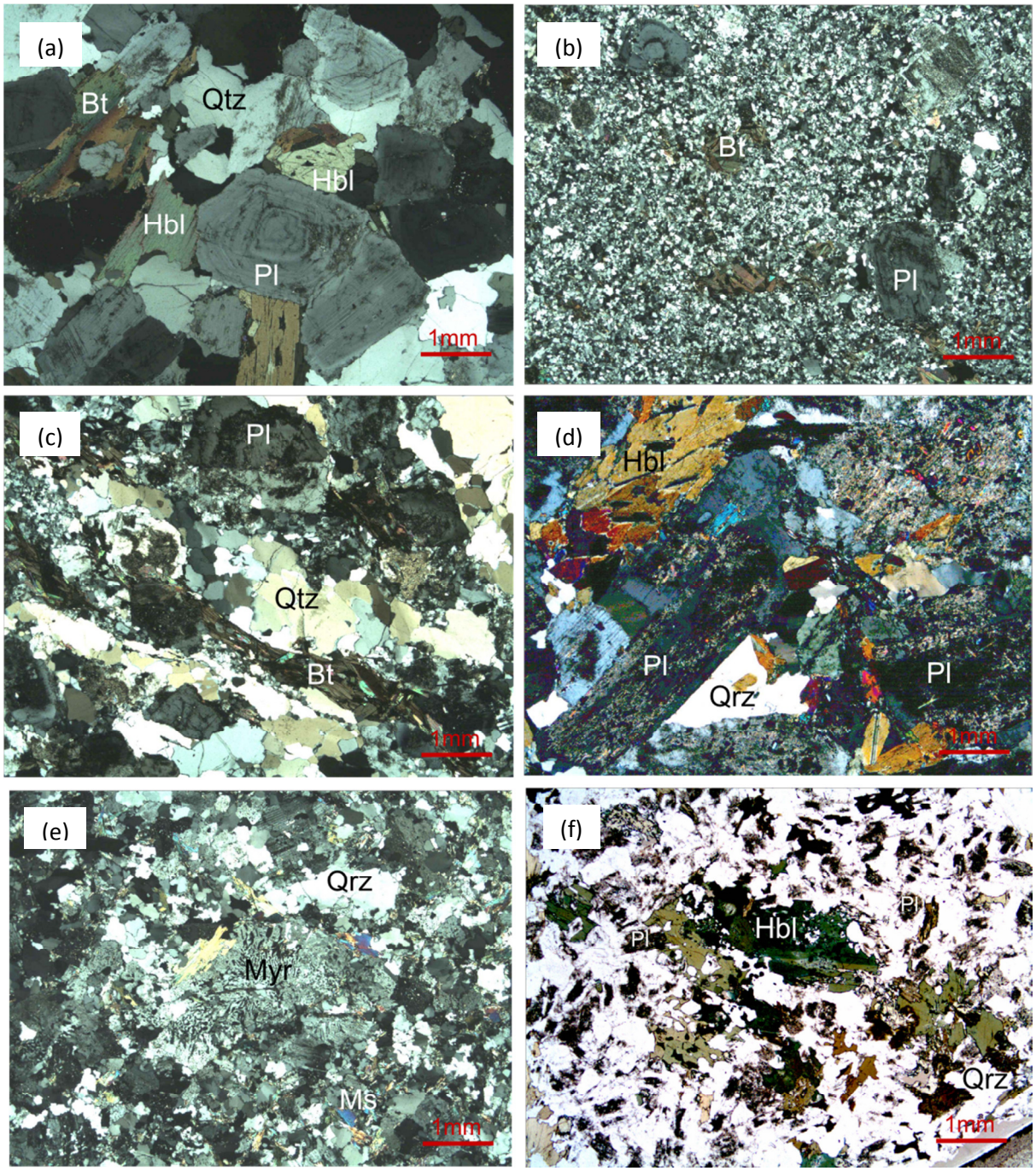

Fig. 5. Photomicrographs of Nelshoogte TTGs. (a) Undeformed coarse-grained tonalite (NLG11R) (cross polarized). Normal zoning is found in plagioclase. (b) Porphyritic trondhjemite (NLG12R) (cross polarized). (c) Foliated coarse-grained trondhjemite (NLG34R) (cross polarized). (d) Hypidiomorphic-granular coarse-grained tonalite (NLG35R) (cross polarized). (e) Xenomorphic-granular fine-grained trondhjemite (aplite) (NLG29R) (cross polarized). (f) Xenomorphic-granular medium-grained granodiorite (NLG30R) (plane

light); Pl, plagioclase; Qtz, quartz; Bt, biotite; Hbl, hornblende; Ms, muscovite; Myr, myrmekite

5.3. Mineral inclusions in zircon

Many mineral inclusions have been identified within zircon crystals from zircon separates from trondhjemites and tonalites (NLG1R, NLG8R, NLG11R, NLG12R, NLG21R, NLG35R and NLG41R). The mineral inclusion assemblages are shown in Table 3. They are mainly apatite (50%), feldspar (10%), epidote (10%), chlorite (5%), quartz (5%), biotite (5%), titanite (5%), magnetite (<5%) and rutile (<5%).

Table 3. Mineral inclusions in zircons.

sample	Pl(Ab)	Pl(An)	Pl(Ab-An)	Kfs	Bt	Qtz	Ep	Chl	Ap	Tit	Ilm	Mag	Rt	Sulphide
NLG1R	▲				▲	▲	▲	▲	▲	▲	▲			▲
NLG8R	▲			▲	▲	▲	▲	▲	▲	▲	▲	▲		
NLG12R			▲		▲		▲		▲					
NLG11R			▲		▲				▲	▲				
NLG35R	▲	▲	▲	▲	▲	▲	▲	▲	▲	▲			▲	
NLG41R			▲	▲	▲	▲	▲	▲	▲	▲				

Ab = albite, An = anorthite, Ap = apatite, Bt = biotite, Chl = chlorite, Ep = epidote, Ilm = ilmenite, Kfs = K-feldspar, Mag = magnetite, Ms = muscovite, Pl = plagioclase, Qtz = quartz, Rt = rutile, Tit = titanite, Zr = zircon

5.4. Mineral chemistry

Plagioclase

Table 4 shows the major-element compositions of plagioclase. In trondhjemites, they vary from An_9 to An_{21} with rim compositions of An_2 to An_{19} They are mainly oligoclase. In tonalites/granodiorites, they vary from An_{15} to An_{33} with rim compositions of An_{17} to An_{27}. They are also mainly oligoclase, but more calcic than oligoclase in trondhjemite. The plagioclase core compositions of coarse-grained TTGs are more calcic than rim composition. The maximum core to rim compositional range observed is 14 mol% An. Plagioclase

zonation (An_{4-24}) is simply a reflection plagioclase phase relations and the slow rate of diffusion within feldspar crystals in cooling.

Hornblende

Hornblendes in the Nelshoogte and the Kaap Valley tonalites/granodiorites are calcic amphiboles (Table 4). They are mainly magnesio-hornblende. Hornblendes in sample 19/6-11C (M-gd tonalite) are ferro-tschermakite (or ferroan-pargasite). Mg# is negatively correlated with Al (Fig. 6). Pargasitic amphibole is more typical of andesitic, basaltic andesitic and basaltic magmas than to dacitic magmas (Eichelberger, 1978; Ewart, 1982).

Biotite

The compositions of biotites in the Nelshoogte TTG and the Kaap Valley tonalite/granodiorite are shown in Table 4. Some of those crystals are altered and replaced by chlorite, epidote or sphene within layers. Biotites in the Kaap Valley tonalite/granodiorite contain more Ti than biotites in the Nelshoogte TTG. Biotites in the Nelshoogte trondhjemite contain less Ti. There is no difference for Mg#. Al in biotites in the Kaap Valley tonalite/granodiorite is less than others (Fig. 7).

Table 4. Mineral compositions.

Plagioclase

Sample	NLG2R		NLG11R		NLG12R			NLG21R	
	core	rim	core	rim	core	rim	groundmass	core	rim
SiO_2	63.90	64.42	62.89	64.15	62.90	62.67	65.76	65.90	66.71
Al_2O_3	21.70	21.31	22.57	21.91	23.42	23.53	22.01	20.36	19.97
TiO_2	0.00	0.02	0.03	0.02				0.03	0.02
FeO^T	0.05	0.03	0.10	0.10				0.06	0.04
CaO	3.95	3.47	5.02	4.21	4.76	4.95	2.93	2.11	1.73
Na_2O	9.09	9.29	8.35	8.78	9.57	9.43	10.83	10.31	10.70
K_2O	0.09	0.12	0.19	0.24	0.17	0.18	0.10	0.29	0.11
BaO	0.05	0.03	0.03	0.06				0.03	0.08
total	98.84	98.67	99.17	99.48	100.89	100.76	101.62	99.09	99.36
Si	2.86	2.88	2.81	2.85	2.76	2.75	2.85	2.92	2.95

Al	1.14	1.12	1.19	1.15	1.21	1.22	1.12	1.06	1.04
Ti	0.00	0.00	0.00	0.00				0.00	0.00
Fe	0.00	0.00	0.00	0.00				0.00	0.00
Ca	0.19	0.17	0.24	0.20	0.22	0.23	0.14	0.10	0.08
Na	0.79	0.80	0.72	0.76	0.81	0.80	0.91	0.89	0.92
K	0.01	0.01	0.01	0.01	0.01	0.01	0.01	0.02	0.01
Ba	0.00	0.00	0.00	0.00				0.00	0.00
total	4.98	4.98	4.98	4.98	5.02	5.02	5.02	5.00	5.00
An	19.40	17.13	24.92	20.94	21.59	22.52	13.00	10.17	8.21

Sample	NLG29R	NLG30R	NLG35R		NLG41R		19/6-11C	27/10-1(Kaap Valley)	
			core	rim	core	rim		core	rim
SiO_2	68.63	63.17	63.29	63.50	62.77	63.46	61.22	63.55	62.74
Al_2O_3	20.11	22.65	23.15	22.66	22.48	22.10	23.80	23.24	23.31
TiO2		0.02	0.02	0.01					
FeO^T		0.07						0.05	0.06
CaO	0.73	4.98	5.26	4.83	4.07	3.60	5.61	4.56	4.79
Na_2O	11.26	8.61	8.45	8.73	9.81	10.19	8.79	9.69	9.64
K_2O	0.11	0.11	0.08	0.06	0.15	0.12	0.19	0.30	0.18
BaO		0.05							
total	100.85	99.71	100.25	99.79	99.28	99.47	99.61	101.38	100.72
Si	2.98	2.81	2.80	2.82	2.79	2.81	2.73	2.78	2.76
Al	1.03	1.19	1.21	1.18	1.18	1.16	1.25	1.20	1.21
Ti		0.00	0.00	0.00					
Fe		0.00	0.00	0.00				0.00	0.00
Ca	0.04	0.24	0.25	0.23	0.19	0.17	0.27	0.21	0.23
Na	0.93	0.74	0.72	0.75	0.85	0.87	0.76	0.82	0.82
K	0.01	0.01	0.00	0.00	0.01	0.01	0.01	0.02	0.01
Ba		0.00	0.00	0.00					
total	4.99	4.98	4.98	4.98	5.02	5.02	5.02	5.02	5.03
An	3.86	24.24	25.58	23.44	18.66	16.73	26.09	20.66	21.57

K-feldspar

Sample	13/6-05	16/6-06A	16/6-06-B	16/6-06C	19/6-06C
SiO_2	65.46	64.85	66.39	66.58	64.85
Al_2O_3	17.73	18.11	17.88	17.94	18.11
TiO2	0.04	0.02		0.02	0.02
FeO^T	0.02	0.08		0.04	0.10

MnO	0.04	0.10		0.04	0.10
CaO	0.10	0.06		0.05	0.06
Na_2O	0.69	0.59	0.63	0.64	0.59
K_2O	15.52	15.11	15.75	15.89	15.11
BaO	0.17	2.05		0.36	2.05
total	99.75	100.89	100.66	101.52	100.89
Si	3.03	3.00	3.04	3.03	3.03
Al	0.97	0.99	0.97	0.96	0.98
Ti	<0.01	<0.01		<0.01	<0.01
Fe	<0.01	<0.01	<0.01	<0.01	0.01
Mn	<0.01	<0.01		<0.01	<0.01
Ca	0.01	<0.01		<0.01	0.01
Na	0.06	0.05	0.06	0.06	0.04
K	0.92	0.89	0.92	0.92	0.91
Ba	0.00	0.04		0.01	<0.01
total	4.99	4.99	4.98	4.99	4.98

Hornblende

Sample	NLG11R magnesio-hornblende	NLG30R magnesio-hornblende	NLG35R magnesio-hornblende	19/6-11C ferro-tschermakite -ferroan pargasite	27.10-01 (Kaap Valley) magnesio-hornblende
SiO_2	46.20	45.59	46.72	42.11	47.62
Al_2O_3	7.51	8.43	8.71	11.45	6.43
TiO_2	0.72	1.56	0.78	0.96	1.12
FeO^T	16.66	17.73	13.69	21.03	15.66
MnO	0.31	0.71	0.16	0.38	0.54
MgO	11.75	10.93	12.90	8.46	12.95
CaO	11.69	11.39	12.03	11.06	11.15
Na_2O	1.23	1.39	1.16	1.58	1.39
K_2O	0.54	0.69	0.48	1.04	0.50
Total	96.60	98.40	96.63	98.08	97.35
Si	6.88	6.70	6.87	6.30	6.96
Al	1.28	1.46	1.51	2.02	1.11
Ti	0.08	0.17	0.09	0.11	0.12
Fe	2.15	2.18	1.68	2.63	1.92
Mn	0.04	0.09	0.02	0.05	0.07
Mg	2.57	2.39	2.83	1.89	2.82
Ca	2.00	1.86	1.96	1.84	1.82
Na	0.35	0.41	0.34	0.48	0.41
K	0.11	0.13	0.09	0.21	0.10

total	15.45	15.41	15.39	15.52	15.32
Ca+Na+K	2.45	2.41	2.39	2.52	2.32
Fe+Mn+Mg	4.76	4.66	4.53	4.57	4.80

Biotite

Sample	NLG11R	NLG12R	NLG30R	27/10-01 (Kaap Valley)
Rock type	tonalite	trondhjemite	granodiorite	tonalite/granodiorite
SiO_2	36.72	37.88	37.02	36.57
Al_2O_3	15.15	15.90	16.01	14.31
TiO_2	2.74	2.44	2.73	3.34
FeO	19.15	17.66	19.57	19.36
MnO	0.19	0.29	0.45	0.30
MgO	11.05	10.74	10.91	11.63
CaO	0.22		0.07	0.13
Na_2O			0.11	0.06
K_2O	9.31	9.08	9.01	9.07
Ba			0.16	
Total	94.53	94.01	96.05	94.77
Si	2.88	2.96	2.85	2.85
Ti	0.16	0.14	0.16	0.20
Al	1.40	1.47	1.45	1.32
Fe^{+2}	1.26	1.16	1.26	1.26
Mn	0.01	0.02	0.03	0.02
Mg	1.29	1.25	1.25	1.35
Ca	0.02		0.01	0.01
Na			0.02	0.01
K	0.93	0.91	0.88	0.90
Ba			0.01	
total	7.95	7.91	7.92	7.92
Mg#	50.70	52.02	49.84	51.71

*$FeO^T = FeO + Fe_2O_3$

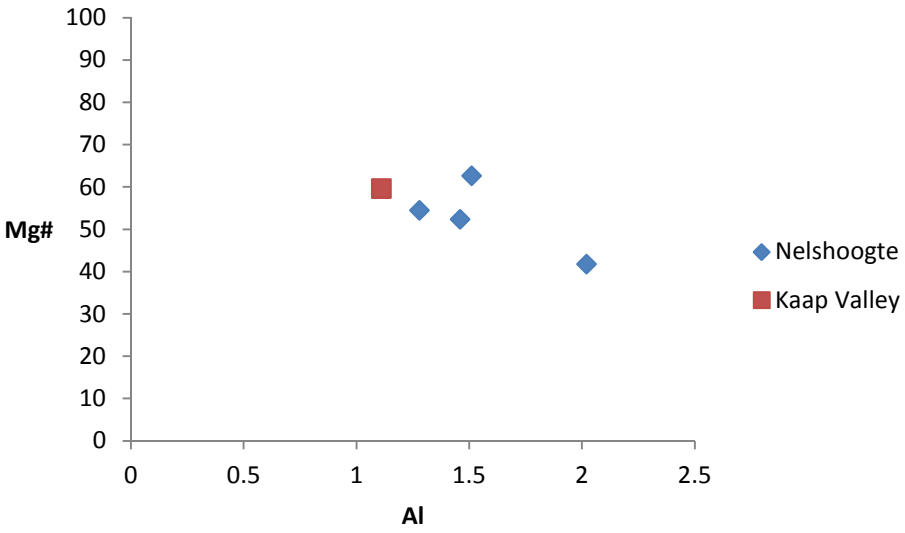

Fig. 6. Mg# vs. Al in hornblende form the Nelshoogte and thr Kaap valley tonalites/granodiorites.

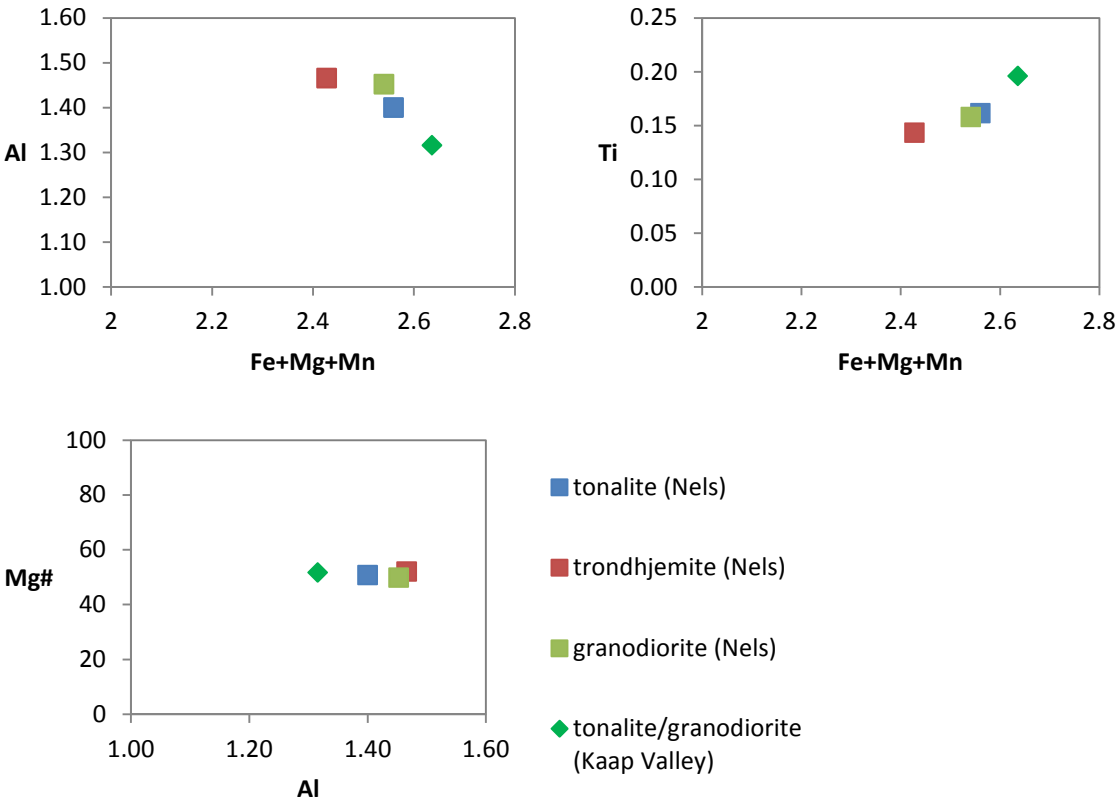

Fig. 7. Al vs. maficity (upper left), Ti vs. maficity (upper right) and Mg# vs. Al (bottom) in biotites in the Nelshoogte TTG and the Kaap Valley TTG.

Chapter 6

Geochemistry

The chemical compositions of the Nelshoogte TTGs are given and are compared with previous data (Yearron, 2003, Moyen, 2011) for other plutons in the BGGT. Chemical variation diagrams, particularly Harker diagrams involving major and trace elements, are useful in detecting inter-relationships between elements and minerals within a pluton or suite. Trends are typically attributed to the evolution of the magma batch through processes such as assimilation of wall rock, mixing (or unmixing), partial melting, crystal fractionation or peritectic assemblage entrainment. However, since it is possible to produce similar trends by both partial melting and crystal fractionation it is perhaps better to consider these diagrams as representing crystal-liquid equilibra (Rollinson, 1993).

6.1. Major elements

Table 5 shows the data of whole-rock major-element compositions of the Nelshoogte TTGs. The classification into rock types and the variations of Al_2O_3, MgO, FeO^T, TiO_2, CaO, K_2O, Na_2O, K_2O/Na_2O, A/CNK and Mg# with SiO_2 (Harker diagrams) are shown (Figs. 8 and 9). The variations of the Nelshoogte TTGs including Yearron (2003)'s and Moyen (2011)'s data are shown in Figures 9a and 9b, and the variations of other TTGs in the BGGT for the ~3500 Ma pluton (Steynsdorp), ~ 3450 Ma plutons (Stolzburg, Theespruit Honingklip, Weergevonden, Theeboom and Doornhoek plutons), ~ 3200 Ma plutons (Badplaas, Rooihoogte and Kaap Valley plutons) by Yearron (2003) and Moyen (2011) are shown in Figure 9b. These Barberton TTGs show wide ranges of values on the diagrams. Al_2O_3, MgO, TiO_2, CaO, FeO^T and Mg# show negative correlations, and Na_2O has a flat distribution of points. The Nelshoogte and other ~ 3200 Ma TTGs show tight correlations for these major elements, however, ~ 3500 Ma and ~ 3450 Ma TTGs show rough correlations. For the Nelshoogte TTGs (Fig. 9a), tonalites show slightly different trends from those of the granodiorites, e.g. in Al_2O_3, TiO_2, K_2O, K_2O/Na_2O, FeO^T and A/CNK. For ~ 3200 Ma TTGs, the Badplaas-domain TTGs show different trends from the Kaap Valley TTGs in Al_2O_3, TiO2, FeO^T and A/CNK. The ranges of the Nelshoogte trondhjemites/granites overlap with the ranges of ~ 3200 Ma Badplaas domain TTGs and ~ 3450 Ma TTGs. The ranges of the

Nelshoogte tonalites/granodiorites overlap with the ranges of the Kaap Valley tonalites/granodiorites.

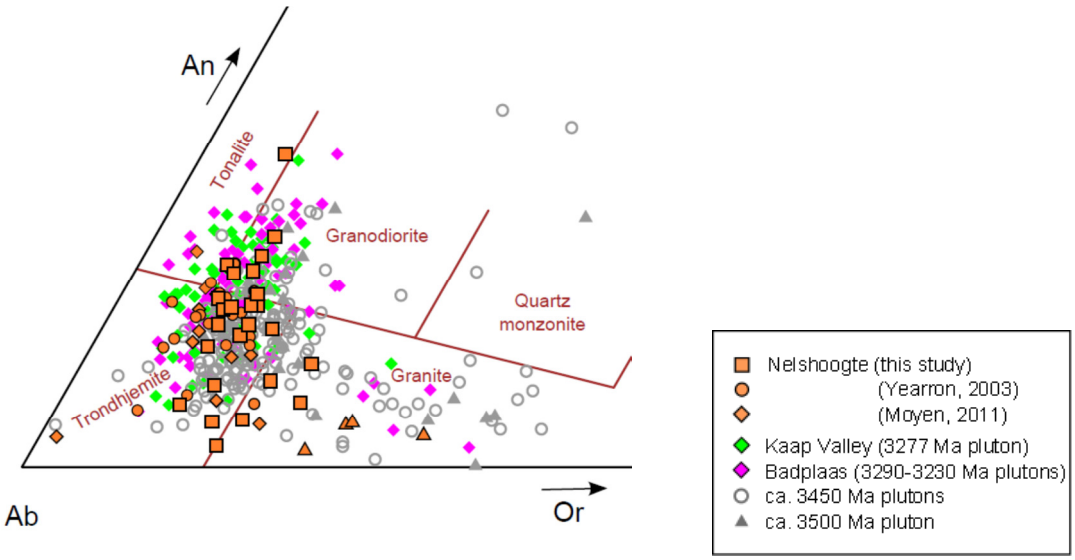

Fig. 8. Normative feldspar composition in An–Ab–Or classification diagram (O'Connor, 1965) to define the rock type for TTGs in the Nelshoogte pluton and other plutons in the BGGT (Yearron, 2003; Moyen, 2011).

Table 5. Whole-rock major- and trace-element compositions

	NLG1R	NLG4R	NLG7R	NLG8R	NLG9R	NLG10R	NLG11R	NLG12R	NLG13R	NLG14R	NLG16R	NLG17R	NLG18R	NLG19R	NLG20R
Rock type	C-gd trondhjemite	C-gd granodiorite	C-gd trondhjemite	C-gd trondhjemite	Potassic granite	M-gd trondhjemite	C-gd tonalite	F-gd trondhjemite	C-gd granodiorite	C-gd granodiorite	C-gd trondhjemite	Potassic granite	C-gd granodiorite	M-gd trondhjemite	M-gd trondhjemite
SiO_2	72.70	71.24	69.99	70.82	76.06	75.16	68.18	73.29	69.45	69.31	71.37	75.37	70.54	74.77	70.57
TiO_2	0.20	0.29	0.36	0.37	0.01	0.20	0.30	0.25	0.34	0.40	0.29	0.02	0.32	0.22	0.34
Al_2O_3	15.91	16.06	15.73	16.05	14.34	15.30	17.46	15.53	16.51	16.32	16.18	14.47	15.59	15.13	16.36
FeO^T	1.57	2.38	2.48	2.97	0.55	1.32	2.41	1.62	2.80	3.06	2.16	0.63	2.81	1.33	2.46
MgO	0.60	1.01	1.23	1.21	0.14	0.44	1.42	0.70	1.59	1.81	1.11	0.05	1.34	0.49	1.97
MnO	0.04	0.05	0.03	0.06	0.02	0.02	0.05	0.03	0.06	0.07	0.04	0.03	0.06	0.03	0.06
CaO	2.63	2.80	3.07	2.62	0.33	0.69	3.69	2.11	3.24	3.18	2.58	0.77	3.47	1.28	1.94
Na_2O	4.67	4.55	5.27	4.70	5.18	5.11	5.25	4.80	4.54	4.61	4.93	4.88	4.41	5.12	4.93
K_2O	1.62	1.52	1.74	1.09	3.28	1.73	1.13	1.59	1.35	1.11	1.24	3.73	1.35	1.57	1.26
P_2O_5	0.06	0.09	0.09	0.09	0.07	0.03	0.10	0.08	0.12	0.14	0.09	0.05	0.11	0.05	0.11
org. total	99.84	99.39	99.40	99.70	99.66	99.41	99.31	99.68	99.46	99.48	99.46	100.06	99.37	99.13	99.81
Trace elements(ppm)															
Sc	4.14	6.60	7.28	7.28	3.66	3.62	8.20	4.67	6.63	7.56	4.69	3.08	6.78	3.78	7.26
Ti	1280.00	1820.33	2108.07	2157.04	550.06	1222.44	1819.16	1549.50	2158.32	2572.66	1771.06	412.65	1977.68	1418.26	2145.17
V	21.93	40.37	49.48	55.83	6.72	14.44	39.20	24.56	50.79	54.86	35.29	8.27	48.38	16.32	46.68
Cr	17.26	22.76	52.56	17.29	5.33	7.61	52.96	18.90	29.50	29.97	29.24	7.43	32.79	7.87	41.03
Ni	9.73	18.74	33.57	16.84	6.49	6.36	26.97	15.21	23.97	22.74	22.59	5.27	24.25	6.80	26.76
Cu	10.89	15.99	14.21	16.18	3.07	20.61	15.64	12.04	8.69	20.49	18.50	8.82	15.29	11.18	15.59
Zn	37.54	39.44	37.02	53.51	21.06	36.36	35.35	49.87	50.85	52.41	38.41	21.86	47.85	36.78	55.76
Ga	18.86	18.79	22.64	20.15	19.56	20.80	19.81	20.21	20.10	18.35	19.86	20.52	18.16	19.50	19.41
Rb	38.27	43.46	66.10	30.28	120.13	63.32	41.75	48.12	34.74	30.57	27.21	98.75	36.35	47.26	53.92
Sr	481.23	488.91	489.22	451.75	138.31	229.98	655.89	407.52	513.79	548.03	535.84	162.72	461.38	305.25	412.70
Y	3.38	6.45	7.78	5.00	3.17	2.74	3.98	2.70	6.52	8.54	3.44	3.31	5.55	2.83	4.68
Zr	83.89	106.08	78.67	73.63	29.75	95.34	107.64	99.46	104.84	141.79	112.93	26.31	113.08	93.86	106.09
Nb	2.80	3.13	5.50	3.41	5.17	3.48	2.00	2.69	3.55	4.35	1.63	4.63	3.19	2.96	2.69
Mo	0.56	1.02	0.30	0.43	0.39	0.48	1.28	0.38	0.46	0.49	0.35	0.49	0.45	0.42	0.28
Cd	0.43	< 0.5	0.29	0.33	0.22	0.20	0.23	0.18	0.29	0.37	0.48	0.29	< 0.5	0.29	0.32
Sn	1.12	1.63	2.02	1.31	1.42	1.55	2.28	1.33	1.43	1.83	1.54	1.45	1.98	1.70	1.56
Cs	0.45	1.43	2.15	0.96	4.86	2.75	2.71	1.73	0.91	0.92	0.52	1.37	0.52	1.04	1.37
Ba	200.66	266.16	718.11	230.38	252.67	140.70	170.41	204.83	283.22	298.19	258.80	204.60	229.79	209.16	192.83
La	8.87	16.85	6.80	11.01	7.93	10.75	8.30	9.71	19.50	18.35	12.37	5.85	19.42	10.96	10.11
Ce	17.50	32.06	15.17	23.27	16.47	22.16	15.72	20.43	37.57	35.15	24.33	11.82	35.64	22.25	21.74
Pr	1.83	3.24	1.77	2.27	1.62	2.21	1.74	2.04	3.88	3.76	2.43	1.15	3.48	2.23	2.37
Nd	7.20	11.47	6.88	8.64	5.73	7.43	6.90	7.16	14.46	14.85	8.96	4.11	12.60	7.82	9.95
Sm	1.44	2.24	1.73	1.66	1.33	1.29	1.58	1.56	2.37	2.52	1.69	0.99	2.08	1.31	2.26
Eu	0.42	0.64	0.43	0.59	0.31	0.39	0.64	0.47	0.80	0.92	0.62	0.25	0.55	0.49	0.59
Gd	0.63	1.61	1.60	1.37	0.91	1.01	1.17	1.11	1.92	2.21	1.10	0.66	1.46	1.03	1.53
Tb	0.16	0.26	0.24	0.16	0.12	0.14	0.17	0.12	0.21	0.27	0.14	0.12	0.18	0.11	0.21
Dy	0.69	1.28	1.27	0.98	0.66	0.57	0.76	0.53	1.27	1.82	0.75	0.52	1.07	0.54	1.12
Ho	0.13	0.23	0.24	0.19	0.12	0.14	0.16	0.10	0.24	0.27	0.14	0.10	0.20	0.11	0.21
Er	0.38	0.65	0.69	0.44	0.33	0.28	0.40	0.29	0.63	0.78	0.30	0.27	0.55	0.24	0.45
Tm	0.05	0.09	0.10	0.07	0.03	0.08	0.05	0.04	0.10	0.14	0.05	0.04	0.07	0.03	0.09
Yb	0.40	0.60	0.70	0.45	0.23	0.28	0.39	0.27	0.54	0.77	0.24	0.29	0.46	0.25	0.44
Lu	0.05	0.07	0.12	0.07	0.05	0.05	0.07	0.04	0.09	0.13	0.06	0.03	0.10	0.03	0.06
Hf	2.53	2.66	2.03	1.96	1.33	2.37	2.42	2.36	2.40	3.40	2.41	1.46	2.78	2.43	2.31
Ta	0.28	0.29	0.35	0.16	0.56	0.38	0.14	0.23	0.30	0.35	0.15	0.58	0.25	0.24	0.25
Pb	6.25	5.66	5.28	6.15	5.48	5.76	5.14	6.10	5.32	4.55	5.26	9.04	5.73	6.10	2.96
Th	2.76	2.88	3.99	1.15	1.99	3.79	1.32	2.07	2.54	2.62	1.38	1.48	3.09	2.35	1.88
U	0.44	0.57	1.24	0.41	0.95	1.17	0.53	0.66	0.47	0.82	0.31	1.41	0.48	0.62	0.32

Table 5 (continued)

Rock type	NLG21R C-gd trondhjemite	NLG22R Potassic granite	NLG24R M-gd granite	NLG26R C-gd granite	NLG29R F-gd trondhjemite	NLG30R M-gd granodiorite	NLG31R C-gd trondhjemite	NLG32R Potassic granite	NLG34R C-gd granite	NLG35R C-gd tonalite	NLG36R M-gd granite	NLG38R M-gd trondhjemite	NLG40R M-gd trondhjemite	NLG41R M-gd trondhjemite	NLG42R C-gd trondhjemite
SiO_2	78.33	76.38	73.48	73.28	77.99	66.81	72.17	73.78	74.25	61.89	73.66	74.68	74.93	74.85	72.36
TiO_2	0.08	0.01	0.20	0.22	0.07	0.51	0.18	0.01	0.19	0.37	0.20	0.12	0.13	0.10	0.21
Al_2O_3	13.68	14.35	16.15	15.84	14.35	16.49	16.59	15.70	15.08	18.83	14.99	15.23	15.22	15.17	16.43
FeO^T	0.40	0.50	1.34	1.53	0.76	3.90	1.40	0.52	1.38	3.60	1.52	1.07	1.20	0.96	1.64
MgO	0.04	0.05	0.38	0.81	0.10	2.08	0.43	0.01	0.57	3.39	0.17	0.41	0.28	0.15	0.61
MnO	0.01	0.02	0.03	0.03	0.01	0.06	0.04	0.01	0.03	0.06	0.05	0.04	0.03	0.02	0.05
CaO	0.88	0.77	1.39	0.82	0.29	4.08	2.40	0.57	1.61	6.17	4.39	1.04	2.16	2.19	2.56
Na_2O	5.29	4.39	4.78	5.23	4.67	4.42	5.01	4.42	4.31	4.37	4.33	4.66	4.78	4.59	4.74
K_2O	1.30	3.47	2.20	2.17	1.73	1.43	1.73	4.95	2.54	1.09	0.63	2.71	1.24	1.93	1.32
P_2O_5	0.00	0.06	0.05	0.07	0.02	0.21	0.05	0.04	0.05	0.22	0.05	0.03	0.02	0.03	0.09
org. total	99.37	99.57	99.76	100.10	99.44	99.39	99.34	99.54	99.61	99.84	99.11	99.12	99.41	99.35	99.44
Trace elements(ppm)															
Sc	3.61	2.76	3.16	4.10	3.06	9.43	3.90	2.84	4.21	13.80	3.07	3.22	2.97	3.21	3.74
Ti	387.96	350.96	934.91	1101.46	458.10	2555.46	920.42	319.85	1011.15	2017.33	1144.23	705.49	832.65	642.47	1203.78
V	5.00	5.61	12.33	19.22	8.05	67.91	17.43	6.98	16.48	82.18	17.54	10.36	11.22	10.07	18.51
Cr	24.23	6.87	5.83	7.83	5.66	51.78	10.61	6.35	10.83	54.19	6.64	9.57	4.99	6.17	8.12
Ni	5.68	3.35	7.77	9.46	7.22	38.72	9.07	6.47	10.24	39.36	6.59	8.38	6.40	6.31	7.00
Cu	< 7	3.16	18.11	8.66	16.76	28.79	6.07	< 5	7.75	45.34	5.46	5.92	7.84	5.90	11.28
Zn	16.43	25.10	39.15	37.37	16.42	55.82	43.95	20.67	38.72	47.25	36.69	28.25	27.75	29.56	49.55
Ga	17.93	18.67	19.01	21.69	21.02	18.75	20.23	23.39	20.07	17.83	18.78	18.68	17.31	18.47	19.64
Rb	32.62	79.45	68.67	70.11	54.90	42.47	54.58	122.24	55.94	26.27	18.24	74.24	33.34	32.52	45.27
Sr	194.37	163.92	349.47	310.00	106.68	546.22	410.96	56.54	333.55	922.93	520.96	318.72	352.68	341.28	449.07
Y	2.73	2.08	1.85	3.17	4.69	9.14	2.46	14.26	3.14	5.73	3.16	3.19	2.53	1.27	5.45
Zr	42.62	29.91	85.46	94.01	46.16	113.74	67.48	51.02	75.84	57.18	76.52	56.26	58.47	50.56	85.18
Nb	2.00	2.22	2.08	2.57	6.76	4.65	2.45	25.51	3.53	1.45	2.20	3.23	2.86	2.03	3.34
Mo	0.56	0.50	0.47	0.50	0.41	0.43	0.21	0.33	0.39	0.67	0.44	0.47	0.74	0.47	0.32
Cd	< 0.5	0.18	0.25	0.59	0.23	0.56	0.29	0.35	< 0.5	< 0.5	0.20	< 0.5	< 0.5	0.11	< 0.5
Sn	1.55	0.71	1.63	1.95	2.22	2.03	1.73	1.06	1.52	1.52	1.15	1.40	1.20	1.14	1.26
Cs	1.18	1.86	1.33	2.16	1.00	2.26	2.67	2.45	1.18	0.98	0.38	1.58	1.94	0.92	2.07
Ba	184.06	246.03	284.13	246.79	456.66	323.88	195.08	77.38	223.31	142.66	87.28	331.86	108.37	443.15	151.06
La	12.31	5.18	9.01	7.89	12.40	17.80	6.58	1.48	6.06	6.65	7.96	8.26	6.77	6.70	7.86
Ce	24.53	11.34	18.10	16.87	24.49	34.08	14.33	7.65	12.42	14.70	14.92	17.83	15.58	13.46	15.99
Pr	2.76	1.11	1.66	1.77	2.60	4.15	1.41	0.56	1.27	2.00	1.58	1.75	1.49	1.33	1.64
Nd	10.12	4.19	6.01	6.61	8.73	16.94	4.94	2.77	5.09	9.70	6.11	8.69	5.33	4.91	6.11
Sm	1.70	0.96	1.09	1.16	1.61	3.40	0.87	1.37	1.19	2.47	1.16	1.10	1.01	0.86	1.32
Eu	0.68	0.33	0.41	0.44	0.36	1.00	0.37	0.21	0.38	0.86	0.38	0.32	0.34	0.41	0.41
Gd	1.40	0.64	0.66	1.11	1.07	2.50	0.67	1.59	0.95	2.06	0.68	0.89	0.64	0.49	0.93
Tb	0.10	0.08	0.07	0.13	0.16	0.32	0.08	0.38	0.13	0.23	0.15	0.10	0.10	0.06	0.14
Dy	0.62	0.50	0.40	0.56	0.86	1.86	0.45	2.58	0.58	1.28	0.63	0.56	0.56	0.35	0.96
Ho	0.07	0.07	0.06	0.10	0.15	0.33	0.11	0.55	0.11	0.22	0.12	0.11	0.12	0.05	0.17
Er	0.23	0.16	0.24	0.30	0.39	0.84	0.25	1.57	0.30	0.61	0.28	0.32	0.23	0.08	0.49
Tm	0.04	0.03	0.04	0.05	0.05	0.13	0.03	0.28	0.04	0.07	0.07	0.05	0.04	0.02	0.08
Yb	0.22	0.11	0.25	0.30	0.38	0.68	0.25	2.01	0.27	0.47	0.33	0.29	0.28	0.10	0.51
Lu	0.03	0.02	0.04	0.03	0.06	0.13	0.04	0.26	0.05	0.07	0.09	0.05	0.04	0.01	0.09
Hf	1.55	1.02	1.90	2.20	1.76	2.79	1.75	2.72	2.20	1.63	2.08	1.71	1.82	1.32	1.98
Ta	0.26	0.23	0.17	0.26	0.48	0.28	0.20	5.74	0.26	0.13	0.27	0.28	0.33	0.10	0.40
Pb	6.25	8.03	7.26	3.08	6.24	5.44	8.12	17.25	7.59	3.45	11.99	7.26	6.08	6.36	6.34
Th	4.39	1.65	2.13	1.44	3.86	2.18	1.39	7.55	2.80	0.74	2.16	2.08	1.72	0.91	1.39
U	0.67	0.77	0.54	0.69	1.35	0.40	0.37	6.96	0.49	0.26	0.62	0.68	0.56	0.22	0.76

(a)

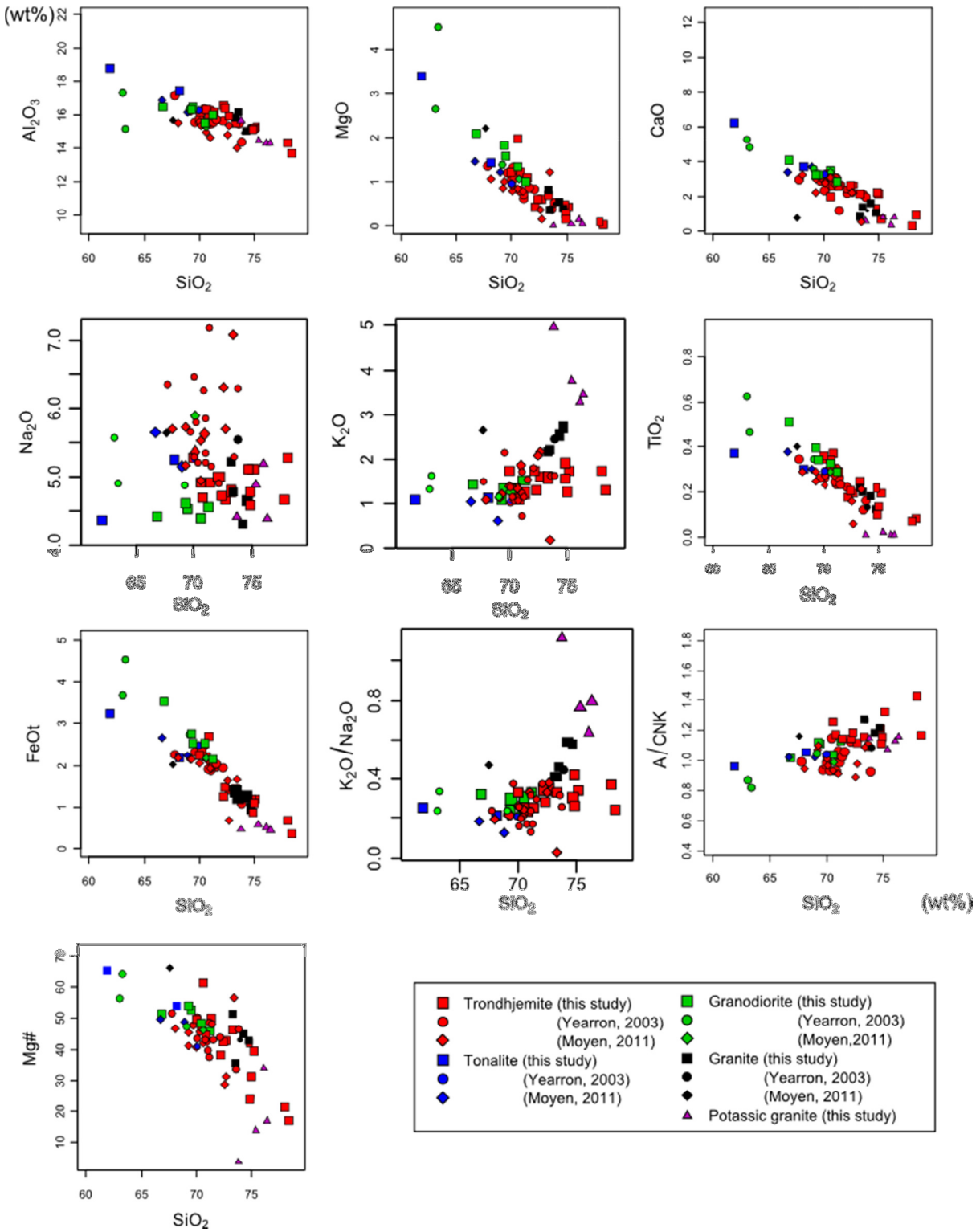

(b)

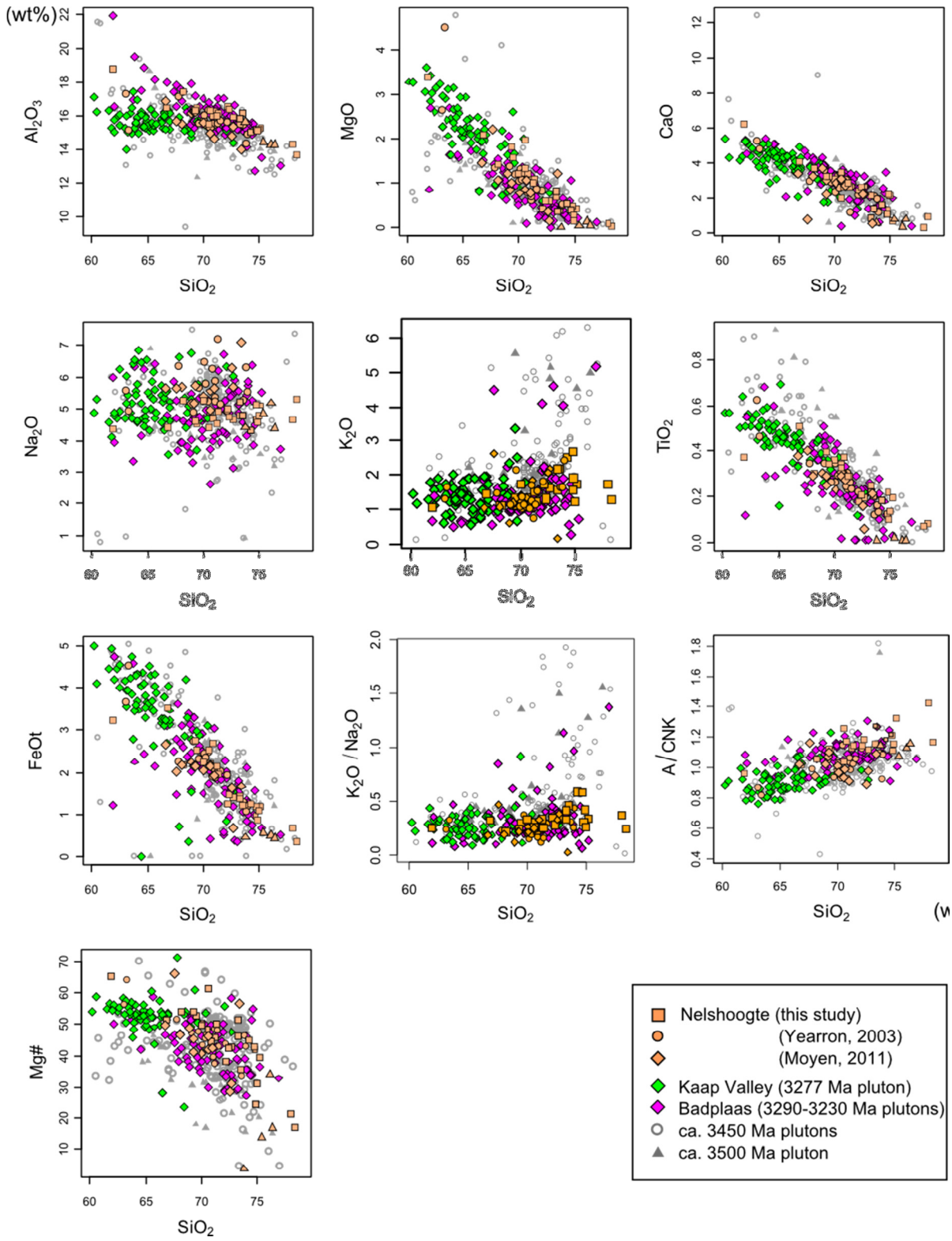

Fig. 9. Major elements compositions against SiO_2. (a) the Nelshoogte TTGs (b) ~ 3200 Ma TTGs and older (~ 3450 Ma and ~ 3500 Ma) TTGs (Yearron, 2003; Moyen 2011).

6.2. Trace elements

The whole-rock trace-element variations of the Nelshoogte TTGs are displayed in Table 5. These data, together with those of with Yearron (2003) and Moyen (2011) are plotted against SiO_2 (Fig. 10a and 10b). The variations of TTGs in the BGGT for the ~ 3500 Ma pluton (Steynsdorp), ~ 3450 Ma plutons (Stolzburg, Theespruit Honingklip, Weergevonden, Theeboom and Doornhoek plutons) and ~ 3200 Ma plutons (Badplaas, Rooihoogte and Kaap Valley plutons) by Yearron, (2003) and Moyen (2011) are also shown in Figure 10b. For the Nelshoogte TTGs, they show tight negative correlations with Cr, Ni, Sr, Zr, HREE and P_2O_5, weak negative correlations with LREE and positive correlation with Rb. The tonalites show different trends from the trend of the granodiorites in Ba, Y, Zr and LREE. The trondhjemites/granites show wide ranges in Rb and Ba. The granodiorites are enriched in Ba, Y, Nb, P_2O_5 and REEs. For ~ 3200 Ma TTGs, they show tight negative correlations with HREE and P_2O_5, weak negative correlations with Cr, Ni, Sr, Zr, and Ba. The Badplaas domain TTGs show different trends from the Kaap Valley TTGs, in Cr, Ni, Sr, Y, Zr, La, Nb and P_2O_5. The ranges of the Badplaas domain TTGs overlap with the ranges of the Nelshoogte trondhjemites/tonalites, and the ranges of the Kaap Valley tonalities/granodiorites overlap with the ranges of the Nelshoogte granodiorites. The variations for ~ 3500 Ma and ~ 3450 Ma TTGs are more scattered. They show wide ranges in Sr, Zr, Nb, Rb, Ba and REEs.

(a)

(ppm)

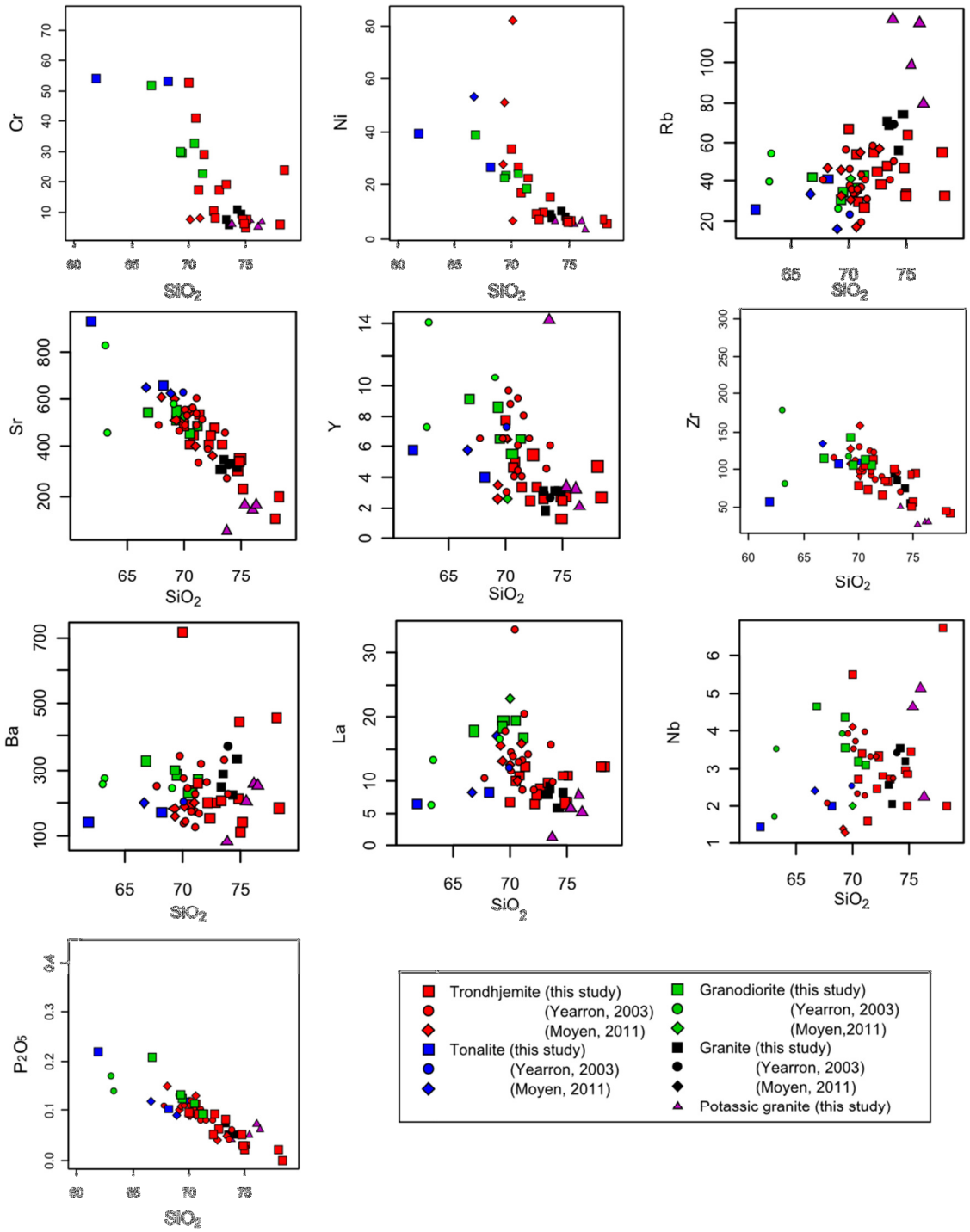

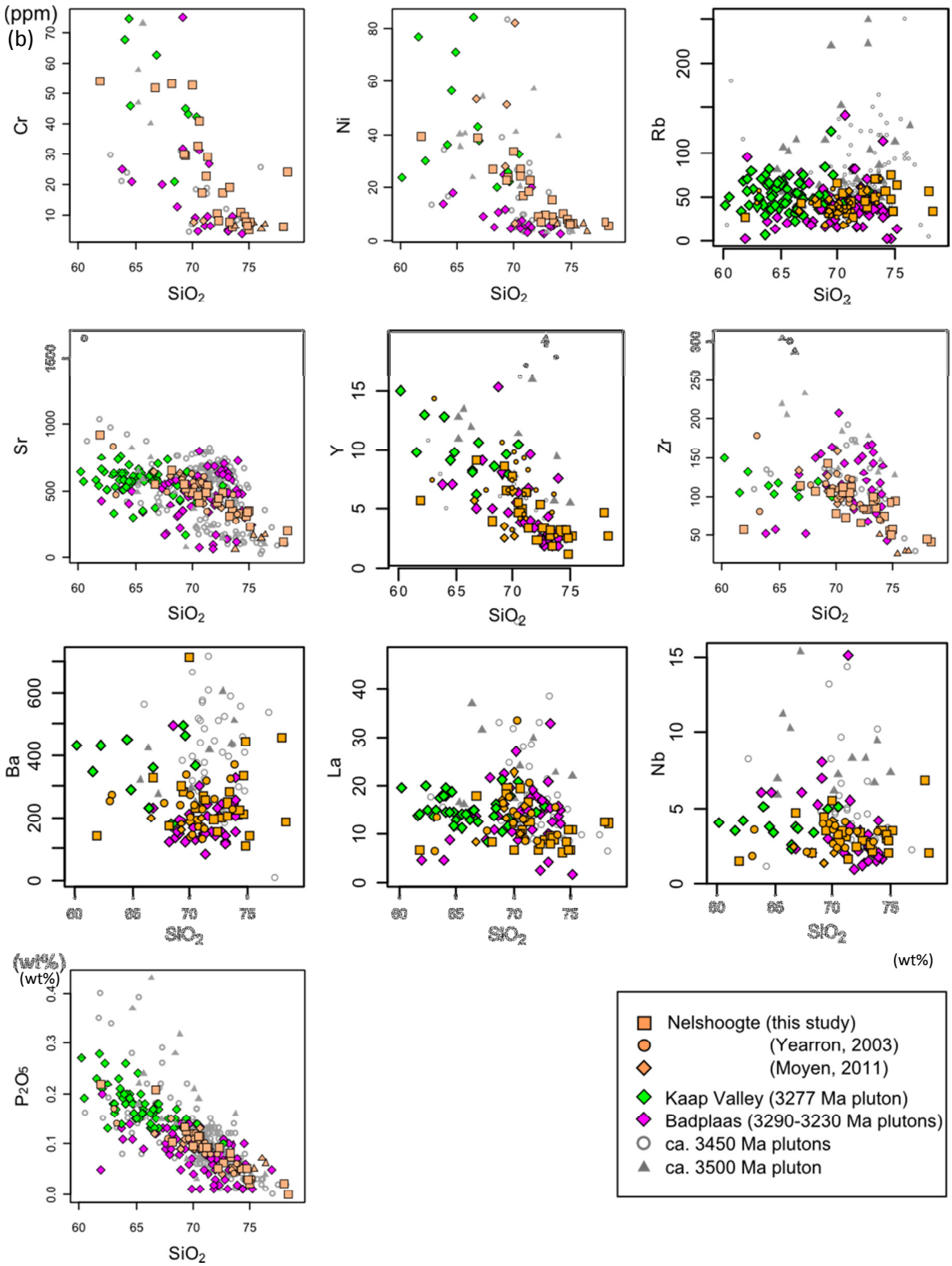

Fig. 10. Trace elements compositions against SiO_2. (a) Nelshoogte TTGs (b) ~ 3200 Ma TTGs and ~ 3500 Ma and ~ 3450 Ma TTGs in the BGGT (Yearron, 2003; Moyen, 2011).

6.3. Multi-element (spider) diagrams

In Figure 11, the spider diagrams display trace-element values of TTGs in ~3500 Ma pluton, ~ 3450 Ma plutons, ~ 3200 Ma plutons and the Nelshoogte pluton, normalised to MORB (Pearce, 1983). These plots of TTGs in the BGGT show clearly enriched LILE (Rb, K, Ba and Th), positive Ce anomaly and depletions in Ta, Nb, P, Ti and Y. The patterns of the Nelshoogte trondhjemites/granites and granodiorites are similar in LILE contents, but the granodiorites are more enriched in Ce and HFSEs. The Nelshoogte TTGs show similar patterns to ~ 3200 Ma plutons and ~ 3500 Ma and ~ 3450 Ma plutons in the BGGT. The patterns of the ~ 3500 Ma TTGs show slightly enriched HFSE compared with ~ 3450 Ma TTGs. Among ~ 3200 Ma plutons, the patterns of the Kaap Valley TTGs shows more enriched HFSE patterns. The patterns of the Kaap Valley TTGs overlap with the Nelshoogte granodiorites. The patterns of the Badplaas domain TTGs overlap with the patterns of the Nelshoogte trondhjemites/granites.

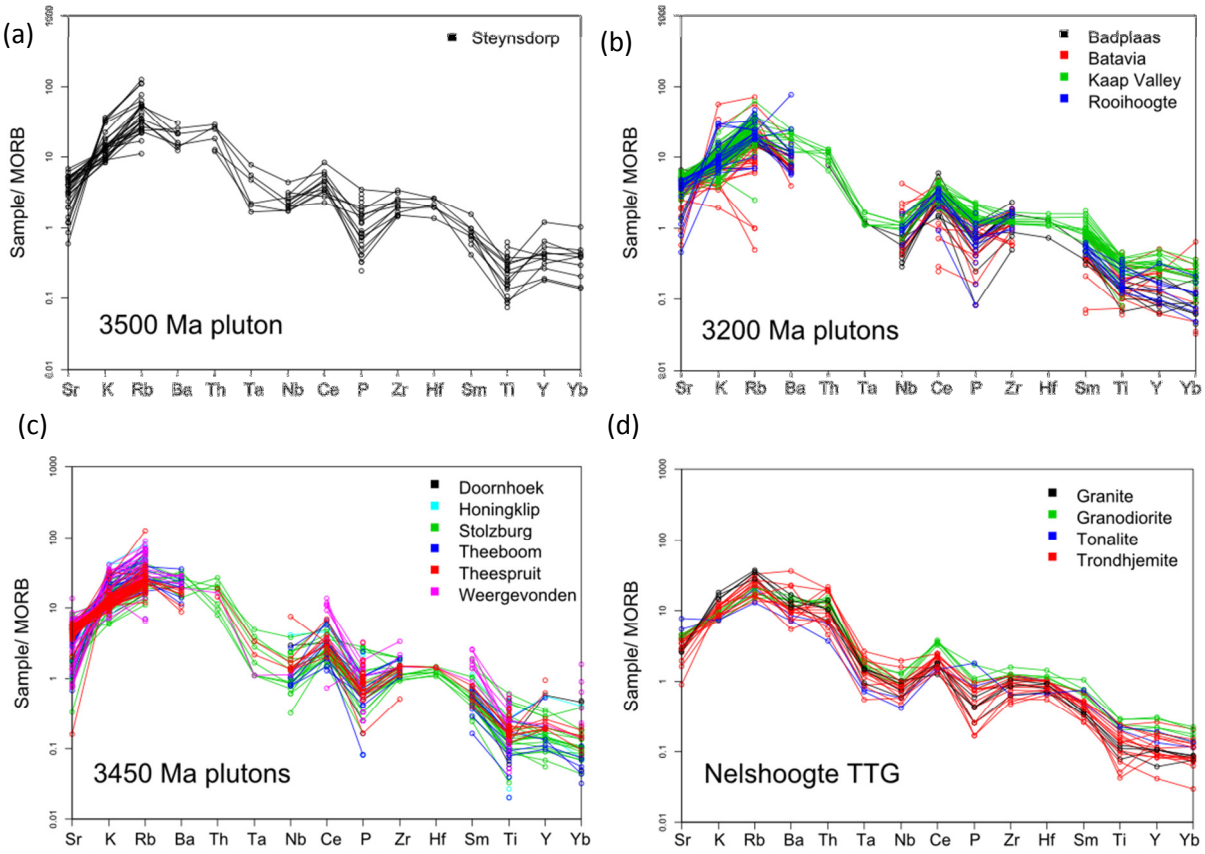

Fig. 11. The spider diagram displays compositions of trace-element values of TTGs in (a) ~ 3500 Ma pluton, (b) ~ 3450 Ma plutons, (c) ~ 3200 Ma plutons and (d) the Nelshoogte pluton in the BGGT (the sources of data for (a), (b) and (c) is from Yearron, 2003; Moyen, 2011) normalised to MORB (Pearce, 1983).

6.4. REE

Figure 12 illustrates the REE patterns of ~ 3500 Ma TTGs (Steynsdorp pluton), ~ 3450 Ma TTGs (Doornhoek, Honingklip, Stolzburg, Theeboom, Theespruit, Weergevonden and Weltreder plutons), ~ 3200 Ma TTGs (Badplaas, Batavia, Kaap Valley and Rooihoogte plutons) (Yearron, 2003; Moyen, 2011) and the Nelshoogte TTGs, normalised to the values for chondrites (McDonough and Sun, 1995). All samples from the BGGT are typically LREE-enriched and HREE-depleted. For the Nelshoogte TTGs, granodiorites are more enriched in all REEs than trondhjemite/granites. The tonalites contain lower LREE, higher

MREE (with a small positive Eu anomalie) compared to others rocks. NLG21R (a trondhjemite/pegmatite) shows a positive Eu anomaly. The Nelshoogte TTGs show similar patterns to ~ 3450 Ma and ~ 3200 Ma TTGs. Especially, the patterns of the Nelshoogte trondhjemites/granites are similar to the patterns of the Badplaas domain TTGs, and the patterns of the Nelshoogte granodiorites are similar to the patterns of the Kaap Valley TTGs. The ~ 3500 Ma plutons show flatter patterns.

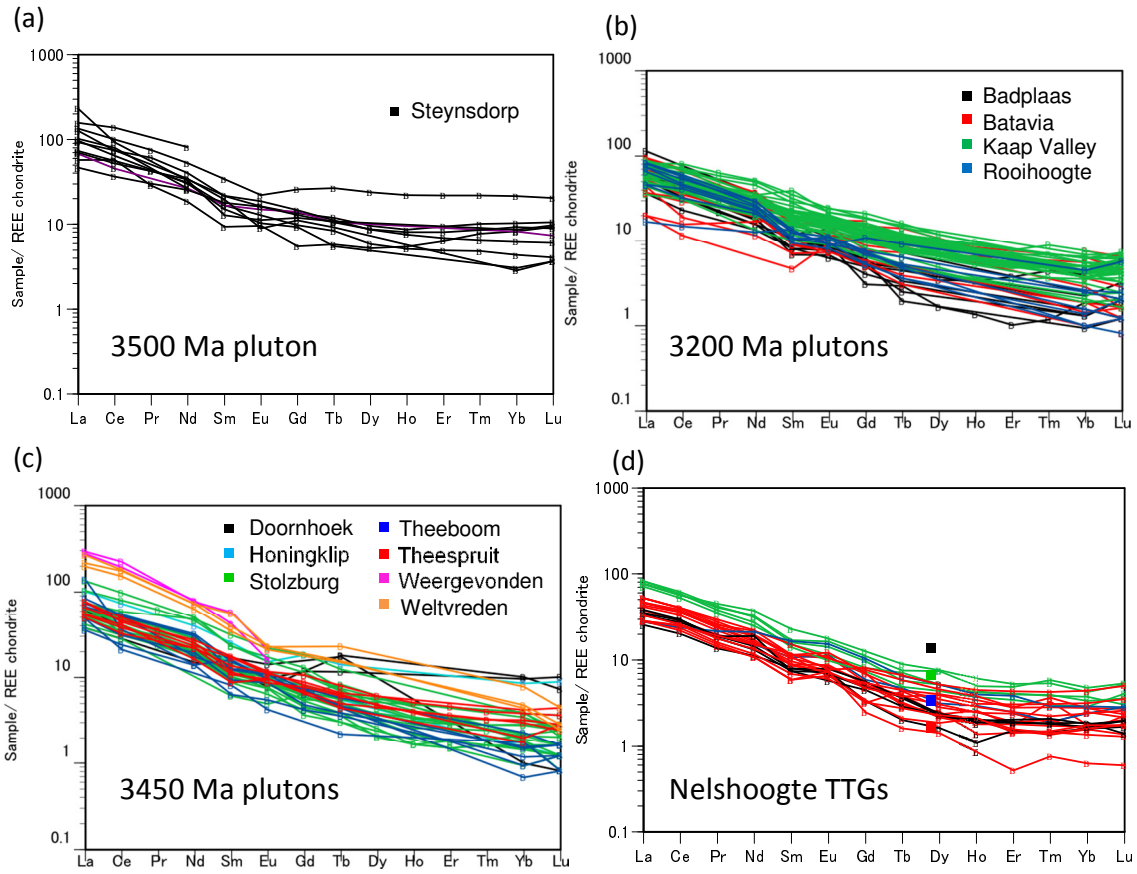

Fig. 12. REE patterns of TTGs in (a) ~ 3500 Ma pluton, (b) ~ 3450 Ma plutons, (c) ~ 3200 Ma plutons and (d) the Nelshoogte pluton in the BGGT (the sources of data for (a), (b) and (c) are from Yearron, 2003; Moyen, 2011) normalised to chondrite (McDonough and Sun, 1995).

Chapter 7

Geochronology

7.1 U-Pb zircon age

Zircon grains were extracted from 6 samples (NLG1R, NLG8R, NLG11R, NLG12R, NLG35R and NLG41R) from the Nelshoogte pluton (see Section 4 for analytical techniques). The samples were selected by different SiO_2 contents (61.89-74.85 wt%). U-Pb ages were obtained (Tables 6 and 7, Fig. 14). All samples except NLG35R contain zircon grains that show magmatic zoning in CL images (Fig. 13), and no particular evidence of inheritance. Determining the presence of inherited cores was difficult. Only one zircon grain from NLG41R yielded older ages (3353 Ma). This might be not inherited, because the grain is fractured, not a fully crystal. It might be from the the other rock (e.g. wall rock of the greenstone) when the trondhjemite intruded (Figs. 13 and 14). The U and Pb concentrations and Th/U ratios from grain spots are calculated relative to GJ-1 reference zircon (Frei and Gerdes, 2009). The calculated $^{207}Pb/^{235}U$, $^{206}Pb/^{238}U$ and $^{207}Pb/^{206}Pb$ ratios using the U and Pb concentrations and Th/U ratios (discordant less than 2%) from each samples represent different ages between ca. 3350 and 3150 Ma. Concordia ages are calculated using concordant $^{207}Pb/^{235}U$, $^{206}Pb/^{238}U$ and $^{207}Pb/^{206}Pb$ ages with the exception of older ages (ca. 3350 Ma) and younger ages (ca. 3150 Ma). The concordia ages for the Nelshoogte pluton are inferred as between 3232 and 3215 Ma for the 6 samples. There are no significant differences between the samples. The ages of all concordant samples are the same.

Table 6. U–Pb data for six samples from the Nelshoogte pluton.

Grain. spot	RATIOS						AGES [Ma]						Conc.
	$^{207}Pb/^{235}U^{b}$	2 σ[d]	$^{206}Pb/^{238}U^{b}$	2 σ[d]	$^{207}Pb/^{206}Pb^{c}$	2 σ[d]	$^{207}Pb/^{235}U$	2 σ	$^{206}Pb/^{238}U$	2 σ	$^{207}Pb/^{206}Pb$	2 σ	%
NLG1R													
zircon 08	24.00	0.71	0.665	0.018	0.2617	0.0029	3268	97	3287	91	3257	17	101
zircon 11	23.17	0.91	0.660	0.025	0.2547	0.0024	3234	127	3266	124	3214	15	101
zircon 15	22.90	0.74	0.649	0.020	0.2558	0.0020	3223	104	3226	101	3221	12	100
zircon 20	23.59	0.82	0.664	0.022	0.2577	0.0023	3252	114	3283	111	3233	14	101
zircon 24	22.90	0.70	0.648	0.018	0.2564	0.0027	3223	98	3219	91	3225	17	100
zircon 25	22.86	0.73	0.648	0.019	0.2558	0.0028	3221	102	3221	96	3221	17	100
zircon 28	21.61	0.69	0.627	0.019	0.2499	0.0030	3167	102	3139	93	3184	19	99
zircon 33	23.50	0.89	0.666	0.023	0.2559	0.0041	3248	123	3291	114	3221	25	101
zircon 49	23.74	0.67	0.664	0.018	0.2593	0.0026	3258	93	3283	87	3243	16	101
zircon 51	23.23	0.69	0.647	0.018	0.2605	0.0026	3236	96	3215	90	3250	16	99
zircon 54	22.43	0.70	0.647	0.019	0.2513	0.0029	3202	100	3218	93	3193	18	100

zircon 55	22.64	0.64	0.638	0.017	0.2572	0.0026	3212	91	3183	85	3230	16	99
zircon 61	23.72	0.87	0.666	0.023	0.2583	0.0037	3257	120	3291	112	3236	22	101
zircon 63	22.88	1.06	0.644	0.028	0.2575	0.0035	3222	149	3206	141	3232	22	100
zircon 64	22.98	0.76	0.651	0.020	0.2560	0.0035	3226	107	3232	98	3222	22	100
NLG 8R													
zircon 07	22.13	0.91	0.644	0.024	0.2491	0.0040	3189	131	3205	121	3179	25	101
zircon 08	23.15	0.85	0.651	0.022	0.2578	0.0040	3233	118	3233	107	3233	24	100
zircon 09	22.25	0.76	0.640	0.020	0.2523	0.0034	3195	109	3187	100	3199	21	100
zircon 14	21.23	0.61	0.631	0.016	0.2441	0.0031	3149	90	3152	81	3147	20	100
zircon 16	22.25	0.64	0.641	0.018	0.2516	0.0020	3195	92	3195	89	3195	13	100
zircon 23	22.96	0.67	0.650	0.018	0.2563	0.0027	3225	94	3228	88	3224	16	100
zircon 24	23.31	0.88	0.655	0.023	0.2583	0.0034	3240	122	3247	115	3236	21	100
zircon 26	20.41	0.59	0.609	0.016	0.2432	0.0026	3111	90	3064	82	3141	17	99
zircon 27	22.94	0.67	0.651	0.018	0.2556	0.0026	3225	94	3232	89	3220	16	100
zircon 36	23.31	0.73	0.659	0.020	0.2566	0.0024	3240	101	3262	97	3226	15	101
zircon 41	22.04	0.60	0.627	0.016	0.2549	0.0022	3186	87	3138	81	3216	14	99
zircon 46	21.85	0.90	0.626	0.025	0.2530	0.0026	3177	131	3136	125	3204	16	99
zircon 50	23.03	0.91	0.652	0.024	0.2561	0.0032	3228	127	3238	121	3223	20	100
zircon 51	22.79	1.06	0.653	0.030	0.2532	0.0023	3218	150	3240	148	3205	14	101
zircon 61	22.90	1.06	0.646	0.028	0.2569	0.0036	3223	149	3214	141	3228	22	100
zircon 72	23.09	0.95	0.649	0.025	0.2582	0.0033	3231	133	3223	127	3235	20	100
NLG11R													
zircon 072	22.11	1.17	0.639	0.029	0.251	0.007	3189	168	3184	113	3192	43	100
zircon 073	23.06	0.73	0.653	0.018	0.256	0.004	3229	103	3241	70	3222	26	101
zircon 074	20.41	0.81	0.621	0.021	0.238	0.005	3111	124	3115	84	3109	33	100
zircon 075	22.77	0.91	0.647	0.022	0.255	0.005	3217	129	3218	87	3217	32	100
zircon 076	23.07	1.03	0.652	0.025	0.257	0.006	3230	145	3237	97	3226	36	100
zircon 077	21.32	0.63	0.631	0.016	0.245	0.004	3153	93	3152	63	3154	24	100
zircon 078	21.32	0.66	0.626	0.017	0.247	0.004	3153	97	3135	66	3165	25	99
zircon 080	22.05	0.66	0.639	0.016	0.250	0.004	3186	96	3185	65	3187	25	100
zircon 085	23.30	0.68	0.654	0.016	0.259	0.004	3240	94	3242	63	3238	24	100
zircon 086	22.09	0.71	0.639	0.017	0.251	0.004	3188	102	3184	69	3190	26	100
zircon 087	21.66	0.66	0.629	0.016	0.250	0.004	3169	97	3144	65	3185	25	99
zircon 088	23.12	0.93	0.652	0.022	0.257	0.005	3232	130	3236	87	3230	33	100
zircon 089	22.68	0.99	0.650	0.024	0.253	0.006	3213	140	3227	94	3204	35	101
zircon 090	22.86	0.88	0.649	0.021	0.256	0.005	3221	124	3223	83	3220	31	100
zircon 092	21.83	0.67	0.636	0.017	0.249	0.004	3176	97	3172	65	3178	25	100
zircon 093	22.24	0.84	0.641	0.021	0.252	0.005	3194	121	3192	81	3196	31	100
zircon 094	22.24	0.78	0.635	0.019	0.254	0.005	3194	112	3169	75	3210	29	99
zircon 098	22.77	1.36	0.651	0.033	0.254	0.008	3217	192	3231	130	3209	48	101
zircon 099	21.66	0.68	0.632	0.017	0.249	0.004	3169	100	3158	67	3176	26	99
zircon 100	22.66	1.37	0.652	0.034	0.252	0.008	3212	195	3236	132	3198	49	101
zircon 102	23.14	1.37	0.651	0.033	0.258	0.008	3233	192	3231	129	3234	48	100
zircon 104	21.29	0.67	0.634	0.017	0.243	0.004	3152	99	3166	67	3143	26	101
zircon 105	22.70	0.78	0.646	0.019	0.255	0.005	3214	111	3214	74	3214	28	100
zircon 107	22.98	0.82	0.652	0.020	0.256	0.005	3226	116	3236	77	3220	30	101
zircon 111	22.89	0.95	0.649	0.023	0.256	0.006	3222	134	3223	89	3222	34	100
zircon 113	22.39	0.69	0.642	0.017	0.253	0.004	3201	99	3196	66	3204	26	100
zircon 115	22.78	0.98	0.651	0.024	0.254	0.006	3217	138	3234	92	3207	35	101
zircon 116	22.69	0.94	0.650	0.023	0.253	0.006	3214	133	3227	89	3205	34	101
zircon 124	21.96	0.67	0.636	0.016	0.250	0.004	3182	98	3175	65	3187	26	100
zircon 126	22.81	0.81	0.650	0.020	0.255	0.005	3219	115	3227	76	3214	30	100
zircon 128	23.11	0.80	0.652	0.019	0.257	0.005	3231	112	3238	74	3227	29	100
zircon 129	23.68	1.00	0.662	0.024	0.259	0.006	3255	138	3276	92	3242	35	101
zircon 130	23.10	0.74	0.651	0.018	0.257	0.004	3231	104	3234	68	3230	27	100
zircon 131	21.70	0.85	0.637	0.021	0.247	0.005	3170	125	3177	83	3166	33	100
zircon 133	23.34	0.97	0.657	0.023	0.258	0.006	3241	135	3254	90	3233	35	101
NLG12R													
zircon 007	23.38	1.10	0.655	0.025	0.259	0.007	3243	153	3248	97	3239	43	100
zircon 008	23.64	1.12	0.653	0.025	0.262	0.007	3254	154	3241	97	3262	43	99
zircon 014	22.52	1.12	0.644	0.026	0.254	0.007	3206	159	3204	101	3208	45	100
zircon 015	22.15	1.21	0.639	0.028	0.251	0.008	3190	174	3184	112	3194	48	100
zircon 016	22.77	1.34	0.642	0.031	0.257	0.008	3217	189	3198	123	3230	51	99
zircon 020	22.55	1.20	0.640	0.027	0.256	0.008	3208	170	3188	108	3220	48	99
zircon 021	22.61	1.07	0.644	0.024	0.255	0.007	3210	151	3203	94	3214	45	100
zircon 023	23.31	1.34	0.651	0.031	0.260	0.009	3240	186	3231	119	3246	52	100
zircon 025	22.06	1.24	0.636	0.029	0.252	0.008	3186	179	3174	115	3195	51	99
zircon 026	23.47	1.43	0.655	0.033	0.260	0.009	3247	198	3246	128	3247	54	100
zircon 035	22.63	1.24	0.646	0.028	0.254	0.009	3211	176	3212	110	3211	52	100
zircon 036	21.58	1.18	0.633	0.027	0.247	0.008	3165	172	3163	107	3166	52	100
zircon 039	22.39	1.73	0.648	0.041	0.251	0.011	3201	247	3219	162	3189	67	101
zircon 041	22.20	1.46	0.643	0.034	0.250	0.010	3193	209	3201	134	3188	60	100
zircon 042	22.22	2.24	0.639	0.056	0.252	0.013	3193	323	3187	219	3198	78	100
zircon 047	23.04	1.84	0.649	0.043	0.257	0.012	3229	257	3224	166	3231	70	100
NLG35R													
zircon 007	23.01	0.93	0.652	0.023	0.2562	0.0053	3228	130	3235	88	3223	32	100
zircon 010	23.43	0.81	0.657	0.020	0.2589	0.0046	3245	113	3254	77	3240	27	100
zircon 011	23.43	0.85	0.657	0.021	0.2586	0.0047	3245	117	3256	80	3238	29	101
zircon 012	23.47	0.83	0.654	0.020	0.2604	0.0047	3247	115	3243	78	3249	28	100
zircon 014	23.11	0.87	0.655	0.021	0.2560	0.0049	3231	121	3246	83	3222	30	101
zircon 016	23.22	0.70	0.658	0.017	0.2559	0.0039	3236	97	3260	67	3221	24	101
zircon 020	23.26	0.75	0.654	0.018	0.2581	0.0042	3238	105	3243	71	3235	25	100
zircon 021	23.10	0.73	0.651	0.018	0.2576	0.0041	3231	102	3230	69	3232	25	100
zircon 023	23.62	0.75	0.658	0.018	0.2605	0.0041	3253	103	3259	70	3250	25	100
zircon 025	23.17	0.78	0.651	0.019	0.2582	0.0044	3234	108	3231	73	3236	26	100
zircon 029	23.08	0.83	0.654	0.020	0.2560	0.0047	3230	116	3244	79	3222	28	101
zircon 033	23.20	0.67	0.653	0.016	0.2578	0.0037	3235	93	3239	64	3233	23	100
zircon 035	22.98	0.77	0.650	0.019	0.2563	0.0043	3226	108	3230	73	3224	26	100
zircon 036	23.15	0.84	0.655	0.021	0.2564	0.0048	3233	118	3247	80	3225	29	101
zircon 038	23.03	0.86	0.652	0.021	0.2561	0.0049	3228	120	3237	81	3223	30	100
zircon 040	23.16	0.86	0.655	0.021	0.2566	0.0049	3234	120	3246	81	3226	30	101
zircon 042	23.21	0.70	0.650	0.017	0.2588	0.0040	3236	98	3230	66	3239	24	100
zircon 047	22.94	0.70	0.651	0.017	0.2556	0.0040	3224	99	3232	67	3220	24	100
zircon 048	23.44	0.90	0.656	0.022	0.2590	0.0051	3245	125	3253	85	3241	31	100
zircon 051	22.92	0.76	0.654	0.019	0.2544	0.0043	3224	108	3242	73	3212	27	101
zircon 053	23.20	0.75	0.659	0.018	0.2552	0.0042	3235	104	3265	71	3217	26	101
zircon 054	23.32	0.91	0.655	0.022	0.2583	0.0052	3240	126	3246	85	3237	31	100
zircon 055	23.36	0.78	0.658	0.019	0.2576	0.0044	3242	108	3258	73	3232	26	101
zircon 064	23.10	0.84	0.657	0.021	0.2550	0.0048	3231	118	3256	80	3216	29	101
zircon 065	23.24	0.81	0.653	0.019	0.2581	0.0046	3237	112	3240	76	3235	28	100
zircon 066	22.97	0.92	0.650	0.022	0.2564	0.0053	3226	129	3228	87	3225	32	100

zircon 068	23.20	0.99	0.652	0.024	0.2579	0.0057	3235	138	3238	93	3234	34	100
NLG41R													
zircon 007	23.26	0.80	0.659	0.020	0.2562	0.0044	3238	111	3261	76	3224	27	101
zircon 008	24.43	0.89	0.667	0.021	0.2656	0.0048	3286	120	3295	82	3280	28	100
zircon 010	22.60	0.63	0.643	0.016	0.2550	0.0034	3210	89	3200	61	3216	21	100
zircon 011	23.19	0.69	0.657	0.017	0.2558	0.0037	3235	96	3257	66	3221	23	101
zircon 012	26.18	1.13	0.684	0.026	0.2776	0.0060	3353	145	3359	98	3350	33	100
zircon 013	23.52	0.70	0.659	0.017	0.2589	0.0038	3249	97	3262	67	3240	23	101
zircon 014	23.56	0.80	0.659	0.020	0.2592	0.0044	3250	111	3264	76	3242	26	101
zircon 016	24.11	0.72	0.661	0.017	0.2646	0.0038	3273	97	3271	67	3275	23	100
zircon 026	23.33	0.71	0.655	0.017	0.2583	0.0039	3241	99	3248	68	3236	23	100
zircon 027	23.17	0.65	0.659	0.016	0.2551	0.0035	3234	91	3263	63	3216	21	101
zircon 028	23.59	0.79	0.656	0.019	0.2610	0.0043	3252	108	3251	74	3253	26	100
zircon 038	23.43	1.00	0.660	0.024	0.2576	0.0056	3245	139	3266	95	3232	34	101
zircon 047	23.10	0.65	0.652	0.016	0.2568	0.0035	3231	92	3238	63	3227	22	100
zircon 050	22.21	0.61	0.636	0.015	0.2531	0.0034	3193	87	3175	60	3204	21	99
zircon 054	22.53	0.64	0.648	0.016	0.2520	0.0035	3207	91	3222	63	3197	22	101

[a]Corrected for background and within-run Pb/U fractionation and normalised to reference zircon GJ-1 (ID-TIMS values/measured value); $^{207}Pb/^{235}U$ calculated using $(^{207}Pb/^{206}Pb)/(^{238}U/^{206}Pb * 1/137.88)$

[b]Rho is the error correlation defined as the quotient of the propagated errors of the $^{206}Pb/^{238}U$ and the $^{207}Pb/^{235}U$ ratio

[c]Quadratic addition of within-run errors (2 SD) and daily reproducibility of GJ-1 (2 SD)

[d]Corrected for mass-bias by normalising to GJ-1 reference zircon (~0.6 per atomic mass unit) and common Pb using the model Pb composition of Stacey & Kramers (1975)

Table 7. Zircon samples and mean ages for U-Pb dating.

Sample	Rock type	Colour	Shape	Zoning	Concordia age (Ma)
NLG1R	trondhjemite	purple	prismatic	magmatic zoning	3227 ± 5
NLG8R	trondhjemite	pale brown	prismatic	magmatic zoning	3222 ± 5
NLG11R	tonalite	purple	prismatic	magmatic zoning	3220 ± 6
NLG12R	trondhjemite	purple or colourless	prismatic	magmatic zoning	3215 ± 12
NLG35R	tonalite	pale brown	prismatic to rounded	no zoning	3232 ± 5
NLG41R	trondhjemite	purple or colourless	prismatic	magmatic zoning	3225 ± 6

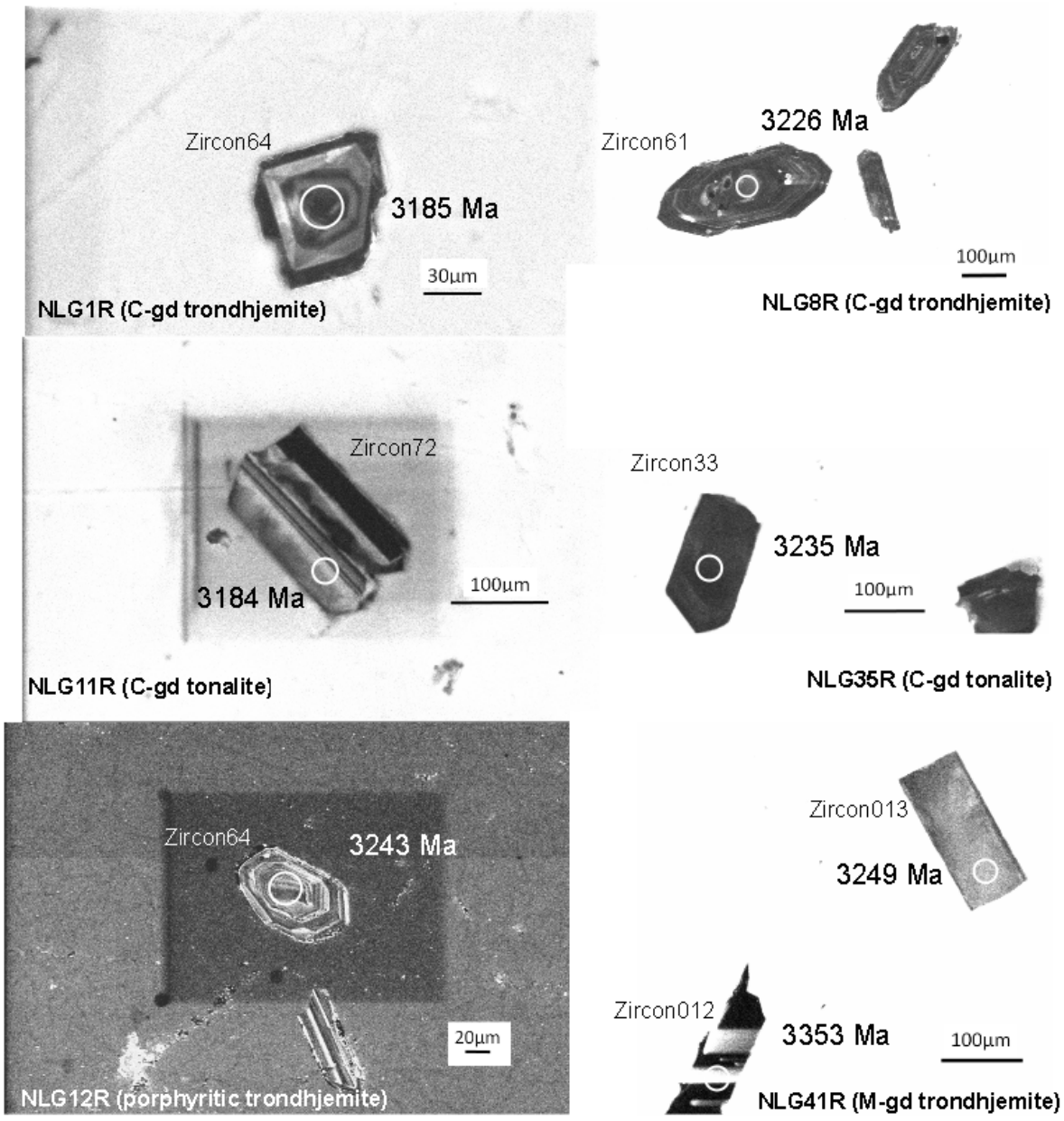

Fig. 13. CL images of zircons dated by U-Pb analysis. Circles define position of laser spots.

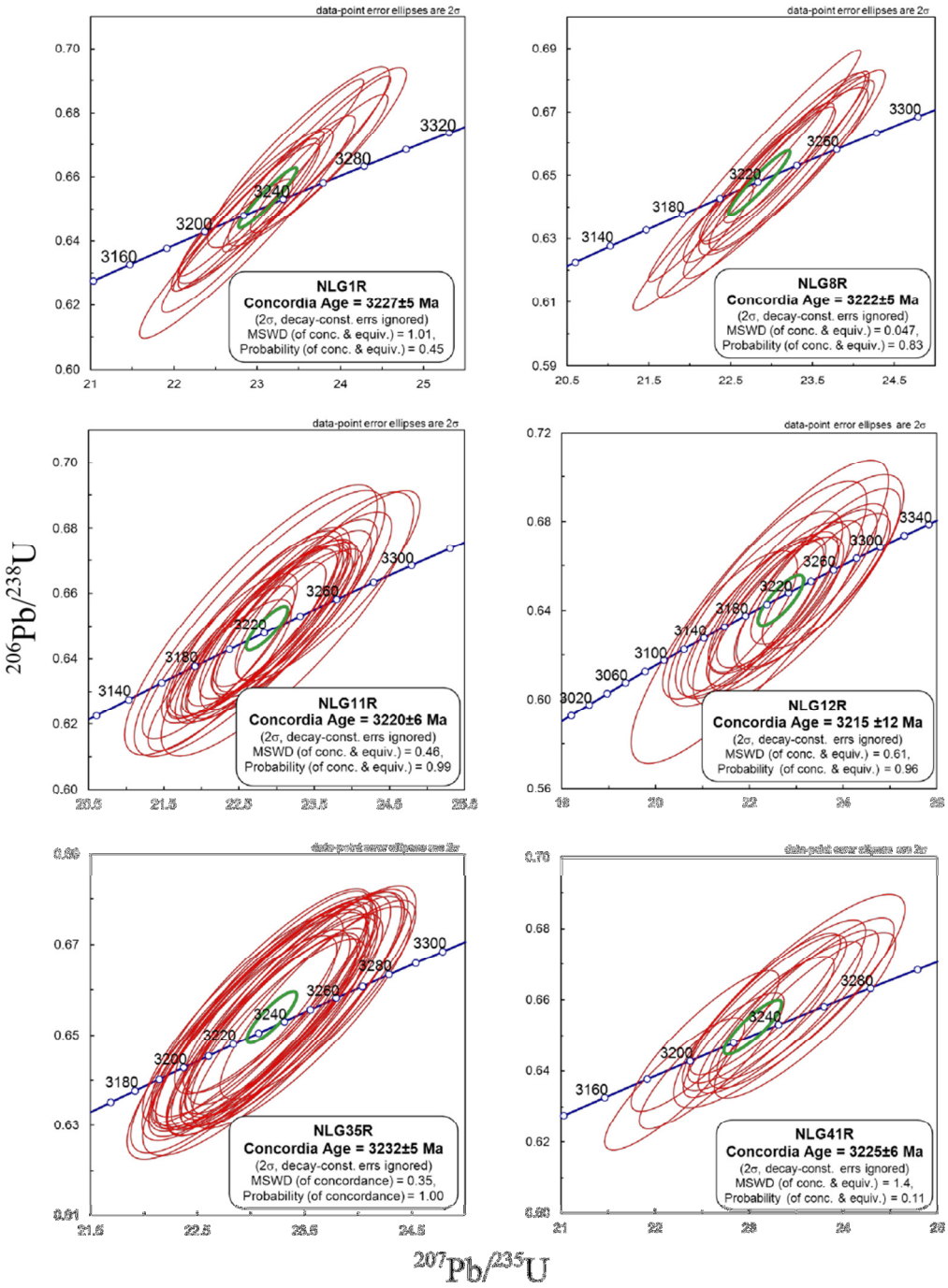

Fig. 14. U-Pb concordia diagram for zircons from sample NLG1R, NLG8R, NLG11R, NLG12R, NLG35R and NLG41R. The small green ellipses in the centre of the groups represent weighted mean error ellipses.

7.2 Hf isotopic analysis of zircon

Zircon can retain its primary Lu–Hf isotopic signature through high-grade metamorphism, due to its ability to remain a closed system during thermal resetting. The Lu-Hf system of zircon is more resistant to alteration processes than U-Pb (Patchett, 1983; Kinny et al., 1991; Kinny and Maas, 2003). This, in conjunction with the use of zircon as a U–Pb geochronometer makes the Lu–Hf isotope system in zircon ideal to study the radiogenic isotopic evolution of the early Archaean gneiss (e.g., Patchett et al., 1981; Vervoort et al., 1996; Vervoort and Blichert-Toft, 1999).

The same zircon grains used for U-Pb ages with discordance of less than 2% were analyzed, and the data are listed in Tables 8 and 9. The εHf(t) values for the Nelshoogte trondhjemites/tonalites comprised between + 0.1 to + 1.9 and T_{DM} model ages were inferred as ca. 3330- 3230 Ma. This indicates that the source of the zircons could have been extracted from the mantle 20 to 100 Myr before the crystallisation of the TTGs. Sample NLG11R (tonalite) shows slightly higher εHf(t) and older T_{DM} age than other Nelshoogte samples, however, the errors for the model ages are more than ± 50 Ma. These values and ages for all the Nelshoogte samples can also be the same witin errors.

Table 8. Lu–Hf isotope compositions of zircon cores from the Nelshoogte pluton by LA-MC-ICP-MS

	$^{176}Yb/^{177}Hf$ [a]	±2s	$^{176}Lu/^{177}Hf$ [a]	±2s	$^{178}Hf/^{177}Hf$	$^{180}Hf/^{177}Hf$	∑Hf [b] (V)	$^{176}Hf/^{177}Hf$	±2s [c]	$^{176}Hf/^{177}Hf(t)$ [d]	εHf(t) [d]	±2s [c]	TNC [e] (Ga)	age [f] (Ma)	±2s
NLG1R															
zircon11	0.01870	18	0.00077	6.2	1.46713	1.88658	9.186	0.28077	19	0.28072	0.907	0.67	3.289	3227	8.636
zircon15	0.02542	23	0.00095	6.7	1.46712	1.88670	8.514	0.28080	23	0.28074	1.413	0.81	3.261	3227	8.636
zircon20	0.02728	41	0.00102	12.5	1.46714	1.88661	9.873	0.28079	27	0.28072	0.886	0.97	3.290	3227	8.636
zircon24	0.02390	21	0.00096	6.4	1.46714	1.88671	5.350	0.28078	27	0.28072	0.740	0.96	3.298	3227	8.636
zircon25	0.01984	19	0.00075	5.5	1.46707	1.88658	6.005	0.28079	26	0.28075	1.670	0.94	3.247	3227	8.636
zircon28	0.02677	28	0.00099	8.3	1.46713	1.88663	6.538	0.28079	27	0.28073	1.056	0.95	3.281	3227	8.636
zircon33	0.03587	41	0.00130	11.2	1.46720	1.88647	13.415	0.28083	24	0.28075	1.909	0.86	3.234	3227	8.636
zircon49	0.02018	17	0.00078	5.3	1.46713	1.88670	6.235	0.28078	30	0.28073	1.203	1.08	3.273	3227	8.636
zircon51	0.02729	25	0.00104	7.2	1.46717	1.88661	10.581	0.28079	15	0.28073	0.957	0.53	3.286	3227	8.636
zircon54	0.02173	18	0.00083	5.4	1.46709	1.88652	12.324	0.28078	16	0.28073	1.035	0.57	3.282	3227	8.636
zircon55	0.03650	56	0.00140	19.9	1.46713	1.88671	6.049	0.28083	29	0.28074	1.620	1.04	3.250	3227	8.636
zircon61	0.02685	22	0.00103	6.4	1.46711	1.88659	12.445	0.28079	22	0.28072	0.944	0.77	3.287	3227	8.636
zircon63	0.02218	22	0.00086	6.9	1.46715	1.88653	13.062	0.28078	18	0.28073	1.096	0.63	3.279	3227	8.636
zircon64	0.01897	15	0.00074	4.5	1.46723	1.88666	13.376	0.28077	18	0.28072	0.744	0.64	3.298	3227	8.636
NLG 8R															
zircon07	0.01883	17	0.00080	5.4	1.46712	1.88671	13.512	0.28078	22	0.28073	1.029	0.77	3.278	3222	8.636
zircon08	0.02054	19	0.00092	7.0	1.46704	1.88669	6.686	0.28079	19	0.28073	0.956	0.68	3.282	3222	8.636
zircon09	0.02350	22	0.00102	8.1	1.46711	1.88652	16.751	0.28079	19	0.28073	0.882	0.67	3.286	3222	8.636
zircon14	0.02515	32	0.00111	12.3	1.46712	1.88657	13.438	0.28080	22	0.28073	1.083	0.79	3.275	3222	8.636
zircon16	0.02067	18	0.00092	6.5	1.46720	1.88662	13.021	0.28079	13	0.28073	0.934	0.46	3.284	3222	8.636
zircon23	0.01360	20	0.00066	7.1	1.46712	1.88673	8.595	0.28078	25	0.28074	1.306	0.89	3.263	3222	8.636
zircon24	0.01941	16	0.00088	5.6	1.46711	1.88661	6.819	0.28080	24	0.28075	1.631	0.86	3.245	3222	8.636
zircon26	0.02011	20	0.00091	7.8	1.46717	1.88676	17.074	0.28080	21	0.28075	1.556	0.74	3.249	3222	8.636
zircon27	0.01761	15	0.00079	5.2	1.46712	1.88661	7.756	0.28080	25	0.28075	1.695	0.87	3.241	3222	8.636
zircon36	0.02380	22	0.00106	7.5	1.46720	1.88673	6.889	0.28079	26	0.28072	0.726	0.92	3.295	3222	8.636
zircon41	0.02322	30	0.00103	11.5	1.46711	1.88647	12.835	0.28079	15	0.28073	0.956	0.54	3.282	3222	8.636
zircon46	0.03855	35	0.00152	11.1	1.46717	1.88660	14.317	0.28084	17	0.28075	1.632	0.60	3.245	3222	8.636
zircon50	0.02094	27	0.00096	10.5	1.46716	1.88665	7.044	0.28078	24	0.28072	0.729	0.85	3.295	3222	8.636
zircon61	0.02192	18	0.00085	5.4	1.46714	1.88652	13.420	0.28078	14	0.28073	1.060	0.51	3.277	3222	8.636

zircon72	0.01589	16	0.00074	7.2	1.46713	1.88663	13.256	0.28079	24	0.28074	1.534	0.85	3.250	3222	8.636
NLG11R															
zircon72	0.02824	23	0.00112	7.1	1.46714	1.88651	8.286	0.28082	21	0.28075	1.613	0.74	3.244	3220	8.636
zircon74	0.01563	18	0.00069	6.4	1.46714	1.88670	7.573	0.28080	25	0.28076	1.987	0.89	3.224	3220	8.636
zircon78	0.02855	52	0.00116	19.4	1.46723	1.88647	5.630	0.28082	27	0.28075	1.589	0.96	3.246	3220	8.636
zircon80	0.01258	11	0.00046	3.6	1.46713	1.88655	11.582	0.28079	21	0.28076	1.907	0.74	3.228	3220	8.636
zircon88	0.01981	20	0.00071	6.4	1.46715	1.88661	9.461	0.28081	23	0.28076	2.106	0.81	3.217	3220	8.636
zircon93	0.02215	21	0.00084	6.1	1.46708	1.88667	5.963	0.28080	25	0.28075	1.534	0.89	3.249	3220	8.636
zircon94	0.01590	15	0.00063	4.6	1.46716	1.88661	7.334	0.28080	20	0.28077	2.219	0.72	3.211	3220	8.636
zircon102	0.01409	18	0.00059	6.8	1.46707	1.88670	5.894	0.28078	26	0.28075	1.537	0.92	3.249	3220	8.636
zircon107	0.02150	20	0.00086	6.7	1.46713	1.88666	5.870	0.28079	25	0.28074	1.319	0.88	3.261	3220	8.636
zircon111	0.02332	25	0.00096	8.8	1.46710	1.88666	5.640	0.28081	26	0.28075	1.613	0.92	3.244	3220	8.636
zircon113	0.02519	26	0.00105	9.2	1.46711	1.88660	6.238	0.28082	25	0.28076	1.942	0.89	3.226	3220	8.636
zircon115	0.01443	21	0.00060	8.0	1.46706	1.88660	6.735	0.28080	24	0.28077	2.253	0.87	3.209	3220	8.636
zircon116	0.01422	13	0.00060	4.3	1.46709	1.88658	6.170	0.28080	27	0.28076	2.052	0.96	3.220	3220	8.636
zircon124	0.02599	27	0.00098	8.0	1.46720	1.88648	13.539	0.28083	14	0.28077	2.228	0.51	3.210	3220	8.636
zircon126	0.02332	26	0.00087	8.5	1.46715	1.88651	9.290	0.28082	18	0.28077	2.382	0.65	3.202	3220	8.636
zircon128	0.02200	25	0.00101	8.9	1.46715	1.88658	6.783	0.28081	22	0.28074	1.468	0.79	3.252	3220	8.636
zircon129	0.01024	9	0.00045	3.0	1.46718	1.88666	6.678	0.28078	16	0.28075	1.839	0.58	3.232	3220	8.636
zircon131	0.01181	11	0.00047	3.4	1.46709	1.88673	4.980	0.28080	23	0.28077	2.260	0.83	3.208	3220	8.636
zircon133	0.01618	14	0.00070	5.2	1.46706	1.88659	6.833	0.28079	24	0.28075	1.649	0.85	3.242	3220	8.636
NLG12R															
zircon07	0.02608	24	0.00107	7.9	1.46712	1.88648	10.536	0.28077	21	0.28071	0.081	0.76	3.325	3215	8.636
zircon08	0.01960	18	0.00084	6.3	1.46718	1.88649	13.539	0.28077	13	0.28071	0.313	0.46	3.312	3215	8.636
zircon14	0.01544	16	0.00062	5.2	1.46715	1.88666	15.125	0.28075	16	0.28071	0.172	0.58	3.320	3215	8.636
zircon15	0.01751	17	0.00072	5.8	1.46713	1.88655	13.353	0.28076	17	0.28072	0.376	0.62	3.309	3215	8.636
zircon16	0.02694	30	0.00111	10.5	1.46708	1.88651	14.513	0.28077	15	0.28070	-0.239	0.52	3.343	3215	8.636
zircon20	0.02700	30	0.00109	11.2	1.46709	1.88660	9.046	0.28078	23	0.28071	0.078	0.81	3.325	3215	8.636
zircon21	0.03964	42	0.00151	13.5	1.46712	1.88655	13.057	0.28079	17	0.28069	-0.432	0.62	3.354	3215	8.636
zircon23	0.02239	19	0.00095	6.5	1.46712	1.88652	8.642	0.28076	20	0.28070	-0.208	0.71	3.341	3215	8.636
zircon25	0.01742	15	0.00074	5.1	1.46708	1.88660	14.314	0.28076	15	0.28071	0.296	0.52	3.313	3215	8.636
zircon26	0.02426	31	0.00092	10.0	1.46718	1.88666	14.011	0.28077	16	0.28071	0.138	0.57	3.322	3215	8.636
zircon35	0.02225	19	0.00093	6.0	1.46715	1.88652	15.189	0.28078	15	0.28072	0.497	0.54	3.302	3215	8.636

zircon36	0.02147	18	0.00087	5.5	1.46712	1.88660	11.534	0.28075	17	0.28070	-0.346	0.61	3.349	3215	8.636
zircon39	0.01815	15	0.00076	4.8	1.46708	1.88656	13.240	0.28075	14	0.28070	-0.062	0.50	3.333	3215	8.636
zircon41	0.02294	20	0.00093	6.6	1.46711	1.88658	12.439	0.28078	19	0.28072	0.407	0.66	3.307	3215	8.636
zircon42	0.02886	34	0.00119	12.1	1.46710	1.88665	12.282	0.28079	17	0.28071	0.312	0.61	3.312	3215	8.636
NLG35R															
zircon11	0.02812	25	0.00113	8.2	1.46710	1.88646	5.444	0.28079	21	0.28072	0.796	0.73	3.299	3232	8.636
zircon12	0.02352	20	0.00095	6.3	1.46715	1.88654	5.567	0.28078	20	0.28072	0.922	0.69	3.292	3232	8.636
zircon14	0.03498	28	0.00132	8.0	1.46717	1.88657	9.447	0.28080	17	0.28071	0.640	0.61	3.308	3232	8.636
zircon16	0.02028	17	0.00083	5.5	1.46706	1.88646	10.521	0.28077	18	0.28072	0.712	0.65	3.304	3232	8.636
zircon20	0.02626	23	0.00101	6.9	1.46712	1.88651	9.813	0.28079	17	0.28072	1.010	0.62	3.287	3232	8.636
zircon21	0.02140	18	0.00084	5.2	1.46716	1.88659	14.931	0.28077	16	0.28072	0.722	0.56	3.303	3232	8.636
zircon23	0.02079	19	0.00082	5.5	1.46713	1.88646	10.682	0.28077	17	0.28072	0.989	0.59	3.289	3232	8.636
zircon25	0.02772	26	0.00110	8.7	1.46712	1.88654	11.371	0.28079	16	0.28072	0.777	0.57	3.300	3232	8.636
zircon33	0.02013	17	0.00083	5.5	1.46709	1.88651	10.835	0.28076	16	0.28071	0.535	0.56	3.314	3232	8.636
zircon35	0.02291	23	0.00096	8.2	1.46712	1.88652	9.782	0.28078	18	0.28072	0.879	0.63	3.295	3232	8.636
zircon36	0.02469	23	0.00102	8.4	1.46708	1.88651	5.322	0.28079	19	0.28073	1.076	0.67	3.284	3232	8.636
zircon38	0.01453	12	0.00062	4.0	1.46715	1.88652	10.719	0.28076	14	0.28072	0.778	0.52	3.300	3232	8.636
zircon42	0.01870	18	0.00075	6.0	1.46714	1.88647	12.108	0.28077	17	0.28072	1.049	0.61	3.285	3232	8.636
zircon48	0.02171	19	0.00089	6.2	1.46713	1.88674	9.893	0.28079	18	0.28073	1.284	0.63	3.272	3232	8.636
zircon51	0.02317	19	0.00093	6.0	1.46713	1.88658	11.551	0.28077	17	0.28071	0.577	0.61	3.311	3232	8.636
zircon53	0.03222	28	0.00117	7.3	1.46713	1.88670	6.361	0.28078	18	0.28071	0.500	0.66	3.316	3232	8.636
zircon54	0.02394	19	0.00097	6.0	1.46712	1.88652	10.186	0.28078	19	0.28072	0.817	0.66	3.298	3232	8.636
zircon64	0.02126	17	0.00083	5.1	1.46710	1.88652	11.587	0.28078	18	0.28073	1.267	0.65	3.273	3232	8.636
zircon65	0.02074	22	0.00083	7.8	1.46715	1.88654	6.725	0.28077	20	0.28072	0.966	0.71	3.290	3232	8.636
zircon66	0.02372	28	0.00090	9.1	1.46706	1.88659	12.140	0.28077	17	0.28071	0.603	0.59	3.310	3232	8.636
zircon68	0.02443	20	0.00097	6.0	1.46711	1.88660	5.628	0.28079	24	0.28073	1.266	0.84	3.273	3232	8.636
NLG41R															
zircon07	0.02315	31	0.00068	8.6	1.46711	1.88660	12.207	0.28075	24	0.28071	0.239	0.85	3.325	3225	8.636
zircon08	0.02588	31	0.00097	7.6	1.46717	1.88647	12.509	0.28078	19	0.28072	0.660	0.69	3.301	3225	8.636
zircon10	0.01184	10	0.00038	2.5	1.46720	1.88647	10.200	0.28074	17	0.28072	0.594	0.62	3.305	3225	8.636
zircon11	0.02163	19	0.00084	5.8	1.46707	1.88662	17.287	0.28076	17	0.28070	0.142	0.61	3.330	3225	8.636
zircon12	0.09019	175	0.00289	50.5	1.46713	1.88666	1.276	0.28089	28	0.28071	0.551	1.01	3.307	3225	8.636
zircon13	0.02136	20	0.00083	6.5	1.46714	1.88652	12.473	0.28077	16	0.28072	0.711	0.55	3.298	3225	8.636

zircon14	0.00579	8	0.00019	2.5	1.46716	1.88663	10.540	0.28071	19	0.28070	-0.114	0.66	3.344	3225	8.636
zircon16	0.02513	27	0.00105	9.7	1.46710	1.88660	6.660	0.28077	23	0.28070	0.106	0.83	3.332	3225	8.636
zircon26	0.01743	23	0.00068	8.7	1.46715	1.88652	13.046	0.28075	17	0.28071	0.372	0.61	3.317	3225	8.636
zircon27	0.01895	26	0.00075	9.7	1.46714	1.88660	12.988	0.28077	17	0.28072	0.724	0.61	3.298	3225	8.636
zircon28	0.01144	15	0.00042	4.9	1.46711	1.88673	6.216	0.28074	27	0.28072	0.626	0.96	3.303	3225	8.636
zircon28b	0.01343	14	0.00048	4.6	1.46710	1.88661	9.949	0.28075	21	0.28072	0.744	0.75	3.297	3225	8.636
zircon38	0.01701	18	0.00069	6.7	1.46717	1.88666	13.281	0.28076	16	0.28072	0.640	0.58	3.302	3225	8.636
zircon47	0.04128	36	0.00163	11.3	1.46713	1.88661	11.964	0.28081	18	0.28070	0.170	0.64	3.328	3225	8.636
zircon54	0.01802	16	0.00053	4.7	1.46713	1.88673	13.850	0.28074	24	0.28071	0.231	0.84	3.325	3225	8.636
Plesovice (n=10)	0.00668	23	0.00017	6.0	1.46718	1.88675	19.424	0.28247	20	0.28247	-3.653	0.73	1.177	338	3.000
GJ-1 (n=28)	0.00699	5	0.00027	0.4	1.46714	1.88663	10.644	0.28200	19	0.28200	-14.339	0.67	1.981	606	6.000
JMC 475 (n=8)					1.46718	1.88670	15.000	0.28215	8						

Quoted uncertainties (absolute) relate to the last quoted figure. The effect of the inter-element fractionation on the Lu/Hf was estimated to be about 6 % or less based on analyses of the GJ-1 and Plesoviče zircon. Accuracy and reproducibility was checked by repeated analyses (n = 30 and 20, respectively) of reference zircon GJ-1 and Plesoviče (data given as mean with 2 standard deviation uncertainties)

(a) $^{176}Yb/^{177}Hf = (^{176}Yb/^{173}Yb)true \times (^{173}Yb/^{177}Hf)meas \times (M^{173}(Yb)/M^{177}(Hf))b(Hf)$, $b(Hf) = \ln(^{179}Hf/^{177}Hf \text{ true} / {}^{179}Hf/^{177}Hf \text{ measured})/ \ln (M^{179}(Hf)/M^{177}(Hf))$, M=mass of respective isotope. The $^{176}Lu/^{177}Hf$ were calculated in a similar way by using the $^{175}Lu/^{177}Hf$ and b(Yb).

(b) Mean Hf signal in volt.

(c) Uncertainties are quadratic additions of the within-run precision and the daily reproducibility of the 40ppb-JMC475 solution. Uncertainties for the JMC475 quoted at 2SD (2 standard deviation).

(d) Initial $^{176}Hf/^{177}Hf$ and eHf calculated using the apparent Pb-Pb age determined by LA-ICP-MS dating (see column f), and the CHUR parameters: $^{176}Lu/^{177}Hf = 0.0336$, and $^{176}Hf/^{177}Hf = 0.282785$ (Bouvier et al., 2008).

(e) Two stage model age in billion years using the measured $^{176}Lu/^{177}Lu$ of each spot (first stage = age of zircon), a value of 0.0113 for the average continental crust (second stage), and a juvenile crust (NC) $^{176}Lu/^{177}Lu$ and $^{176}Hf/^{177}Hf$ of 0.0384 and 0.28314, respectively.

(f) apparent Pb-Pb age determined by LA-ICP-MS

Table 9. Average Hf isotope compositions of zircon cores from the Nelshoogte pluton by LA-MC-ICP-MS. The number of εHf(t) indicates evolution of the crust and T_{DM} age represents the age of the source rock.

Sample	rock type	$^{176}Hf/^{177}Hf(t)$	εHf(t)	T_{DM} age (Ga)
NLG1R	trondhjemite	0.28073±0.00002	1.2±0.7	3.275
NLG8R	trondhjemite	0.28074±0.00002	1.2±0.7	3.270
NLG11R	tonalite	0.28076±0.00002	1.9±0.6	3.230
NLG12R	trondhjemite	0.28071±0.00002	0.1±0.6	3.325
NLG35R	tonalite	0.28072±0.00001	0.9±0.5	3.296
NLG41R	trondhjemite	0.28071±0.00002	0.4±0.6	3.314

Chapter 8

Discussion

8.1. Interpretation for the field relationship, rock textures and mineral inclusions

There are sharp contacts between tonalite/granodiorite and trondhjemite (and also between mafic rock/greenstone and trondhjemite) in the Nelshoogte pluton. Also many dykes/intrusions of TTGs, potassic granite and mafic rocks in this pluton suggest that there was some later magmatism around the pluton. Especially, intrusions of TTGs suggest there were some different compositions of magma batches around the pluton and the Nelshoogte TTGs reflect these different magmas due to long-lived magmatism. The NE-trending foliations were mostly found in southern and southwestern part of the pluton. This may be explained by Kisters et al. (2003) hypothesis that those structures were caused by deep crustal exhumation in response to extensional collapse of the BGB at ca. 3220 Ma. This implies that the response of the southern, high-grade metamorphic TTG terrain to exhumation and uplift is likely to be different to that of the 3236 Ma Nelshoogte pluton along the northern margin of the Stolzburg schist belt. The Nelshoogte pluton represents a largely early- to syn-D2 pluton and although it contains a pervasive gneissosity along its margins, it has not presented a lower crustal basement to the supracrustal rocks as the older Stolzburg pluton in the south. The Nelshoogte pluton shows the markedly different fabric development from the Stolzburg pluton, namely the lack of constrictional-type fabrics in gneisses of the Nelshoogte pluton, and the lineation pattern, that deviates from the unidirectional L1 lineation pattern in the SSB and Stolzburg pluton. Top-to-the-NE extensional shearing inferred for the upper-plate greenstone sequence is, in the present-day upright orientation of the greenstones, only manifest by relatively rare oblique sinistral supracrustal-up, Nelshoogte pluton-down shear sense indicators along the northern margin of the SSB. Most shear sense indicators rather point to oblique off-the-dome kinematics which are possibly related to the later diapiric steepening of fabrics.

Euhedral plagioclase in the foliated texture has resisted the deformation and shows primary magmatic textures. The myrmekite is attributed to solid-state replacement of K-feldspar accompanying deformation. This texture is interpreted to mean that foliated trondhjemites in

the eastern to southern part near the margin of the BGB were affected by metamorphic events related with early- to syn-D2 deep-crustal exhumation in the BGGT at ca 3220 Ma (Kisters et al., 2003). The porphyritic texture implies that this type of trondhjemites is intrusion. They indicate that slow crystallization to form the phenocrysts and more rapid cooling to form the groundmass, at shallow emplacement depths (e.g. Swanson, 1977; McMillan, 1986). Also the myrmekite formed by rapid cooling when it emplaced. Biotite aggregates suggest the breakdown of clinopyroxene or hornblende. Small grains in the xenomorphic granular texture indicate inward crystallization due to rapid cooling in the contact with the country rocks of the greenstone belt (Figs. 4c and 5f). Normal zoning in plagioclase in the granitic texture indicates that cores reflect crystallization at relatively high temperatures, so that they are relatively rich in Ca and Al, and successive outer zones are progressively richer in Na and Si, presumably in response to falling temperature. The hypidiomorphic-granular texture implies relatively slower crystallization in warmer system. Plagioclase and hornblende crystallized first, prior to quartz. In Figures 11 and 12, this rock (NLG35R) shows different trace-element and REE patterns to other Nelshoogte TTGs, and has positive Sr and Eu anomalies. Also U-Pb age of this sample shows only the same age. This suggests that plagioclase crystals cumulated in the magma chamber, perhaps due to thermal convection of the magma. Renjith (2013) suggests that repeated recharge-recycling processes have produced various populations of plagioclase with different micro-textural stratigraphy. Plagioclase develops sieve-texture during the decompression of H_2O-undersaturated magma process (Nelson and Montana, 1992) or reaction with hotter Ca-rich melt (Tsuchiyama, 1985). The close association of synneusis texture implies that during their growth crystals were repeatedly in motion may be due to dynamically active convection or turbulence of the crystallizing magma. The sieve texture and synneusis texture in plagioclase from sample NLG35R may be explained by these suggestions. The existence of hornblende in the core of plagioclace suggests either plagioclase nucleated on hornblende or mafic melt entered the crystal through the crack.

Chlorite inclusion in magmatic zircon suggests that mafic melt/fluid gets into zircon through the crack. Probably, after the zircon crystallised in the magma batch, the other magma batch gets into the batch (Table 3).

These intrusions, textures, and inclusions in the Nelshoogte pluton suggest different types of magma batches. This variety within the pluton may be caused by long-lived magmatism during syn-D2 event in the BGGT (Kisters et al., 2010).

8.2. Implications of the major-element variations in whole-rocks and minerals

8.2.1. Whole-rocks

Nelshoogte TTGs and also other Barberton TTGs present a wide range of major-element variation. The TTGs are dominated by quartz, plagioclase, biotite and amphibole, with accessory apatite, allanite, Fe-Ti oxide and titanite. The following mechanisms are considered as possible explanations for the variations: 1) assimilation of greenstone belt rocks, 2) fractional crystallization, 3) magma mixing, and 4) peritectic assemblage entrainment.

1) *Assimilation of wall rocks (greenstone belt rocks)*

Assimilation, it is not demonstrable from the major-element data. In many cases, assimilation models based on isotope or trace-element data, fail to pass the test of agreeing with the major-element chemistry of the modelled 'hybrid' rocks (e.g. O'Hara, 1980; Clemens et al., 2009, 2010). Compositions of mafic rocks and TTG on Harker diagrams (Fig. 15) show that there are no correlations or linear trends between TTGs and mafic rocks including greenstone belt rocks (e.g. on plots of SiO_2 vs TiO_2, Al_2O_3, K_2O, P_2O_5, Rb, Sr Ba and Zr). Clemens and Stevens (2012) noted that bulk assimilation might take place by either mechanical disaggregation of ingested xenoliths or by reactive dissolution and precipitation of crystals. These ideas have been effectively debunked by consideration of the energetic consequences of these processes (Spera and Bohrson, 2001; Glazner, 2007). Essentially, the energy consumed in these processes results in considerable cooling, crystallisation and the formation of a hybrid magma so highly crystallised that it would be immobile and incapable of undergoing further magmatic evolution. For the Nelshoogte pluton, the thermal energy to melt the wall rock was not available, because the contacts with the Stolzburg schist belt to the south (Kisters, et al., 2003), with greenstone to the east, and with mafic rocks to the north, are sharp. Therefore, there is no evidence for assimilation by wall rocks (greenstones) or post-3.0 Ga mafic rocks within the pluton.

2) *Fractional crystallization*

TTG rocks are dominated by quartz, plagioclase, biotite and amphibole, with accessory apatite, allanite, Fe-Ti oxide and titanite. Crystallisation and fractionation of these minerals would explain the negative linear trends displayed by CaO, Al_2O_3, MgO, FeO^T and TiO_2 on Harker diagrams. The trends are characterised by quite tight inter-element correlation on the diagrams. The decrease in TiO_2, MgO, FeO^T and CaO as SiO_2 increase is consistent with the removal of early-formed plagioclase, pyroxene and magnetite, and later hornblende and biotite, from the cooling liquids (initial gabbroic, tonalitic, or quartz dioritic parental magmas). MgO and FeO^T are incorporated into the typically early-formed mafic minerals. CaO may have been removed by either a clinopyroxene, a calcic plagioclase, or both (e.g. Bowen, 1915). Also the CaO variation could be explained by the fractionation of a feasible amount of the kind of early plagioclase that the rocks contain. The variations of these major-elements for the Nelshoogte and other ~ 3200 Ma TTGs represent tight negative trends (Fig. 9). Therefore, the trends of ~ 3200 Ma TTGs and the Nelshoogte TTGs could be explained by fractional crystallization of the minerals that crystallized when the magma was cooling. However, possibilities for other processes, such as magma mixing, source and *P-T* control on melt chemistry and peritectic assemblage entrainment still need to be considered.

3) *Magma mixing*

Janoušek et al. (2004) noted that it is difficult to explain some unusual whole-rock geochemical variations by any model other than magma-mixing (Holub, 1997; Gerdes et al., 2000), but also many linear trends can be interpreted equally well by alternative petrogenetic scenarios (DePaolo, 1981; Chappell et al., 1987; Wall et al., 1987; Albarède, 1995). Radiogenic isotopes may be sensitive indicators of open-system behaviour, but some variation can be attributed to derivation of the magmas from isotopically heterogeneous sources (Gerdes, 2001), or to crustal contamination (DePaolo, 1981). Even in cases in which mixing took place, it could have been a multistage process, or there may have been limited isotopic contrasts between mixing end-members, or both (Bateman, 1995). This level of possible complication makes mixing models difficult to test rigorously, and this tends to decrease their usefulness. It is generally always possible to construct a mixing model if you

use enough mixing end members. Another problem can be with identification of end members. The residual melt within small hybrid masses and enclaves could conceivably undergo chemical exchange with remaining host magma (Pin et al., 1990; Holden et al., 1991; Elburg, 1996; Waight et al., 2000). These uncertainties demonstrate that magma mixing cannot be evaluated merely on geochemical grounds. Therefore this emphasises the combined implications of field relationships, textures, mineral chemistry, the whole-rock and mineral geochemistry of major and trace elements and radiogenic isotopes (Vernon, 1990; 1991; Hibbard, 1991; 1995; Elburg et al., 1995). I shall return to this discussion after reviewing Hf isotopes studies (see Section 8.5.2).

4) Proportions of entrained restitic or peritectic phases

Granitic rock compositions are controlled primarily by the melting reactions in the protoliths (Clemens et al., 2010). At granulite-facies conditions, granitic melts have highly variable K/Na, Na/Ca, Mg# and A/CNK, reflecting variations in source composition and degree of melting. Elements with low solubilities in the melt, but significant concentrations in the reactants, are closely coupled in all crustally derived magmas, because the compositions of the magmas are controlled by the concentrations of the entrained peritectic phases (Clemens et al., 2011; Clemens and Stevens, 2012). These authors suggested that the chemical variability typically exhibited in granitic suites and individual plutons is inherited directly from the protoliths by two main mechanisms: (i) Source control of the melt composition. This defines the granitic character of the magmas and introduces variations in the concentrations of incompatible elements (e.g. K, Rb, Ba and Na), reflecting the compositions and proportions of the tectosilicate reactant minerals in the source, as well as the buffering residual assemblage. These elements commonly show substantial compositional variations at any given bulk-rock MgO + FeO or maficity value, reflecting compositional variations in the protolith; (ii) Peritectic assemblage entrainment control on magma composition. This process accounts for the strong, positive Ti: Mg+Fe correlation that all granitic associations have in common. Importantly, this correlation, while being a fundamental characteristic of granitic rocks is absent among basalts of all types. Thus, this characteristic, interpreted to have been induced by peritectic assemblage entrainment, is a characteristic of the physical behaviour of melts and crystals during partial melting in the crust (Clemens and Stevens, 2012). This

attribute of granitic magmas poses a substantial challenge to the notion that their chemistry is significantly moulded by mixing with mafic to intermediate mantle-derived magmas.

A/CNK ratios in ~ 3200 Ma TTGs including the Nelshoogte TTGs and ~ 3450 Ma TTGs show negative correlations with maficity (FeO^T + MgO) (Fig. 16). Although ~ 3500 Ma TTGs are also paraluminous to metaluminous, they do not show such correlations. These trends for ~ 3450 Ma and ~ 3200 Ma TTGs are similar. According to mechanism (i) above, this trend indicates that ~ 3450 Ma and ~ 3200 Ma trondhjemites are generated have variations controlled by the nature of their protoliths. The likely partial melting reactions consumed biotite and hornblende and produced a peritectic ferromagnesian assemblage dominated by clinopyroxene. The work of Sisson et al. (2005) in which melting begins at higher temperatures and which produced very much more felsic partial melts coexisting with peritectic pyroxenes and garnets (e.g. Beard and Lofgren, 1991; Rapp and Watson, 1995; Rushmer, 1991; Sen and Dunn, 1994). This is essential to producing the characteristic that I-type rocks have of decreasing A/CNK with increasing maficity, extending into the metaluminous range (Clemens et al., 2011). The other modelling of A/CNK vs SiO_2 (Fig. 17) shows plots of the Nelshoogte TTGs and trends (arrows) of mixing between TTGs as the assumed initial melts and peritectic garnet or clinopyroxene (Cpx). The trend of the Nelshoogte TTGs is between the arrow of melt + garnet and the arrow of melt + Cpx. These arrows showing the degrees and compositions of melting, suggest that peritectic minerals for the Nelshoogte TTGs are indeed garnet and clinopyroxene. Nelshoogte trondhjemites/granites would correspond to ~ 90% melt + ~ 10% peritectic garnet and Cpx, and Nelshoogte tonalites/granodiorites would correspond to magmas with ~ 80% melt + ~ 20% peritectic garnet and Cpx.

Ti contents for ~ 3450 Ma and ~ 3200 Ma TTGs show positive correlations with maficity (Fig. 16). According to mechanism (ii) above, the trend for ~ 3200 Ma plutons is similar to typical I-type behaviour, suggesting that the metamafic source produced entrainable peritectic clinopyroxene because hornblende was a major reactant during partial melting. The production of ilmenite or rutile in the peritectic assemblages ensures that entrainment of this assemblage will produce magmas with compositional arrays that mimic the slope of the trend (Ti-maficity array) that is controlled by the compositions and proportions of the reactant biotite and hornblende (Clemens et al., 2011; Stevens et al., 2007). The ~ 3200 Ma TTGs have different trends (Ti vs. maficity) from the ~ 3450 Ma TTGs due to entrainment of

different proportions of peritectic minerals which are the results of variations in the compositions and proportions of reactant biotite and hornblende. The trend might be controlled by different compositions of peritectic pyroxene for ~ 3450 Ma trondhjemites. This also can explain such heterogeneities that magma mixing is not involved. Farina and Stevens (2011) demonstrated that radiogenic isotope variability in granitic magmas is the inevitable consequence of mineral and larger scale isotopic disequilibrium in typical heterogeneous crustal protoliths and the withdrawal of magma batches in a progressive melting process.

Thus, the different trends between TTGs in the Nelshoogte pluton and also between ~ 3200 Ma plutons suggest that there were some different magma batches in the BGGT at ~ 3200 Ma. The ~ 3200 Ma tonalites/granodiorites were plausibly generated by ~ 3200 Ma trondhjemitic melts with the addition of entrained peritectic garnet and clinopyroxene. The diagrams (Fig. 16) suggest that the protolith of the ~ 3200 Ma plutons has a similar composition. However, fractional crystallization and the *P-T* conditions are still allowed to cause the variations. Perhaps, firstly ~ 3200 Ma TTGs were generated and the different magma batches caused by entrained peritectic phases in a deeper magma chamber at higher temperature. The fractional crystallization may be responsible when the magma was cooling after shifting to shallower magma chambers.

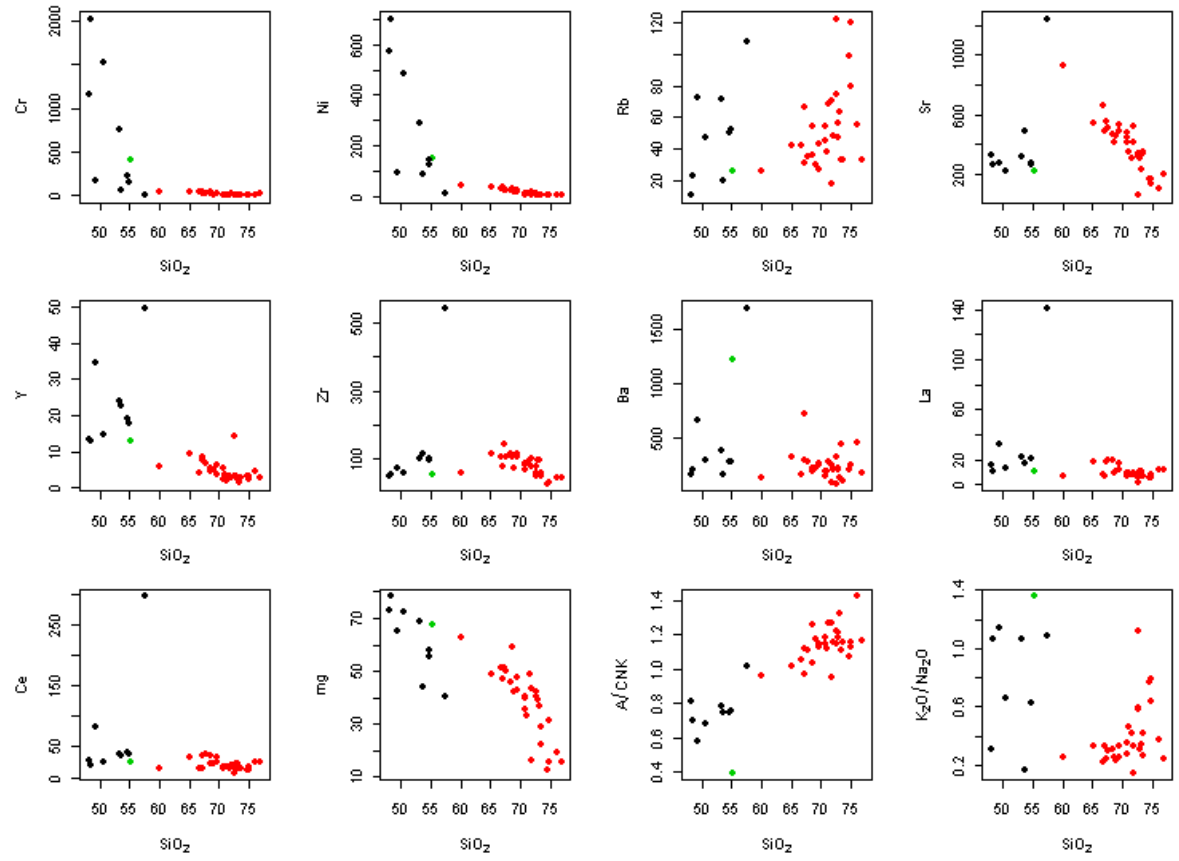

Fig. 15. The variation diagrams of major- and trace-element in Nelshoogte TTGs (red dots), mafic rocks (black dots) and greenstone (green dots) in the Nelshoogte pluton.

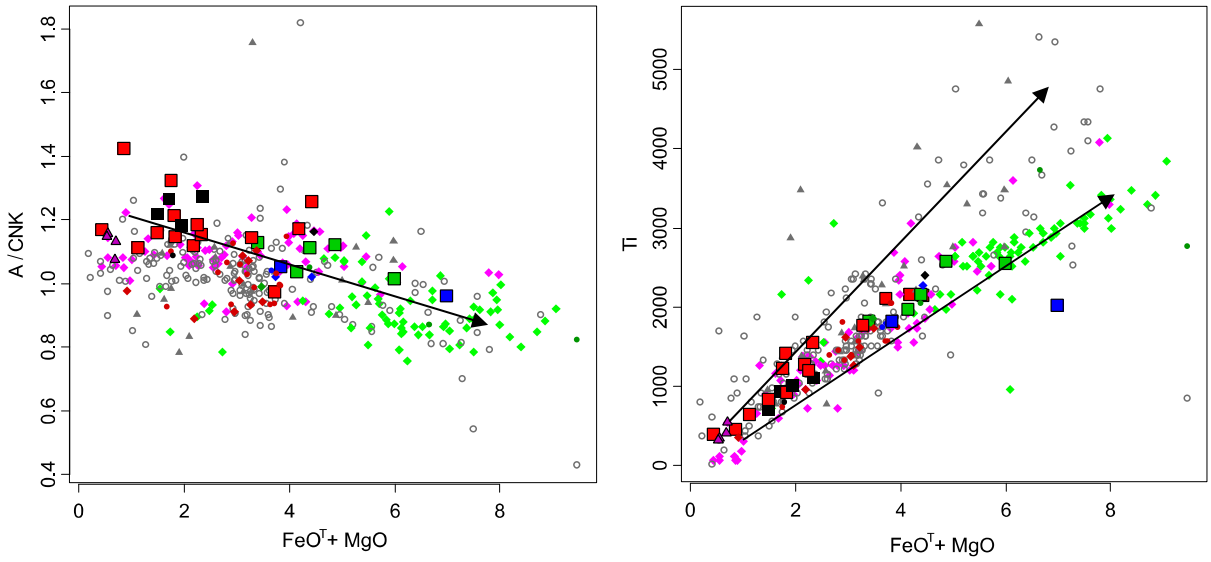

Fig. 16. Major-element modelling, A/CNK vs maficity (left) and Ti vs. maficity (right). Arrows represent mixing between the initial melt and peritectic garnet, clinopyroxene and

ilmenite formed during partial melting of a rock with biotite and hornblende. Symbols are as in Fig. 9.

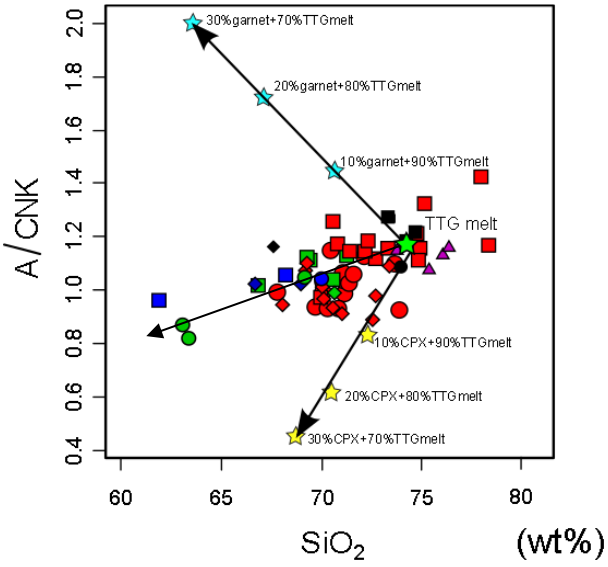

Fig. 17. Major-element modelling, A/CNK vs. SiO_2. Arrows represent mixing compositions of TTG melt + peritectic garnet at 3.8 GPa (light blue stars) (Rapp et al., 1999), TTG melt + clinopyroxene (yellow stars) and the trend of the Nelshoogte TTGs. The starting point (light green star) shows the composition of a Nelshoogte trondhjemite as TTG melt. Symbols are as in Fig. 9a.

8.2.2. Implications of the mineral chemistry and geothermobarometry

Plagioclase

Plagioclase zonation (An_{4-24}) is simply a reflection plagioclase phase relations and the slow rate of diffusion within feldspar crystals in cooling or metamorphic overprint. The core compositions from tonalites/granodiorites are more calsic than the one from trondhjemites. This suggests fractional crystallization in a magma chamber when it was cooling.

Hornblende

The compositions of Al-in-hornblende constrain crystallization pressures of intrusions of 2.6 to 5.9 kbar for the Nelshoogte tonalities/granodiorites and 1.9 kbar for the Kaap Valley granodiorite at 718 °C, 1.7 to 4.7 kbar for the Nelshoogte tonalites/granodiorites and 1.0 kbar for the Kaap Valley granodiorite at 775 °C (Table 9). Here, the temperatures of crystallization were estimated by Yearron (2003), based on the dependence of zircon solubility on melt

composition (Watson and Harrison, 1983). The resulting T_{Zr} values are 718 to 775 °C for the TTG plutons in the BGGT.) Nédélec et al. (2012) also estimated the pressure using Al contents in hornblendes in tonalites from the Nelshoogte pluton, that 4.4 to 5.2 kbar (Schnidit, 1992). This is consistent with the present result of 4.7 to 5.9 kbar for granodiorite 19/6-06C. For other Nelshoogte tonalites/granodiorites estimated pressures are lower (1.7 to 3.7 kbar), based on the lower Al contents of the hornblendes in these rocks.

The calibration is

$$P(kbar)=4.76Al-3.01-[(T°C-675)/85]\times[0.53Al+0.005294(T°C-675)]$$

by Anderson and Smith (1995) using the experimental data of Johnson and Rutherford (1989) and Schmidt (1992).

Biotite

Figure 7 presents the compositional variation of biotites in various rocks from the Nelshoogte and the Kaap Valley plutons. They show no major differences between different rocks, having similar Mg#. This may be because Fe and Mg are easily re-equilibrated in sheet-silicates (Vernon, 1990) or because the biotite only began to crystallize in the mafic end-member after the magma-mixing event (if there was one). There are slight trends in Al and Ti against maficity in different rocks. Ti contents in biotites in the granodiorite/tonalite are higher than in biotites in the trondhjemite. They can be explained by peritectic entrainment (see Section 8.2.1).

Table 10. Pressure estimate.

Sample	P(kbar) **average**	T=718(°C)	T=775(°C)
NLG11R	**2.1**	2.6	1.7
NLG30R	**2.9**	3.4	2.4
NLG35R	**3.1**	3.7	2.6
19/6-11C	**5.3**	5.9	4.7
27.10-01 (Kaap Valley)	**1.4**	1.9	1.0

8.3. Implications of trace-element variations

8.3.1. Causes of trace-element variations

The behaviour of trace-elements depends on the source composition and the residuum with which the magma equilibrated prior to leaving the source if there were no modification of magma compositiojn by mixing, assimilation or crystal fractionation (e.g. Blundy and Wood, 1994; Adam and Green, 2003). Incompatible elements such as the HFSEs (Y, Zr and Nb) and the LREE (La, Ce and Nd) are immobile during low- to medium-grade metamorphism, and are readily accommodated in a variety of minerals. For ~ 3500 Ma and ~ 3450 Ma TTGs in the BGGT, their plots are scattered on Harker diagrams. The trace elements are not so constrained because their concentrations are commonly not buffered by a crystalline phase that contains the element as a major structural constituent. Another factor that contributes to scatter in trace-element concentrations of magmas is the apparently common occurrence of disequilibrium during partial melting (e.g. Bea, 1996). The disequilibrium partial melting may occur by the extreme degree of metamorphism or during the assimilation, suggesting that the slow reaction rates between plagioclase and magma inhibited the dissolution of plagioclase relative to olivine, pyroxene, and opaque oxides (Naslund, 1986).

For the Nelshoogte TTGs, they show tight negative correlations with Cr, Ni, Sr, Zr and Y on Harker diagrams. The different rock phases (trondhjemite, tonalite and granodiorite) represent distinct trends. The fractionation of different minerals results in different trends for the fractionation curves because the different minerals have different crystal-liquid KD values for various elements. For example, tonalites show different trends from trends of granodiorites in Y, Ba, La, Nb and P_2O_5 in the diagrams. The tonalites seem to be cumulates (formed by accumulation of plagioclase crystals) from the trondhjemites, because their REE contents are similar to those of trondhjemites and lower than those of granodiorites. Therefore, the magma of the Nelshoogte tonalites may be caused by accumulation from a parental magma of the Nelshoogte trondhjemites. The enriched compositions of the Nelshoogte granodiorites suggest the magma of the Nelshoogte granodiorites is more enriched than the magma of Nelshoogte trondhjemites. The Nelshoogte granites display distinct trend for Rb and Ba. The different trends in the Nelshoogte TTGs can be caused by different compositions of magmas. Also for ~ 3200 Ma TTGs, the Badplaas domain TTGs and the Kaap Valley TTGs show tight negative correlations with Y and weak negative

correlations with Cr, Ni, Sr, Zr, and Ba. Also, each pluton presents a different trend in Cr, Ni, Sr, Ba, REE, Nb and P_2O_5. The variations of the Nelshoogte trondhjemites/tonalites overlaps with the ranges of the Badplaas TTGs, and the variations of the Nelshoogte granodiorites overlap with the ranges of the Kaap Valley TTGs. These overlaps suggest that the parental magma of the Nelshoogte trondhjemites/tonalites is similar to the magma of the Badplaas TTGs and also the magma of the Nelshoogte granodiorites is similar to the magma of the Kaap Valley TTGs. These variations and similality between the Nelshoogte TTGs and other ~ 3200 Ma TTGs suggest a number of different magma batches, not only one magma batch, were involved in construction of the Nelshoogte pluton. Different magma batches may reflect magmas of other ~ 3200 Ma plutons. Again these variations for ~ 3200 Ma TTGs may be controlled by fractional crystallization, proportion of entrained restitic or peritectic phases, and *P-T* conditions. These different processes might produce different magma batches.

The source composition and the residual assemblage that the magma left behind, as well as the entrainment of peritectic assemblage control the geochemistry. The proportions of entrained restitic or peritectic phases for trace elements are controlled by co-entrainment of the accessory mineral suite. Co-entrainment of the accessory suite controls the concentrations of elements that are hosted within zircon, monazite, xenotime and allanite. This accounts for the fact that elements concentrated in these minerals (e.g. Hf, Zr and REE) correlate positively with compatible major elements that do not reflect their solubilities in the melt, but rather the operation of peritectic assemblage entrainment (Clemens and Stevens, 2012). The negative correlations for Y, La and Zr contents in the Nelshoogte TTGs and other ~ 3200 Ma TTGs in the BGGT are explained by this suggestion that the source compositions control the compositions of TTG. However, the tight trend in the Sr variation for the Nelshoogte TTGs must be caused by fractional crystallization of plasioclase because the trend of CaO can be explained by the fractionation of early plagioclase that the rocks contain.

TTGs exhibit characteristic trace element signatures, with high contents in LREE but very low HREE contents, resulting in high La/Yb ratios. They also show negative Nb–Ta and Ti anomalies; Nb/Ta and Lu/Hf ratios are low while Zr/Sm ratios are high. The lack of both Eu and Sr anomalies associated with the low HREE content are interpreted as reflecting the presence of garnet and amphibole as well as the lack of plagioclase, either as residual or fractionating phases; such that, most often, a high-pressure origin has become implicit in the term ‘Archaean TTG’ (Champion and Smithies, 2003). In this respect too, this trace-element

signature makes TTG rocks different from modern continental crust, which has both higher HREE contents, and negative Eu, Nb–Ta, Sr and Ti anomalies (Moyen and Martin, 2012). As the TTGs are likely to be derived from mafic source rocks, they probably arise by relatively low-proportion partial melting. In this scenario, with a greater volume of residuum than melt, the mineral assemblage in the residuum exerts a very strong influence on the trace-element chemistry of the melt (Foley et al., 2002, 2003; Rapp et al., 2003; Smithies, 2000; Moyen and Martin, 2012).

The multi-element (spider) diagrams and the REE patterns of Nelshoogte TTGs are similar to ~ 3450 Ma and other ~ 3200 Ma TTGs in the BGGT, represents negative Ti–Nb–Ta anomalies, high La/Yb ratio, low Yb abundances and moderate to high Sr/Y at low Y abundances that are signatures of typical Archaean TTG (Figs. 10 and 11). (However, this does not explain the negative Ba anomalies with respect to Rb and Th. One explanation for this could be that this feature is a hydrothermal overprint.) These signatures of typical Archaean TTGs are a result of the influence of certain minerals, particularly garnet and plagioclase. HREE are readily accommodated into garnet. Therefore, depletion in the HREE (i.e. Yb_N values = 1 to 10; Rapp et al., 1991) suggests that these magmas left a source residuum containing abundant garnet. However, the ~ 3500 Ma pluton (Steynsdorp) shows relatively undepleted HREE signatures (Yearron, 2003; Clemens et al., 2006). These imply that garnet had little influence, and that the restite produced during the generation of these oldest magmas was garnet-poor, and therefore that melting occurred at lower P, in crust that was then not as thick as later. There are small positive or no Eu anomalies in the Nelshoogte TTGs. Eu is readily accommodated into plagioclase, so these signatures suggest that plagioclase did not fractionate from these magmas. Also, high Sr contents in these rocks suggest that there was no plagioclase in the residuum. Thus, TTGs in the Nelshoogte pluton were derived from melting of hydrous mafic crust at pressures commonly above 12 to 15 kbar where garnet is stable but plagioclase is not (Moyen and Stevens, 2006).

Most of the 3200 Ma TTGs in the BGGT display similar patterns in the multi-element (spider) diagrams. However, the Nelshoogte and the Kaap Valley tonalites/granodiorites show more enriched REE patterns than the Nelshoogte and the Badpaas trondhjemites/granites. It seems likely that the magmas of 3200 Ma plutons are from similar sources, and that their internal variations are explained by *P-T* condition (see Section 8.3.1) and/or proportion of entrained restitic.

Also, experimental studies of partial melting of amphibolite by different *P-T* condition can explain the trace-element variations. This earlier suggestion by Yearron (2003) and Clemens et al. (2006) that TTG compositions from the BGGT mostly represent unevolved melt compositions. Moyen and Stevens (2007) modelled the differentiation of a ca. 65% SiO_2 tonalite, using three different mineral assemblages and explain that if fractionation played a role in the geochemical evolution of the Barberton TTGs, it was only minor. The geochemical trends for at least some of the plutons are explained by late fractionation (amphibole + plagioclase), probably reflecting liquid-crystal separation during emplacement. It is also unable to change low-Sr rocks into high-Sr rocks and can also not account for the high Sr/Y values in the (high-Sr) trondhjemites, as the fractionation of amphibole + plagioclase has no noticeable effect on Sr/Y values of the melts. It is also possible that the high-Sr (and high Sr/Y) signature of some deeply generated trondhjemites was enhanced by some high-pressure fractionation.

Consequently, the compositions of TTGs from the BGGT mostly represent unevolved melt compositions. The trace-element variations and enriched LREE- and depleted HREE-patterns resemble those of ~ 3450 Ma plutons and other ~ 3200 Ma plutons in the BGGT. This suggests that the magma sources of the Nelshoogte pluton are garnet-rich amphibolites, like the sources of ~ 3450 Ma plutons and other ~ 3200 Ma plutons in the BGGT. The Nelshoogte trondhjemites/tonalites are similar to the Badplaas domain TTGs, and the Nelshoogte granodiorites are similar to the Kaap Valley tonalites/granodiorites. The Nelshoogte TTGs represent similarities to other 3200 Ma TTGs, and different trends and patterns in the diagrams. This suggests that there were different magma batches, involved with other ~ 3200 Ma plutons around the Nelshoogte pluton.

8.3.2. Implications for pressure indicators

Some trace elements (REE, Sr, Y, Nb and Ta) are extremely sensitive to the pressure of melting and are partitioned in markedly different ways in eclogitic (garnet-clinopyroxene-rutile) or amphibolitic (amphibole-plagioclase-ilmenite) assemblages (Martin, 1994; Foley et al., 2002; Klemme et al., 2002; Rapp et al., 2003; Xiong et al., 2005; Moyen and Stevens, 2006; Moyen, 2009). It is also known that the nature and modal proportion of mineral phases

is modified by pressure (e.g., plagioclase is destabilized and garnet stabilized at higher pressures).

Figure 18 compares the La/Yb and Sr/Y ratios of Nelshoogte TTGs and other plutons in the BGGT. The Nelshoogte TTGs show a wide range of La/Yb and Sr/Y ratios, but most of samples plot in the middle of the range, similar values to other TTGs. There are no apparent differences between trondhjemites and tonalites. The granodiorites show slightly lower La/Yb, Sr/Y ratios and higher Yb_N, Y value. This highlights the fact that the TTG suite has low Yb_N and Y values and highly evolved $(La/Yb)_N$ and Sr/Y ratios, typical of Archaean TTGs (Martin, 1986). The arrows on the diagrams represent batch-melting trends for Archaean tholeiites that produce restite compositions of amphibolite, and 7–30% garnet-rich amphibolite or eclogite, as modelled by Atherton and Petford (1993), Martin (1986), Drummond and Defant (1990) and Petford and Atherton (1996). Using the literature-derived trends as a guide, it appears that the TTG suite could have been derived through partial melting of a primitive basaltic source, producing an amphibolitic or eclogitic restite with > 30% garnet (Clemens et al., 2006) (Fig. 18). According to $(La/Yb)_N$ and Sr/Y ratios, the source rock for the Nelshoogte TTGs might typically be an amphibolite containing 10 to 30 % garnet.

REE, Sr, Y, Nb and Ta can indicate the pressure of melting of source rock as described above. However, the Nelshoogte TTGs have variable Sr contents and the boundaries between pressure groups are unclear. In Figure 18, the Nelshoogte TTGs plot in an overlap area that belongs to both the high- and medium-pressure groups. Some additional models from Moyen (2011) were also tested using other trace elements to indicate the pressure of melting (Figs. 19 and 20). In the Nelshoogte pluton, trondhjemites/granites plot in the field for the high-pressure group, indicating P > 25 kbar. The granodiorites plot with the medium-pressure group, indicating P from < 10 to < 25 kbar. Although, La/Yb ratios for tonalites indicate lower pressure than the pressure of trondhjemites and granodiorites, in other plots the tonalites fall in the fields for both high- and medium-pressure groups. The tonalites can also belong to high-pressure group because they must be cumulates of trondhjemites. For other plutons in the BGGT**,** ~ 3500 Ma TTGs plot in the low-pressure field, indicating P < 10 kbar. The ~ 3450 Ma TTGs plot with the high-pressure group, indicating high pressure, and ~ 3200 Ma TTGs indicate high and medium pressure (Moyen and Stevens, 2006; Moyen, 2011).

Furthermore, a recent experimental study (Laurie and Stevens, 2012) suggests that melt generation by high-pressure H_2O-present partial melting of an eclogitic source appears to be a viable petrogenetic model for the formation of the high-pressure trondhjemites, which constitute a component of the Paleo- to Meso-Archaean sodic continental crust. The experimental glasses produced by high-pressure (1.9 to 3.0 GPa) H_2O-present partial melting of an eclogite-facies metabasalt have a peraluminous trondhjemitic composition and their chemical compositions are similar to ~ 3200 Ma trondhjemite in the BGGT. More broadly these experimental melt compositions match the chemical properties of high-pressure-type Archaean TTG, defined by Moyen (2011), in terms of most major, trace and RE elements. In Figure 18, the ranges of melt compositions from Laurie's eclogitic source overlap the compositions of the Nelshoogte trondhjemites. They suggest that the source rock of those trondhjemites is eclogitic and that these magmas were produced by high-pressure H_2O-present partial melting.

However, as discussed above, the source of the Nelshoogte TTGs is also suggested as an amphibolite containing 10 to 30 % garnet. This can be applied for the Nelshoogte granodiorites, suggesting the partial melting by medium pressure. The geodynamic scenario of the medium-pressure type granodiorites must not the same as the high-pressure trondhjemites.

Thus, the source of ~ 3200 Ma plutons appears to resemble similar sources of gneisses from ~ 3450 Ma plutons in the BGGT. However, Archaean TTG gneisses do not show clear-cut compositions characteristic of different pressure groups, which is why defining the exact pressure group of melting is difficult for these rocks. These models, combined with Moyen (2011) indicate that the Badplaas domain TTGs and the Nelshoogte trondhjemites/granites/tonalites belong to the high-pressure group, granodiorites in the Nelshoogte and the Kaap Valley plutons to the medium-pressure group (Figs. 18, 19 and 20). The Badplaas domain TTGs and the Nelshoogte trondhjemites must originate through high-pressure H_2O-present partial melting of an eclogitic source, and the Kaap Valley granodiorites/tonalites and the Nelshoogte granodiorites must originate through medium-pressure partial melting of an amphibolitic containing 10-30 % garnet.

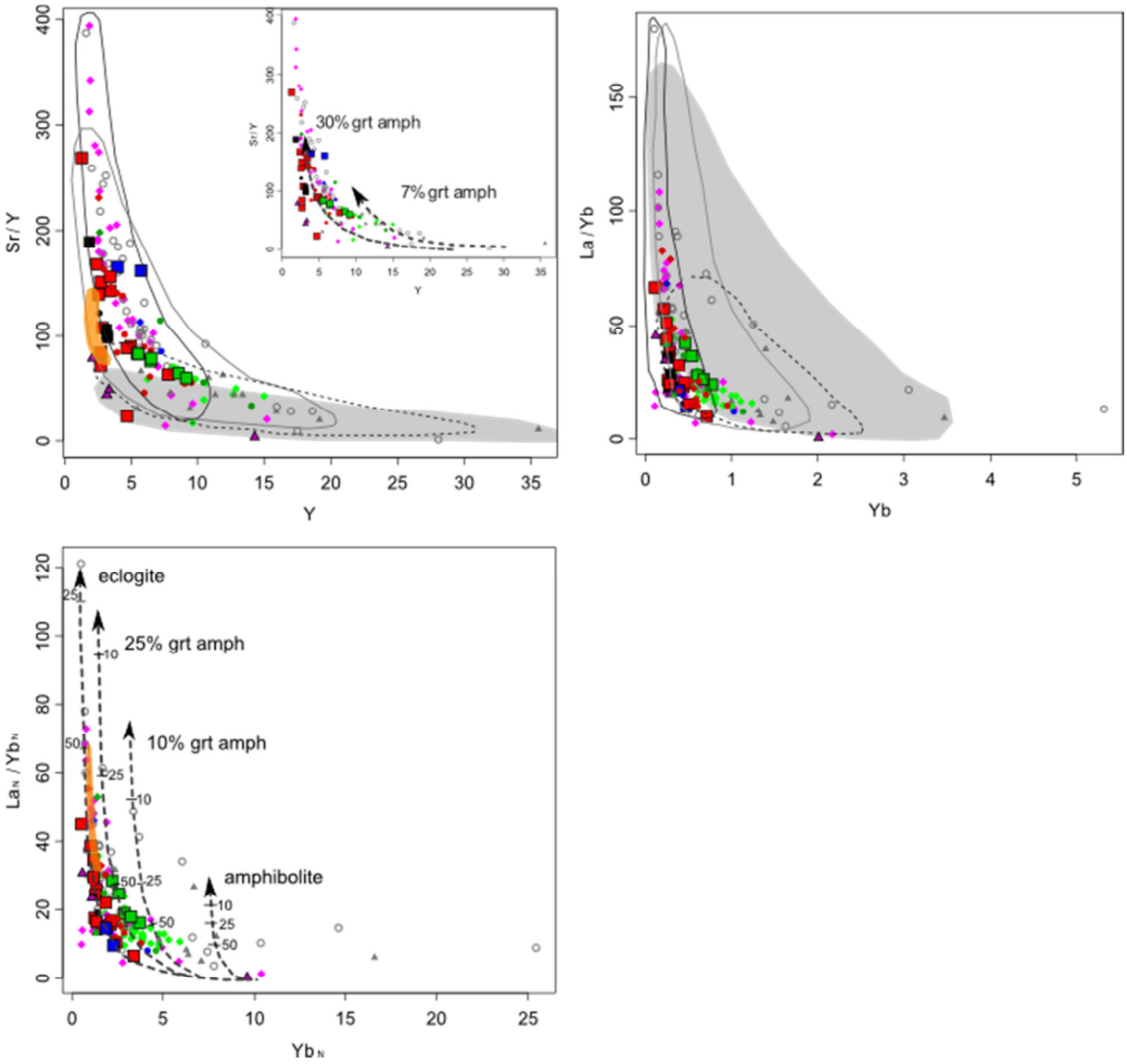

Fig. 18. Trace- and rare earth-element modelling, Sr/Y vs. Y, La/Yb vs. Yb and La_N/Yb_N vs. Yb_N. The low-pressure region is outlined by a dashed line, the medium pressure group is outlined in grey, the high pressure group is outlined in black, and potassic samples are indicated by grey shading (adapted from Moyen, 2011). Arrows represent the calculated melt compositions of Archaean tholeiites with source mineralogies of amphibolite, 7–30% garnet-rich amphibolite or eclogite (adapted from Petford and Atherton, 1996 and Moyen and Martin, 2012). Numbers on each arrow indicate the degree of melting or of fractional crystallisation (Moyen and Martin, 2012). Ranges of the compositions of experimental glasses produced by high-pressure (1.9–3.0 GPa) H_2O-present partial melting of an eclogite-facies metabasalt (Laurie and Stevens, 2012) are shown as orange bars. Symbols are as in Fig. 9.

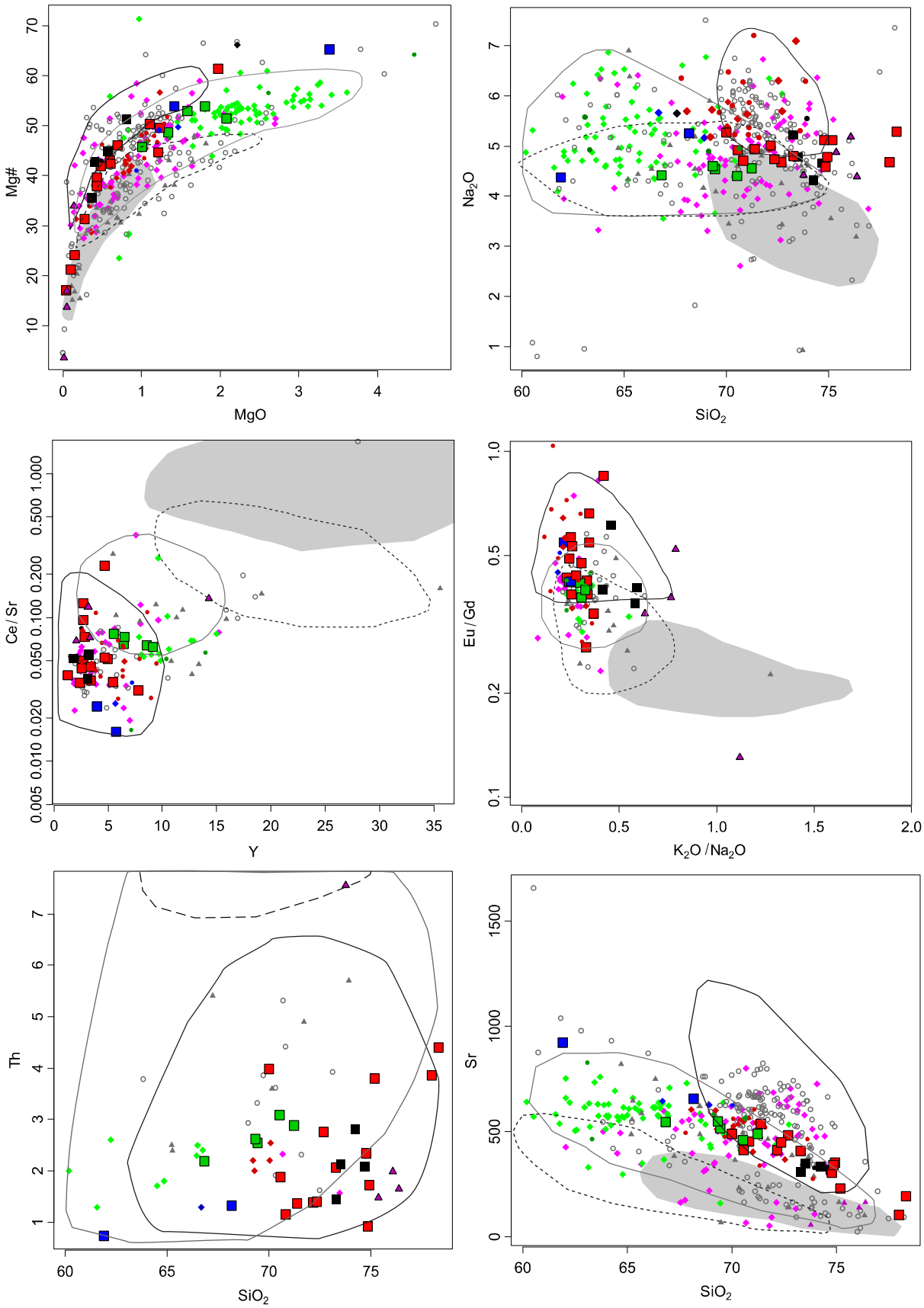

Fig. 19. Trace- and rare-earth-element modelling. In all diagrams, the low-pressure field (LP) is outlined by dashes, the medium-pressure field (MP) by a grey outline, the high-pressure

(HP) field by a black outline, and potassic samples by a grey field, adapted from Moyen (2011). Symbols are as in Fig. 9.

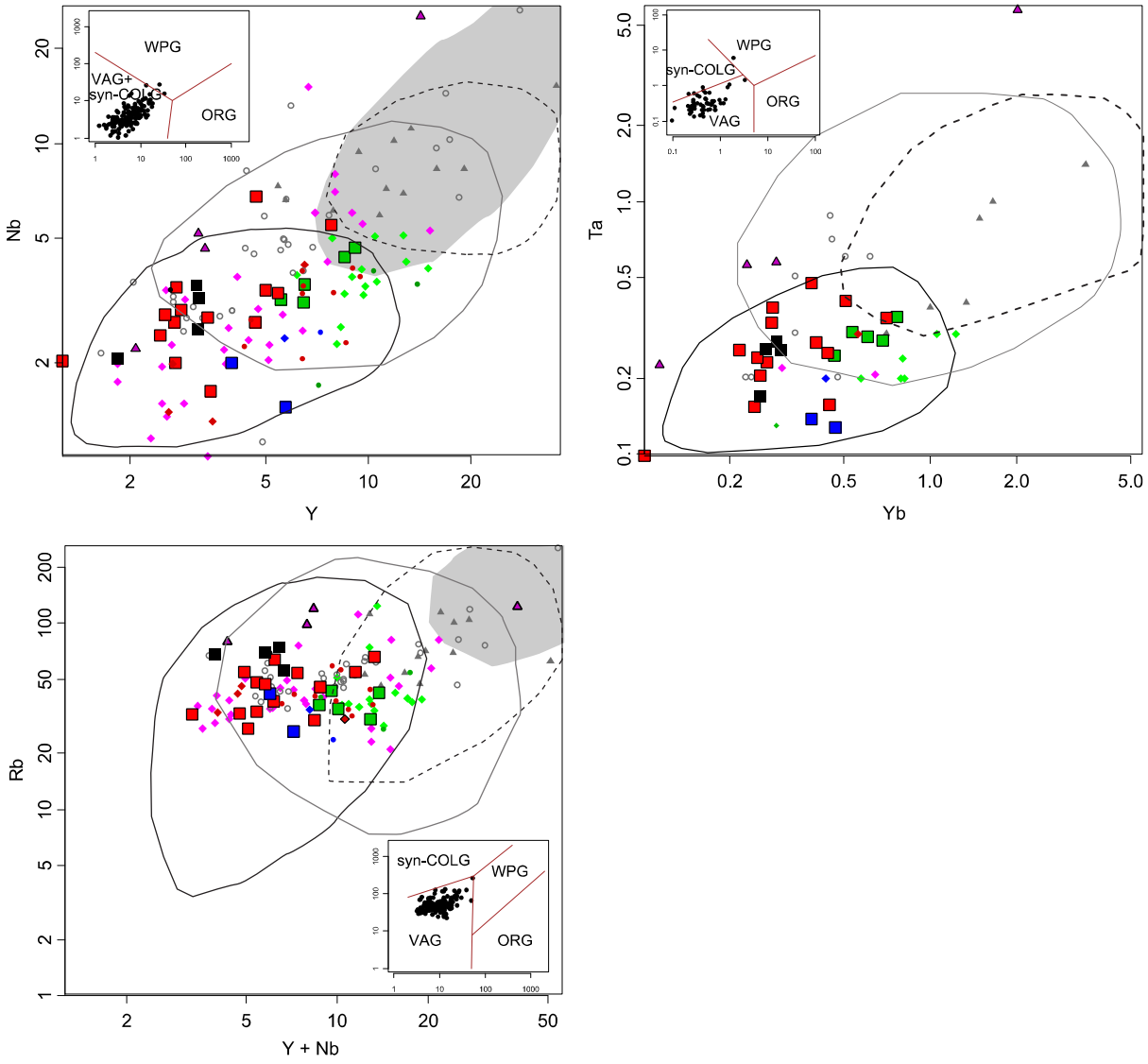

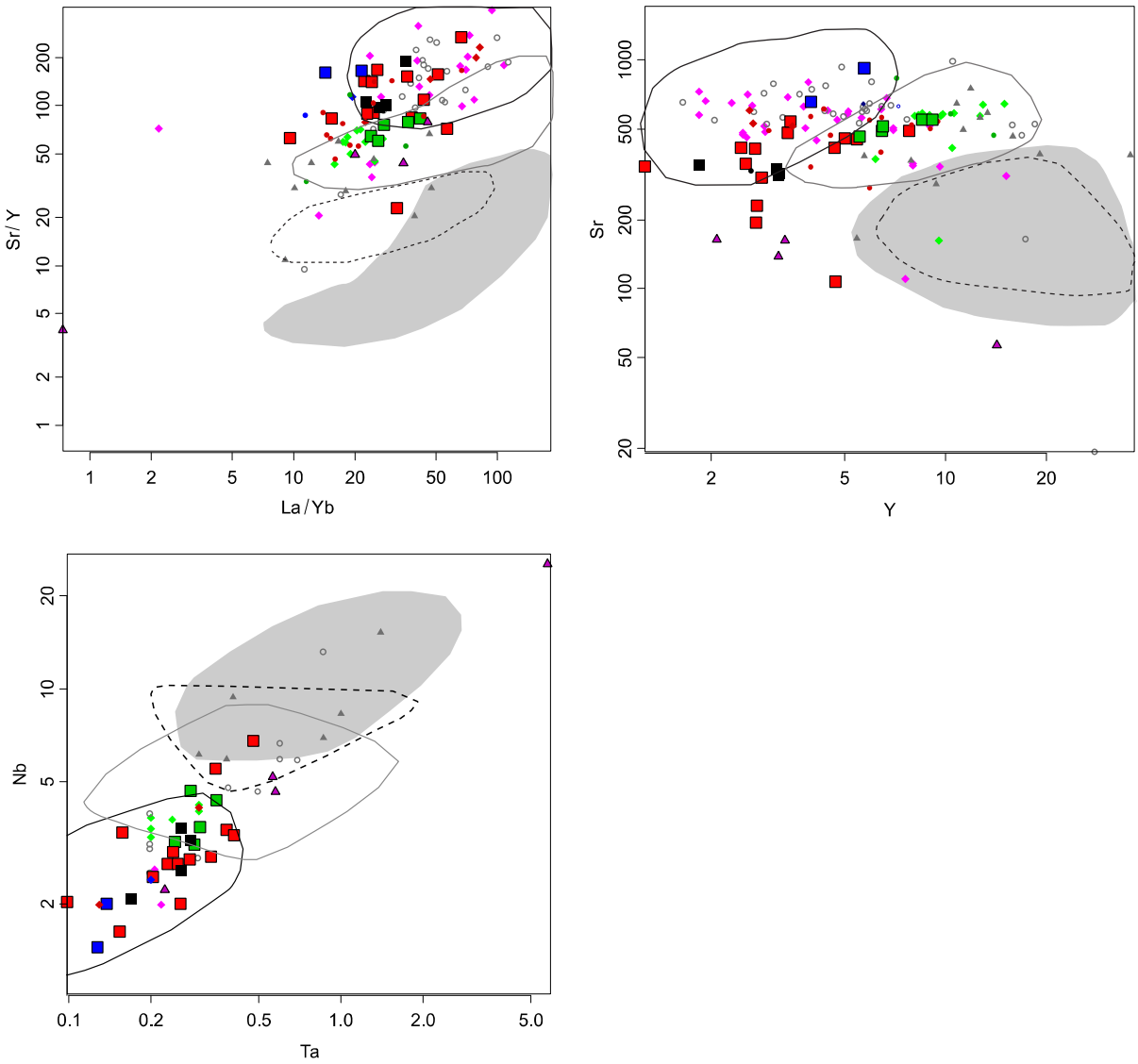

Fig. 20. Trace- and rare-earth-element modelling. In all diagrams, the low-pressure field (LP) is outlined by dashes, the medium-pressure field (MP) by a grey outline, the high-pressure (HP) field by a black outline, and potassic samples by a grey field, adapted from Moyen (2011). Symbols are as in Fig. 9. VAG, volcanic arc granite; COLG, collision granite; WPG, within plate granite; ORG, ocean ridge granite.

8.3.3. Implications of the HFSE contents

Nb and Ta contents are largely controlled by the presence of rutile at high pressures and ilmenite at low pressures during partial melting of metabasaltic sources. Foley et al. (2002) suggest the trace-element characteristics of low Nb/Ta and Nb/La and high Zr/Sm, can be explained by partial melting of amphibolite in the subducting slab where amphiboles have

relatively low Mg#, but not by melting of Mg-rich amphibolites or eclogites in the lower parts of thick oceanic crust. Nb/Ta in the melt is controlled by the Mg# and titanium concentration of the amphiboles during melting of amphibolites. The high Mg# of amphiboles from mantle wedge assemblages above subducting slabs prevents fractionation of Nb from Ta. In contrast, the low-Mg#, low-Ti amphiboles may cause the low Nb/La and low Nb/Ta signatures of arc magmas and crystallize from slab-derived, silica-rich aqueous fluids at high fluid-rock ratios. However, based on the same approach, but with a low Nb/Ta basaltic source (common in the Archaean record), Rapp et al. (2003) arrived at the opposite conclusion that the Archaean TTG residue can be eclogitic.

Rapp et al. (2003) estimate that rutile-TTG melt D values are ~ 55–60 for Nb, and 85–90 for Ta, with a $D^{Nb/Ta} \approx 0.68$, comparable to previous estimates 25 of $D^{rutile/melt} \approx 27$ for Nb and $D^{rutile/melt} \approx 44$ for Ta, with a $D^{Nb/Ta} \approx 0.60–0.67$. It appears that the $D^{rutile/melt}$ used in Foley et al. (2002) in modelling melting of rutile-bearing eclogite were much higher, especially for Nb; combined with a starting material with an assumed chondritic Nb/Ta ratio, their calculations suggested that partial melting of rutile-bearing eclogite would result in TTG liquids with superchondritic Nb/Ta. However, that the subchondritic Nb/Ta ratios of their experimental eclogite residues are comparable to those of rutile-bearing eclogites previously interpreted as being residues from TTG magma generation (Jacob and Foley, 1999; Barth et al., 2001).

Hoffmann et al. (2011) noted that rutile and amphibole play major roles in controlling these ratios because these two phases exhibit oppositional partition coefficient ratios for D_{Nb}/D_{Ta} and D_{Zr}/ D_{Sm} (e.g., Foley et al., 2002; Rapp et al., 2003). However, as discussed above, the partitioning behaviour of Nb and Ta for amphibole remains uncertain. Following Foley et al. (2002) D_{Nb}/D_{Ta} in amphibole is >1, whereas Nb–Ta partition coefficients determined between amphibole and tonalitic melts by Klein et al. (1997) are equal, within error, suggesting no fractionation of the two elements by residual amphibole. The presence of a Ti phase in the residues of TTGs (i.e., rutile, titanite or ilmenite) is suggested by the pronounced negative Ti, Nb and Ta anomalies. The stability of rutile is controlled by (1) the *P–T* conditions during melting, (2) the degree of partial melting, (3) the bulk composition of the protolith and (4) the H_2O content of the mafic protolith (e.g., Green and Pearson, 1986; Ryerson and Watson, 1987; Klemme et al., 2002; Xiong et al., 2006, 2011). At lower pressures, it is likely that ilmenite (e.g., Martin, 1987) or titanite (e.g., John et al., 2011) and amphibole are present,

whereas at pressures exceeding 1.5 GPa, rutile is dominant (e.g., Zack et al., 2002; Xiong et al., 2006; John et al., 2011).

Laurie and Stevens (2012) suggest that the ~ 3200 Ma trondhjemite magmas in the BGGT might have been produced through high-pressure H_2O-present partial melting of an eclogitic source. Also, the Nelshoogte trondhjemites/tonalites represent high pressure of partial melting (see Section 8.3.2). Therefore, it is better to apply the compositions of the high-pressure type Barberton TTGs to the study of Rapp et al. (2003). In Figure 19, most of Nelshoogte TTGs have lower Nb/Ta and higher Zr/Sm ratios and higher Sr contents, corresponds to eclogitic melt (AB-1 by Rapp et al., 2003). Therefore, the source of TTGs in the BGGT may be rutile-bearing eclogitic melt.

For the Nelshoogte granodiorite and the Kaap valley tonalites/granodiorites, suggesting partial melting by medium-pressure, the source must be amphibolitic. Therefore, Foley et al. (2002) should be referred. In Figure 19, Nelshoogte granodiorites have lower Nb/Ta and higher Zr/Sm ratios, corresponding to Foley's 10% of partial melting of amphibolitic source. Some of Nelshoogte TTGs and especially Kaap Valley tonalites/granodiorites have higher Nb/Ta ratio, corresponding to Foley's eclogitic source. These features of HFSE indicate that these medium-pressure rocks reflect the different (eclogitic) melt from the original (amphibolitic) melt or different conditions during melting.

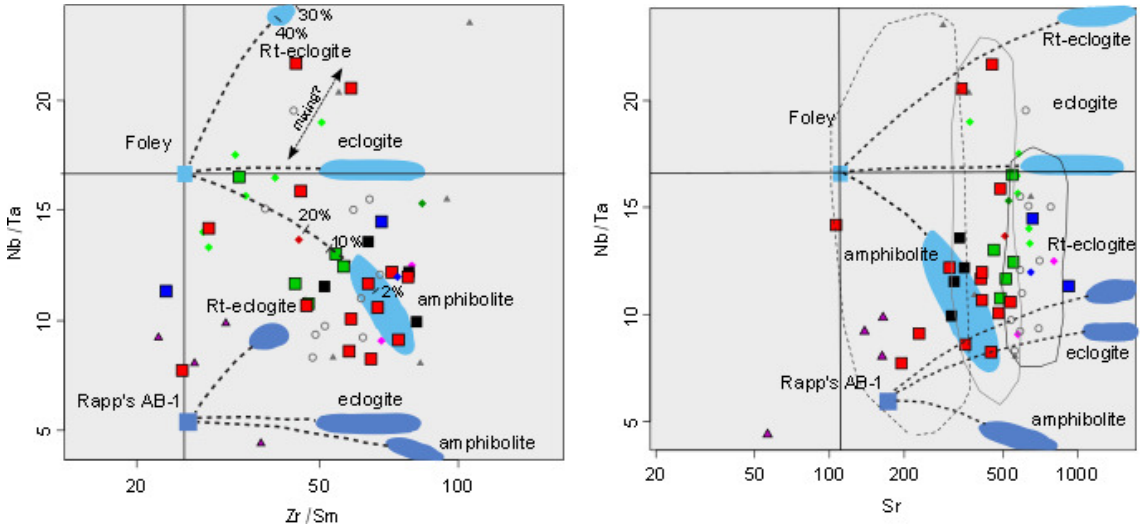

Fig. 21. Nb–Ta systematics. Composition of TTGs from the Nelshoogte pluton and other plutons in BGGT in Nb/Ta vs. Zr/Sm (left) and vs. Sr (right) diagrams. Melting models

(Foley et al., 2002) are overlaid on the diagram, using either Foley's source (light blue square, light blue arrays) or Rapp et al. (2003)'s source AB-1 (blue square, blue arrays). Each of the three models (rutile-eclogite, rutile-free eclogite and amphibolites) is indicated by an array. Numbers on each array indicate the degree of melting (Foley, 2008; Hoffmann, 2011). Symbols are as in Fig. 8.

8.4. Timing of Nelshoogte TTG magmatism in the BGGT

The U-Pb zircon dating shows that each sample has wide range of values except sample NLG35R (tonalite). These data indicates that the initial magmatic may event happen around 3230 Ma in the Nelshoogte pluton. Therefore, the different ages between each phase are within the error different. The concordia ages are inferred as between ca. 3240 and 3210 Ma (Table 7 and Fig. 14).

The period of the magmatism of the Badplaas domain was long (ca. 60 Myr) (Kisters et al., 2010). The spread of ages indicate provably they are overprinted by high temperature of several magma batches such as Badplaas domain plutons and the Kaap Valley pluton, surrounding the Nelshoogte pluton. The U-Pb zircon dating from this study indicates the ages of the magmatism of the Nelshoogte pluton is younger than the inferred U-Pb ages of the Batavia and the Rooihoogte plutons in the Badplaas domain and similar to the ages of younger Badplaas trondhjemite and the Kaap Valley pluton (Fig. 22).

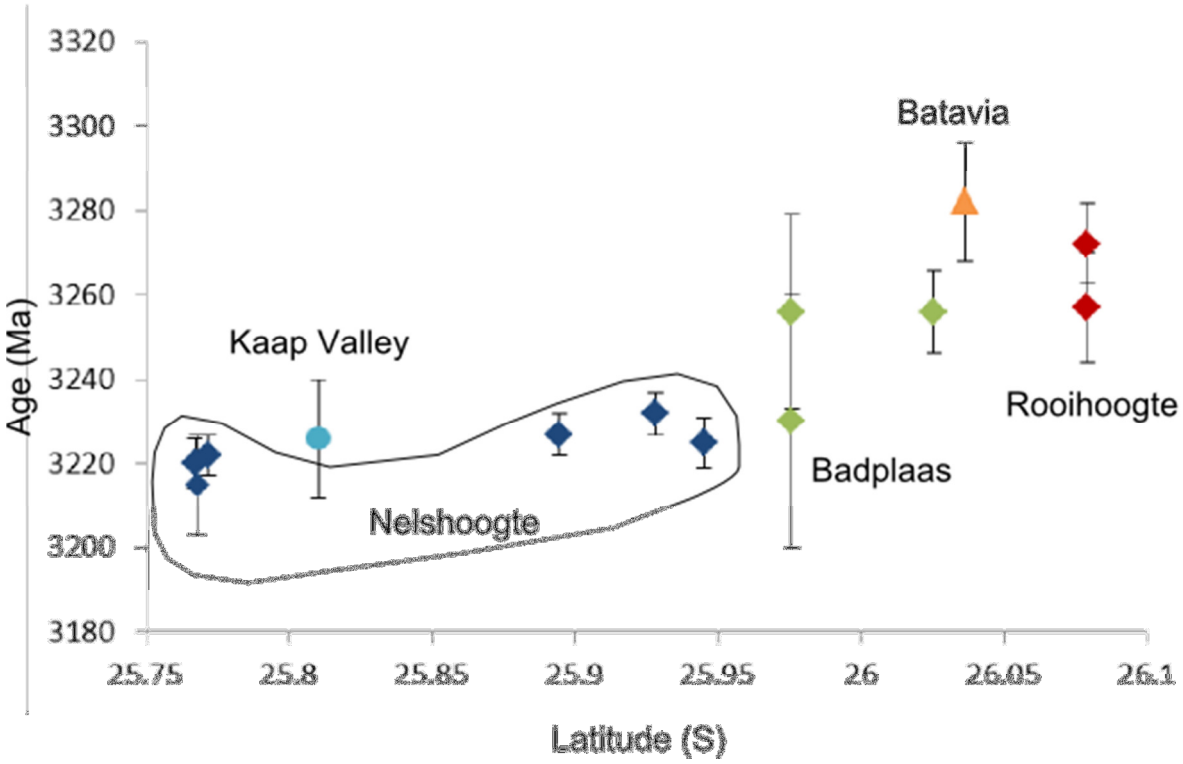

Fig. 22. Age ($^{207}Pb/^{235}U$) vs. latitude. Nelshoogte pluton; blue diamond, Kaap Valley pluton; light blue circle, Badplaas pluton; green diamond, Rooihoogte pluton; red diamond, Batavia pluton; orange triangle (Armstrong et al., 1990; Kisters et al., 2010).

8.5. Petrogenesis of the Nelshoogte pluton

Here, the various petrogenetic models are expanded and tested using the existing knowledgebase on the geodynamic evolution of the proto-Kaapvaal craton at 3300 to 3200 Ma, to arrive at an understanding of why this is the last significant TTG pluton to form and why, following 3200 Ma, crustal magmatic processes switched to producing more potassic calc-alkaline series felsic magmas. Are the source rocks for TTG magmas oceanic crust or arc volcanic rock (greenstone belt rocks)? These discussion leads to improved understanding of the petrogenesis of the BGGT and Archaean TTGs in general.

8.5.1. Interpretation of the Hf isotopes

T_{DM} model ages by U-Pb and Lu-Hf datasets represent the time of extraction of the protolith from a Depleted Mantle. The T_{DM} model ages of ca. 3330 - 3230 Ma indicate that the source

rocks of the Nelshoogte TTGs are 20 to 100 Myr before the crystallisation of the pluton (ca. 3240 - 3210 Ma) (Tables 8 and 9, Figs. 23 and 24). The εHf(t) values and T_{DM} ages for all samples can also be the same witin errors. So it is impossible to find any difference between trondhjemite and tonalite for their Hf isotopic data as well as the U-Pb ages (Fig. 24).

Radiogenic Nd values suggest that the Barberton TTGs were derived from juvenile crustal sources with depleted-mantle signatures. The similarity between the εNd values of the ~ 3450 Ma plutons and the Lower Onverwacht greenstone sequences implies that the greenstone material could be the source-rock of these magmas (Kröner et al., 1996; Yearron, 2003; Sanchez-Garrido, 2012). For ~ 3200 Ma plutons Moyen and Stevens (2007) explain that the relatively enriched signature of 3230–3210 Ma Nelshoogte and 3227 Ma Kaap Valley TTGs could reflect a composite source, consistent with derivation from an enriched mantle source (the Supergroup/supracrustals in the BGB) (Kröner and Tegtmeyer, 1994; Kröner et al., 1996) or from part of the Onverwacht crust (Hamilton et al., 1979).

The Supergroup (ca. 3550–3210 Ma) in the BGB is comprised of three stratigraphic units, which are from the bottom to the top: the Onverwacht Group, Fig Tree Group and Moodies Group. The Onverwacht Group is interpreted to have been deposited in a deep to shallow marine environment between 3550 and 3250 Ma (Lowe and Byerly, 2007; Lowe, 1982), and consists of metamorphosed ultramafic lavas (e.g. komatiites, komatiitic basalts) and mafic lavas (tholeiites), with minor felsic volcanic (dacitic to rhyolitic calc-alkaline) and sedimentary material. The Fig Tree Group, dated at 3260–3223 Ma (Kröner et al., 1991; Byerly et al., 1996), conformably overlies the Onverwacht Group. This group is rich in felsic volcanic and volcaniclastic material, interpreted to have been deposited in a deep (north of the Inyoka fault) to shallow (south of the Inyoka fault) marine environments.

The T_{DM} ages of the Nelshoogte pluton are consistent with ca. 3550–3210 Ma Barberton Supergroup. However, the Nd isotope and Hf isotope studies by Sanchez-Garrido (2012) suggest that the Barberton TTGs (especially for the Kaap Valley samples) and Moodies clasts originate from a different source. Therefore the source rocks of the pluton must originate from oceanic crusts of the Onverwacht and/or the Fig Tree Group.

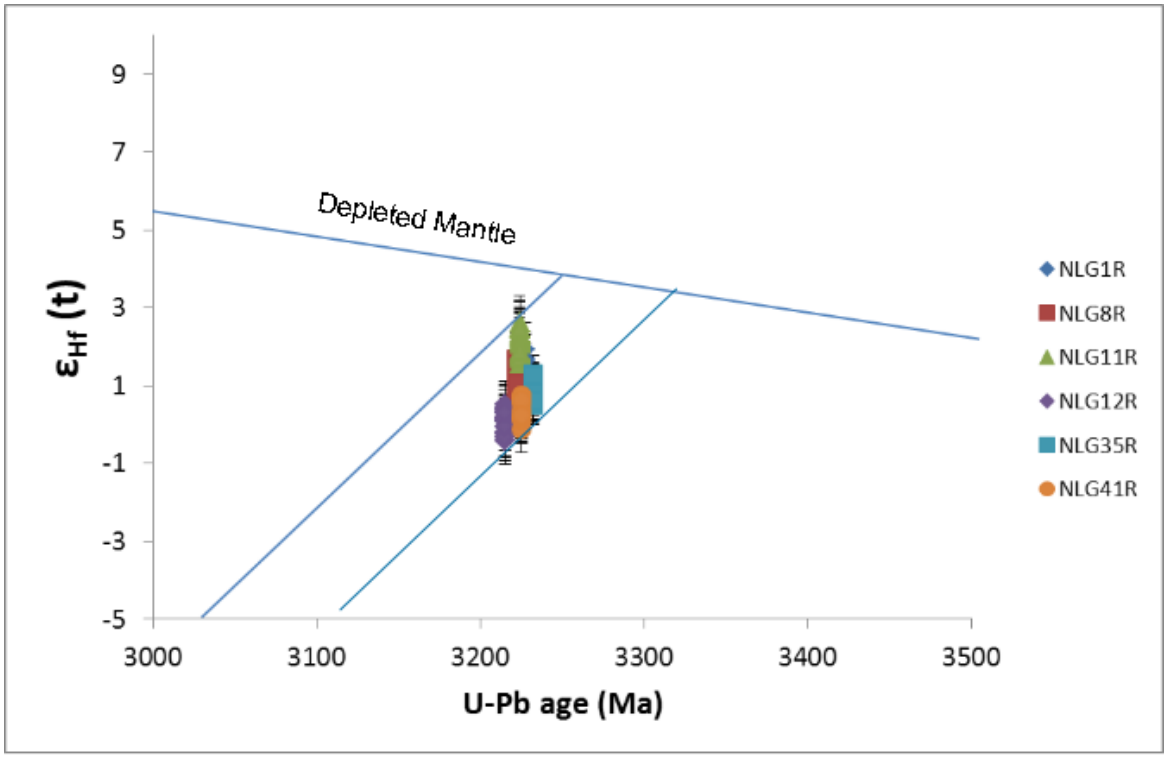

Fig. 23. εHf(t) vs. U-Pb zircon age.

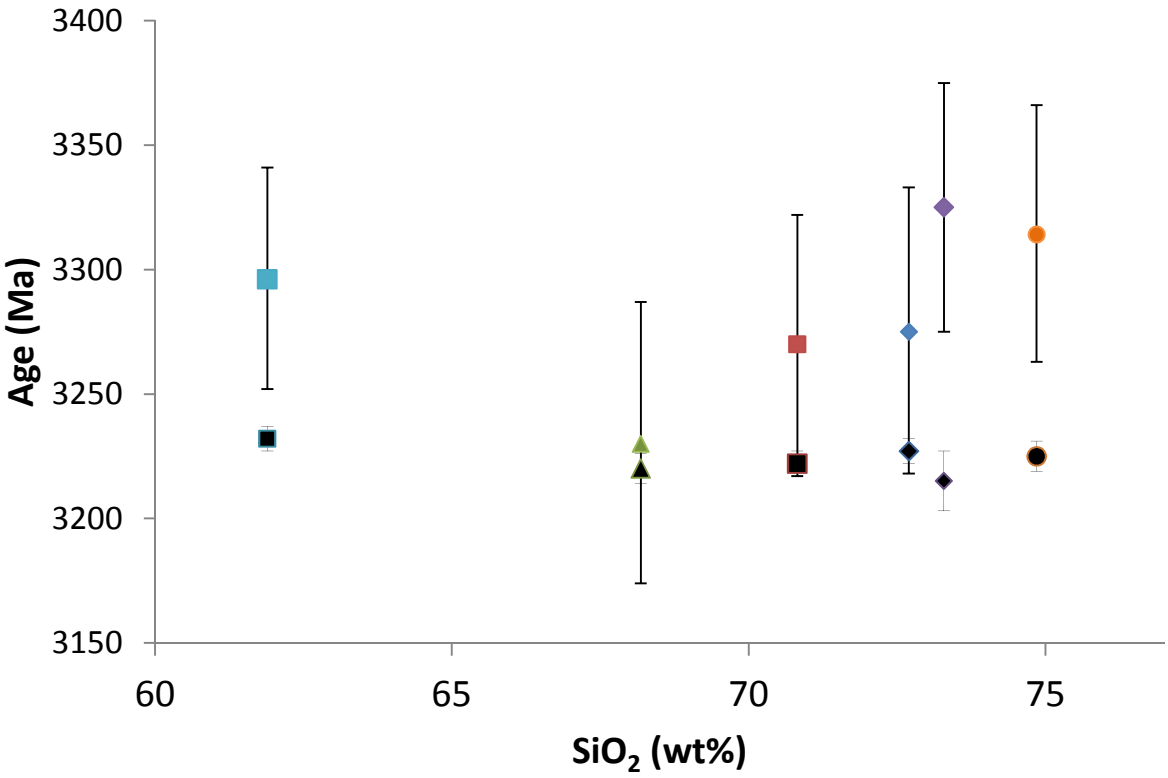

Fig. 24. U-Pb age and Hf isotope age vs. SiO_2. Symbols are as in Fig. 23 represent Hf isotope ages. Black symbols represent U-Pb ages for each sample.

8.5.2. Implications for the geochemistry of ~ 3200 Ma plutons in the BGGT

In the BGGT, different trace element contents in each generation represent that ~ 3500 Ma plutons were generated by low pressure (shallow source), ~ 3450 Ma plutons are high pressure (deep source) and ~ 3200 Ma plutons are both high and medium pressure (Moyen and Stevens, 2006; Moyen et al., 2007; Moyen, 2011). ~ 3200 Ma plutons in the BGGT consist of the Badplaas domain (3270-3260 Ma Rooihoogte pluton, 3290-3230 Ma Badplaas pluton, 3280 Ma Batavia pluton) and the Kaap Valley domain (3234-3215 Ma Nelshoogte pluton and 3227 Ma Kaap Valley pluton) (Fig. 1).

Only ~ 3200 Ma plutons in the BGGT show tight trends with Al_2O_3, MgO, TiO_2, CaO, FeO^T, HREE, P_2O_5, Mg# and A/CNK against silica or maficity (see Section 6, Figs. 9, 10 and 16). However, all the patterns in their multi-element diagrams for Barberton TTGs are similar. So they originate from similar common source. The trends are dominantly caused by proportions of entrained peritectic phases and/or the *P-T* conditions at deeper depth (and minor fractional crystallization at shallower depth). These major- and trace-element variations of the Nelshoogte TTGs are plotted on the ranges that are represented by ~ 3200 Ma TTGs from the Badplaas domain and the Kaap Valley TTGs. The Nelshoogte trondhjemites/granites are similar to the Badplaas trondhjemite, indicating high-pressure of partial melting, and the Nelshoogte granodiorites are similar to the Kaap Valley tonalite/granodiorite, indicating medium-pressure of partial melting (see Sections 6 and 8.3.2).

The hypothesis of the entrained peritectic phase by Clemens and Stevens (2012) suggests that the trondhjemitic magma was generated before the granodioritic magma, because trondhjemitic magma becomes more mafic (granodioritic) by peritectic garnet and clinopyroxene. The *P-T* conditions that high-pressure for 3200 Ma trondhjemite and medium-pressure for 3200 Ma granodiorites were indicated. These suggestions imply the pressure of melting decreased at ~ 3200 Ma.

The isotope characteristics of the Nelshoogte and the Kaap Valley TTGs suggest a slightly enriched source, consistent with oceanic crusts that are the Onverwacht and/or the Fig Tree Group in the BGB. The different Nb/Ta ratios in the Nelshoogte and the Kaap Valley TTGs must be from the source rock that may be the Fig Tree Group.

Therefore these variations for ~ 3200 Ma plutons cannot be explained by magma mixing. The different magma batches may be caused by entrained peritectic assemblage and/or *P-T* conditions.

8.5.3. Is the origin of the basaltic source: thickened crust or subducting slab melt?

The evidences that high pressure of melting of the source rock, the compositional similarities of adakites and Archaean TTGs, and the water-present source lead that the TTGs may be related with a subduction zone. 10 to 30% garnet in a plagioclase-free mafic source that is also fertile, either through the fact that it contains hydrous minerals that can undergo incongruent partial melting, or through providing a ready supply of water to flux melting (e.g. Drummond and Defant, 1990). Moyen et al. (2006) explain that “high pressure” TTGs were derived from hot subduction zone. TTGs encompass at least some degree of geochemical diversity that can be related to differences in melting depth of similar sources. The mineralogical model for amphibolite melting suggests that TTGs formed at $P > 15$ kbar and T between 900°C and 1100°C, corresponding to low (15 °C/km) geothermal gradients that are likely to be attained only in subduction zones (Moyen and Stevens, 2006).

Smithies and Champion (2000) suggest that melting of hydrated basaltic material at the base of thickened crust (e.g. Atherton and Petford, 1993; Petford and Atherton, 1996), may be more appreciate model for most TTG. Tectonic models that incorporate tectonic underplating of oceanic crust, sequential stacking, or obduction, of oceanic crust (De Wit, 1998) and/or successive accretion of oceanic plateau (e.g. Desrochers et al., 1993; Condie, 1997) predict TTG generation mainly at the base of thickened crust and might be more appreciate models of early Archaean crustal growth than modern-style subduction and arc accretion. These suggestions require a lateral tectonic process and thus some form of destruction of crust at convergent plate boundaries. This also leads the tectonic setting of subduction.

For ~ 3450 Ma and ~ 3200 Ma TTGs in the BGGT, many authors sugget that the origin of those TTGs is subducting slab melt (see Section 2). The emplacement of large volumes of TTG magmas in the BGGT has been linked with major episodes of terrane accretion at ~ 3445 and ~ 3230 Ma (De Ronde and De Wit, 1994; De Ronde and Kamo, 2000). De Ronde and De Wit (1994) was the first to attribute each episode to an arc-trench environment. They have trace elements signatures of TTGs for a subduction zone, and the coeval nature of TTG magmatism and dacitic volcanism in the greenstone sequences (De Wit et al., 1987).

Rapp et al. (2003) suggest that TTG magmatism may have taken place beneath granite-greenstone complexes that developed along Archaean intra-oceanic island arcs by imbricate thrust stacking and tectonic accretion of diverse subduction-related terranes. Some eclogitic xenoliths and inclusions in diamonds from the subcratonic mantle may indeed represent residues from partial melting and TTG magmatism (Rollinson, 1997; Jacob and Foley, 1999; Barth et al., 2001). The source for Archaean TTG magmas may have been oceanic crust with variable Nb/Ta ratios, formed in a variety of environments in association with intraoceanic subduction; tectonic imbrication and accretion of these disparate terranes would have led to partial melting and TTG magmatism at the base of overthickened, juvenile arc crust (De Wit, 1998; Kusky and Polat, 1999).

Therefore, ~ 3200 Ma plutons, corresponding to “high pressure” TTGs are probably derived from hot subduction zone. The geochemical variations are also caused by different pressures of melting of source rock. They show distinct pressures in each phase within the Nelshoogte pluton as well as in each ~ 3200 Ma pluton. Furthermore, the U-Pb and Hf isotopic data represent that the origin of the Nelshoogte TTGs corresponds to the Onverwacht group that consists of oceanic mafic rocks in the BGB.

The upper portion of subducting slabs is the hottest due to the thermal effect of the overlying mantle wedge (e.g. van Keken et al., 2002; Peacock et al., 2005). The considerable volume of metamorphic water released during the pre-anatectic history of the slab. This would have induced fluid-present anatexis of the upper layers in the slab (Drummond and Defant, 1990).
In this case, Laurie (2013) interpreted that the emplacement of high pressure- or medium pressure-type TTG magmas by melting of a young and fast or slow slab, may be followed by the formation and emplacement of medium pressure-type TTG granitoids within a collisional orogeny by slab decompression melting which is a consequence of slab breakoff. The

geometries of *P-T* paths of the upper portions of fast subducting slabs and the relevant low-K_2O fluid-present solidus are similar as they both inflect towards higher temperatures. Therefore cooling of the upper mantle by only a small amount during the late Archaean ended fluid-present melting of the slab. This allowed slab water to migrate into the fluid- and meltmetasomatised wedge, which initially resulted in the formation of mantle enriched melts, such as sanukitoids, and thereafter produced fluid-fluxed mantle melts with dominantly intermediate composition that have since been associated with subduction zones.

Moyen et al. (2007) explains that, in the case of slab melting, felsic TTG liquids would form at relatively low melt fractions (Moyen and Stevens, 2006), raising issues surrounding how they are extracted from the source, and their ascent mechanism through a hot mantle wedge. In the case of modern adakites, high Ni, Cr, and Mg contents are ascribed to melt-mantle interactions during ascent (Kelemen, 1995; Smithies, 2000; Martin and Moyen, 2002; Martin et al., 2005). In Archaean collisional margin, slab breakoff will result in the decompression-driven melting of the fertile slab. The Nelshoogte granodiorites and the Kaap Valley TTGs have higher of Ni, Cr and Mg contents and Mg# than in the Badplaas domain TTGs. They may reflect fertile melt and it may be involved with hot mantle wedge.

These geochemical and geochronological features of TTGs from previous studies and this study suggest that the Nelshoogte pluton and other ~ 3200 Ma plutons in the BGGT are originaly derived from oceanic crusts (the Onverwacht Group in the BGB) as well as the origin of older ~ 3450 Ma TTGs. The source may be rutile-bearing eclogitc protolith for ~ 3200 Ma trondhjemites and garnet-bearing amphibolitic protolith for ~ 3200 Ma granodiorites, related with subducting slab breakoff and asthenospheric upwelling.

Chapter 9

Conclusions

- The magma source of the Nelshoogte pluton is similar to that which formed the older TTGs in the BGGT. The REE and trace element patterns resemble those of other TTGs in the BGGT suggest that the magma source is garnet-rich (10 to 30 % garnet) amphibolites or rutile-bearing eclogite. A/CNK-, Ti-maficity correlations show typical I-type like behaviour, confirming the metamafic character of the source and the involvement of a peritectic garnet and clinopyroxene component. The major- and trace-element variations indicate that there were different magma batches within the Nelshoogte pluton. The Nelshoogte granodiorites are similar to the Kaap Valley tonalites/granodiorites and the Nelshoogte tonalitis/trondhjemites/granites are similar to the Badplaas domain TTGs in their major- and trace-element variations.

- Magma compositions possibly reflect different pressures of partial melting. The Nelshoogte TTGs have variable Sr/Y and La/Yb ratios. The trondhjemites/tonalites correspond to high pressure group and the granodiorites correspond to medium pressure group, suggesting a transition from high pressure to medium pressure.

- The U-Pb zircon dating for the Nelshoogte pluton reveals no significant age (apparent age) differences between the trondhjemites and the tonalites; all lie between ca 3240 and 3210 Ma, and Hf isotopes suggest the source rocks are ca. 20 to 100 Myr older than the pluton and the source rock is consistent with the ages of oceanic crusts (the Onverwacht Group and/or the Fig Tree Group) in the BGB.

- The source of ~ 3200 Ma TTGs in the BGGT may be rutile-bearing eclogitc protolith for the Nelshoogte trondhjemites/tonalites and the Badplaas domain TTGs and garnet-bearing amphibolitic protolith for the Nelshoogte and the Kaap Valley granodiorites, related with subducting slab breakoff and asthenospheric upwelling.

References

Albare`de, F., 1995. Introduction to Geochemical Modeling. Cambridge Univ. Press, Cambridge.

Anhaeusser, C.R., 1969. The Stratigraphy, Structure and Gold Mineralization of the Jamestown and Sheba Hills Areas of the Barberton Mountain Land. Ph.D. thesis (unpubl.), Univ. of the Witwatersrand, Johannesburg, 332 pp.

Anhaeusser, C.R., 2001. The anatomy of an extrusive-intrusive Archaean mafic-ultramafic sequence: the Nelshoogte schist belt and Stolzburg Layered ultramafic complex, Barberton greenstone belt, South Africa. South African Journal of Geology 104, 167-204.

Anhaeusser, C.R., Robb, L.J., 1983. Geological and geochemical characteristics of the Heerenveen and Mpuluzi batholiths south of the Barberton greenstone belt and preliminary thoughts on their petrogenesis. Geological Society of South Africa 9, 131–151, Special Publication.

Anhaeusser, C.R., Robb, L.J., Viljoen, M.J., 1981. Provisional geological map of the Barberton greenstone belt and surrounding granitic terrane, eastern Transvaal and Swaziland. Geological Society of South Africa, 1:250.000.

Arculus, R.J., 1994. Aspects of magma genesis in arcs. Lithos 33, 189–208.

Armstrong, R.A., Compston W., De Wit, M.J., Williams, I.S., 1990. The stratigraphy of the 3.5-3.2 Ga Barberton Greenstone Belt revisited: a single zircon ion microprobe study. Earth and Planetary Science Letters 101, 90-106.

Atherton, M.P., Petford, N., 1993. Generation of sodium-rich magmas from newly underplated basaltic crust. Nature 362, 144–146.

Barth, M. G., Foley, S. F., Horn, I., 2002. Partial melting in Archean subduction zones: constraints from experimentally determined trace element partition coefficients between

eclogitic minerals and
tonalitic melts under upper mantle conditions. Precambr. Res. 113, 323–340.

Barton, M., et al., 1983. Geochronological and Sr-isotopic studies of certain units in the Barberton granite-greenstone terrane, South Africa. Spec. Publ. Geol. Soc. S. Afr. 9, 63–72.

Bateman, R., 1995. The interplay between crystallization, replenishment and hybridization in large felsic magma chambers. Earth- Sci. Rev. 39, 91– 106.

Bea F., 1996. Residence of REE, Y, Th and U in granites and crustal protoliths; implications for chemistry of crustal melts. Journal of Petrology 37, 521 –552.

Beard, J.S., Lofgren, G.E., 1991. Dehydration melting and water-saturated melting of basaltic and andesitic greenstones and amphibolites at 1, 3, and 6.9 kb. Journal of Petrology 32, 365–401.

Belcher, R.W., Kisters, A.F.M., Anhaeusser, C.R., 2009. Nelshoogte trondhjemite. Catalogue of Lithostratigraphic Units 10, 17-18.

Belcher, R.W., Kisters, A.F.M., Poujol, M., Stevens, G., 2005. Structural emplacement of the 3.2 Ga Nelshoogte Pluton: implications for the origin of dome-and-keel structures in the Barberton granite greenstone terrain. Geo 2005 conference abstracts, Durban, South Africa, p. 14.

Blichert-Toft, J., Puchtel, I.S., 2010. Depleted mantle sources through time: evidence from Lu–Hf and Sm–Nd isotope systematics of Archean komatiites. Earth and Planetary Science Letters 297, 598–606.

Blundy, J.D., Wood, B.J., 1994. Prediction of crystal-melt partition coefficients from elastic moduli. Nature 372, 452–454.

Bowen, N.L., 1915. The crystallization of haplobasaltic, haplodioritic and related magma. Am. J. Sci., 40: 161–185.

Bouvier, A., Vervoort, J.D., Patchett, P.J., 2008. The Lu–Hf and Sm–Nd isotopic composition of CHUR: constraints from unequilibrated chondrites and implications for the bulk composition of terrestrial planets. Earth and Planetary Science Letters 273, 48–57.

Boynton, W.V., 1984. Cosmochemistry of the rare earth elements: Meteorite studies. In: P. Henderson (Editor), Rare Earth Element Geochemistry. Elsevier, Amsterdam, 63-114.

Brun, J.P., Gapais, D. and Le Theoff, B., 1981. The mantled gneiss domes of Kuopio (Finland): interfering diapirs. Tectonophysics,

Byerly, G.R., Lowe, D.R., Wooden, J.L. and Xie, X., 2002. An Archean Impact Layer from the Pilbara and Kaapvaal Cratons. Science 297, 1325-1327.

Castillo, P.R., 2006. An overview of adakite petrogenesis. Chinese Science Bulletin 51, 257–268.

Champion, D.C., Smithies, R.H., 2003. Slab melts and related processes—Archaean versus Recent. In: Arima, M., Nakajima, T., Ishihara, S. (Eds.), Hutton Symposium V, The Origin of Granites and Related Rocks. Geological Survey of Japan, pp. 19.

Chappell, B.W., White, A.J.R., Wyborn, D., 1987. The importance of residual source material (restite) in granite petrogenesis. J. Petrol. 28, 571– 604.

Clemens, J.D., Darbyshire, D.P.F., Flinders, J., 2009. Sources of post-orogenic calcalkaline magmas: the Arrochar and Garabal Hill–Glen Fyne complexes, Scotland. Lithos 112 (3–4), 524–542.

Clemens, J.D., Helps, P.A., Stevens, G., 2010. Chemical structure in granitic magmas — a signal from the source? Earth and Environmental Science Transactions of the Royal Society of Edinburgh 100 (1–2), 159–172.

Clemens, J.D., Stevens, G., Farina, F., 2011. The enigmatic sources of I-type granites: The peritectic connexion. Lithos 126, 174-181.

Clemens, J.D., Stevens, G., 2012. What controls chemical variation in granitic magmas? Lithos 134–135, 317–329.

Clemens, J.D., Yearron, L.M., Stevens, G., 2006. Barberton (South Africa) TTG magmas: geochemical and experimental constraints on source-rock petrology, pressure of formation and tectonic setting. Precambrian Research 151, 53–78.

Coldwell, B.C., 2008. Evolution of the Peruvian Subduction Margin at 9° S: Evidence from Geochemistry, Experimental Petrology and Melt Inclusions on Adakite-like Ignimbrites. Kingston University, p. 272.

Condie, K.C., 1997. Contrasting sources for upper and lower continental crust: the greenstone connection. Journal of Geology 105, 729-736.

Condie, K.C., 2005. TTGs and adakites: are they both slab melts? Lithos 80, 33–44.

Defant, M.J., Drummond, M.S., 1990. Derivation of some modern arc magmas by melting of young subducted lithosphere. Nature 367, 662–665.

DePaolo, D.J., 1981. Trace element and isotopic effects of combined wallrock assimilation and fractional crystallization. Earth Planet. Sci. Lett. 53, 189– 202.

De Ronde, C.E.J., De Wit, M.J., 1994. Tectonic history of the Barberton greenstone belt, South Africa: 490 million years of Archean crustal evolution. Tectonics 13, 983–1015.

De Ronde, C.E.J., Kamo, S.L., 2000. An Archaean are-arc collisional event: a shortlived (ca. 3 Myr) episode, Weltetvreden area, Barberton Greenstone Belt, South Africa. Journal of African Earth Sciences 30, 219–248.

Desrochers, J.-P., Hubert, C., Ludden, J., Pilote, P., 1993. Accretion of Archean oceanic

plateau fragments in the Abitibi greenstone belt, Canada. Geology 21, 451-454.

De Wit, M.J., 1998. On Archaean granites, greenstones, cratons and tectonics: does the evidence demand a verdict? Precambrian Research 91, 181–226.

De Wit, M.J., Armstrong, R.A., Hart, R.J., Wilson, A.H., 1987. Felsic igneous rocks within the 3.3 to 3.5 Ga Barberton greenstone belt: high crustal level equivalents of the surrounding tonalite-trondhjemite terrain emplaced during thrusting. Tectonics 6, 529-549.

De Wit, M.J., Roering, C., Hart, R.J., Armstrong, R.A., de Ronde, C.E.J., Green, R.W.E., Tredoux, M., Peberdy, E., Hart, R.A., 1992. Formation of an Archaean continent. Nature 357, 553–562.

Diener, J.F.A, Stevens, G., Kisters, A.F.M., and Poujol, M., 2005, Geotectonic evolution of the
Tjakastad Schist belt, Barberton greenstone belt, South Africa: a record of mid-Archaean metamorphism and terrain exhumation. Precambrian Research 143, 87-112.

Ding, L., Ma, C.Q., Li, J., Robinson, P.T., Deng, X.D., Zhang, C., Xu, W., 2011. Timing and genesis of the adakitic and shoshonitic intrusions in the Laoniushan complex, southern margin of the North China Craton: implications for post-collisional magmatism associated with the Qinling Orogen. Lithos 126, 212-232.

Dixon, J.M., 1975. Finite strain and progressive deformation in models of diapiric structures. Tectonophysics 28, 89-124.

Drummond, M.S., Defant, M.J., 1990. A model from trondhjemite–tonalite–dacite genesis and crustal growth via slab melting: Archaean to modern comparisons. Journal of Geophysical Research 95, 21503–21521.

Dziggel, A., Stevens, G., Poujol, M., Anheusser, C.R., Armstrong, R.A., 2002. Metamorphism of the granite-greenstone terrane south of the Barberton greenstone belt, South Africa: an insight into the tectono-thermal evolution of the “lower” portions of the

Onverwacht Group. Precambrian Research 114, 221–247.

Eichelberger, J.C., 1978. Andesite volcanism and crustal evolution. Nature 275, 21–27.

Elburg, M.A., 1996. Evidence of isotopic equilibration between microgranitoid enclaves and host granodiorite, Warburton Granodiorite, Lachlan Fold Belt, Australia. Lithos 38, 1– 22.

Elburg, M.A., Nicholls, I.A., Sie, S.H., 1995. Mineralogical evidence for the origin of mafic microgranular enclaves in Stype granites and volcanics. Nucl. Instrum. Methods Phys. Res., B Beam Interact. Mater. Atoms 104, 464–469.

Ewart, A., 1982. The mineralogy and petrology of Tertiary-Recent orogenic volcanic rocks: with a special reference to the andesitic– basaltic compositional range. In: Thorpe, R.S. (Ed.), Andesites: orogenic andesites and related rocks. Wiley, Chichester, pp. 25–95.

Foley, S.F., Tiepolo, M., Vannucci, R., 2002. Growth of early continental crust controlled by melting of amphibolite in subduction zones. Nature 417, 637–640.

Foley S., 2008. A trace element perspective on Archean crust formation and on the presence or absence of Archean subduction. In: When Did Plate Tectonics Begin? (eds. K.C. Condie and V. Pease). Geological society of America Special Paper 440. 31–50.

Frei D, Gerdes A (2009) Precise and accurate in situ U–Pb dating of zircon with high sample throughput by automated LA-SF-ICPMS. Chem Geol 261: 261–270.

Gerdes, A., 2001. Magma homogenization during anatexis, ascent and/or emplacement? Constraints from the Variscan Weinsberg Granites. Terra Nova 13, 305– 312.

Gerdes, A., Wfrner, G., Finger, F., 2000. Hybrids, magma mixing and enriched mantle melts in post-collisional Variscan granitoids: the Rastenberg Pluton, Austria. In: Franke, W., Haak, V., Oncken, O., Tanner, D. (Eds.), Orogenic Processes: Quantification and Modelling in the Variscan Fold Belt, Special Publication-Geological Society (London), 179, 415–431.

Gerdes A, Zeh A (2006) Combined U–Pb and Hf isotope LA-(MC)-ICP-MS analyses of detrital zircons: comparison with SHRIMP and new constraints for the provenance and age of an Armorican metasediment in Central Germany. Earth Planet Sci Lett 249: 47–61.

Glazner, A.F., 2007. Thermal limitations on incorporation of wall rock into magma. Geology 35 (4), 319.

Green, T. H. & Adam, J. (2003). Experimentally-determined trace element characteristics of aqueous fluid from partially dehydrated mafic oceanic crust at 3.0 GPa, 650–700℃. European Journal of Mineralogy 15, 815–830.

Grosch, E.G., Kosler, J., McLoughlin, N., Drost, K., Slam, J., Pedersen R.B., 2011. Paleoarchean detrital zircon ages from the earliest tectonic basin in the Barberton Greenstone Belt, Kaapvaal craton, South Africa. Precambrian Research 191, 85– 99.

Gorman, B.E., Pearce, T.H. and Birkett, T.C., 1978. On the structure of Archaean greenstone belts. Precambrian Res., 6: 23-41.

Guo, Z., Wilson, M., Liu, J., 2007. Post-collisional adakites in South Tibet: products of partial melting of subduction-modified lower crust. Lithos 96, 205-224.

Hastie, A., Kerr, A., McDonald, I., Mitchell, S., Pearce, J., Millar, I., Barfod, D., Mark, D., 2010. Geochronology, geochemistry and petrogenesis of rhyodacite lavas in eastern Jamaica: a new adakite subgroup analogous to early Archaean continental crust? Chemical Geology 276, 344-359.

Heubeck, C., and Lowe, D.R., 1999, Sedimentary petrography and provenance of the Archean Moodies Group, Barberton greenstone belt, *in* Lowe, D.R., and Byerly, G.R., eds., Geologic evolution of the Barberton greenstone belt, South Africa: Geological Society of America Special Paper 329, 259–286.

Hamilton, P. J., Evensen, N. M., O'Nions, R. K., 1979. Sm-Nd dating of Onverwacht Group Volcanics, southern Africa. Nature 279, 298-300.

Hamilton, W.R., 1995. Subduction systems and magmatism. Geological Society of London 31, 3–28, Special Publication.

Hibbard, M.J., 1991. Textural anatomy of twelve magma-mixed granitoid systems. In: Didier, J., Barbarin, B. (Eds.), Enclaves and Granite Petrology. Elsevier, Amsterdam, pp. 431– 444.

Hibbard, M.J., 1995. Petrography to Petrogenesis. Prentice Hall, New Jersey.

Hoffmann, J.E., Münker, C., Næraa, T., Minik, T.R., Herwartz, D., Garbe-Schönberg, D., and Svahnberg, H., 2011. Mechanisms of Archean crust formation inferred from high-precision HFSE systematics in TTGs. Geochimica et Cosmochimica Acta 75, 4157–4178.

Holden, P., Halliday, A.N., Stephens, W.E., Henney, P.J., 1991. Chemical and isotopic evidence for major mass-transfer between mafic enclaves and felsic magma. Chem. Geol. 92, 135– 152.

Holub, F.V., 1997. Ultrapotassic plutonic rocks of the durbachite series in the Bohemian Massif: petrology, geochemistry and petrogenetic interpretation. Sbor. Geol. Veˇd, Lozˇisk. Geol. Mineral. 31, 5 –26.

Jackson S, Pearson NJ, Griffin WL, Belousova, E.A., 2004. The application of laser ablation – inductively coupled plasma – mass spectrometry to in situ U–Pb zircon geochronology. Chemical Geology 211: 47–69.

Jacob, D. E., Foley, S. F., 1999. Evidence for Archean ocean crust with low high field strength element signature from diamondiferous eclogite xenoliths. Lithos 48, 317–336.

Kamber, B.S., Ewart, A., Collerson, K.D., Bruce, M.C., McDonalds, G.D., 2002. Fluidmobile trace element constraints on the role of slab melting and implications for Archaean crustal growth models. Contrib. Mineral. Petrol. 144, 38–56.

Kamber B. S., Whitehouse M. J., Bolhar R. and Moorbath S., 2005. Volcanic resurfacing and the early terrestrial crust: zircon U–Pb and REE constraints from the Isua Greenstone

Belt, southern West Greenland. Earth Planet. Sci. Lett. 240, 276–290.

Kamo, S.L., Davis, D.W., 1994. Reassessment of Archaean crustal development in the Barberton Mountain Land, South Africa, based on U–Pb dating. Tectonics 13, 165–192.

Kelemen, P.B., 1995. Genesis of high Mg# andesites and the continental crust. Contrib. Mineral. Petrol. 120 (1), 1-19.

Kinny, P.D., Compston, W., Williams, I.S., 1991. A reconnaissance ion-probe study of hafnium isotopes in zircons. Geochimica et Cosmochimica Acta 55, 849–859.

Kinny, P.D., Maas, R., 2003. Lu–Hf and Sm–Nd isotope systems in zircon. In: Hanchar, J.M., Hoskin, P.W.O. (Eds.), Zircon, Reviews in Mineralogy & Geochemistry. Mineralogical Society of America 53, 327–341.

Kisters, A.F.M. and Anhaeusser, C.R., 1995. Emplacement features of Archaean TTG plutons along the southern margin of the Barberton greenstone belt, South Africa. Precambrian Research. 75, 1-15.

Kisters, A.F.M., Belcher, R.W., Poujol, M., and Dziggel, A., 2010. Continental growth and convergence-related arc plutonism in the Mesoarchaean: Evidence from the Barberton granitoid-greenstone terrain, South Africa. Precambrian Research. 178, 15-26.

Kisters, A.F.M., Stevens, G., Dziggel, A., Armstrong, R.A., 2003. Extensional detachment faulting at the base of the Barberton greenstone belt: evidence for a 3.2 Ga orogenic collapse. Precambrian Research 127, 355-378.

Klemme S., Blundy J. D., Wood B. J., 2002. Experimental constraints on major and trace element partitioning during partial melting of eclogite. Geochim. Cosmochim. Acta 66, 3109–3123.

Klemme S., Prowatke S., Hametner K. and Gu¨nther D., 2005. Partitioning of trace elements between rutile and silicate melts: implications for subduction zones. Geochim. Cosmochim.

Acta 69, 2361–2371.

Kröner, A., 2007. The Ancient Gneiss Complex of Swaziland and environs: record of early Archaean crustal evolution in southern Africa. In: Van Kranendonk, M.J., Smithies, R.H., Bennett, V.C. (Eds.), Earth's Oldest Rocks. Elsevier, Amsterdam, 465–480.

Kröner, A., Byerly, G.R. and Lowe, D.R., 1991. Chronology of early Archaean granitegreenstone evolution in the Barberton Mountain Land, South Africa, based on precise dating by single zircon evaporation. Earth and Planetary Science Letters 193, 41–54.

Kröner, A., Hegner, E., Byerly, G.R., Lowe, D.R., 1992. Possible terrane identification in the early Archean Barberton Greenstone Belt, South Africa, using single zircon geochronology. Eos (Trans. Am. Geophys. Union) 73, 616.

Kröner, A., Hegner, E., Wendt, J.I., Byerly, G.R., 1996. The oldest part of the Barberton granitoid-greenstone terrain, South Africa, evidence for crust formation between 3.5 and 3.7 Ga. Precambrian Research 78, 105–124.

Kröner, A., and Tegtmeyer, A., 1994. Gneiss-greenstone relationships in the Ancient Gneiss Complex of southwestern Swaziland, southern Africa, and implications for early crustal evolution: Precambrian Research 67, 109-139.

Kröner, A., Wendt, J.I., Milisenda, C.C., Compston, W., Maphalala, R., 1993. Zircon geochronology and Nd isotopic systematic of the Ancient Gneiss Complex, Swaziland, and implications for crustal evolution, in Kröner, A., ed., The Ancient Gneiss Complex: Overview papers and guidebook for excursion: Swaziland Geological Survey and Mines Department., Bulletin 11, 15-37.

Kusky, T. M. & Polat, A., 1999. Growth of granite-greenstone terranes at convergent margins, and stabilization of Archean cratons. Tectonophysics 305, 43–73.

Lana, C., Buick, I., Stevens G., Rossouw, R., De Wet, W., 2011. 3230-3200 Ma post-orogenic extension and mid-crustal magmatism along the southeastern margin of the

Barberton Greenstone Belt, South Africa. Journal of Structural Geology 33, 844-858.

Lana, C., Tohver, E., Cawood, P., 2010. Quantifying rates of dome-and-keel formation in the Barberton granitoid-greenstone belt, South Africa. Precambrian Research 177, 199-211.

Laurie, A., 2013. The formation of Earth's early felsic continental crust by water-present eclogite melting. PhD thesis, Stellenbosch University, Stellenbosch, South Africa, 66 pp.

Laurie, A., Stevens, G., 2012. Water-present eclogite melting to produce Earth's early felsic crust. Chemical Geology 314–317, 83–95.

Leake, B.E., et al., 1997. Nomenclature of amphiboles: report of the subcommittee on amphiboles of the international mineralogical association commission on new minerals and mineral names. Mineral. Mag. 61, 295– 321.

Li, J., Qin, K., Li, G., Xiao, B., Chen, L., Zhao, J., 2011. Post-collisional ore-bearing adakitic porphyries from Gangdese porphyry copper belt, southern Tibet: melting of thickened juvenile arc lower crust. Lithos 126, 265-277.

Lowe, D.R. (1982). Comparative sedimentology of the principal volcanic sequences of Archean greenstone belts in South Africa, Western Australia, and Canada: implications for crustal evolution. Precambrian Research 17, 1–29.

Lowe, D.R., 1994. Accretionary history of the Archean Barberton Greenstone Belt (3.55–3.22 Ga), southern Africa. Geology 22, 1099–1102.

Lowe, D.R., Byerly, G.R., 1999. Stratigraphy of the west-central part of the Berberton Greenstone Belt, South Africa. In: Lowe, D.R., Byerly, G.R. (Eds.), Geologic Evolution of the Barberton Greenstone Belt, South Africa. Geological Society of America Special Paper 329, 1–36.

Lowe, D.R., Byerly, G.R., 2007. An overview of the geology of the Barberton greenstone belt: implications for early crustal development. In: van Kranendonk, M.J., et al. (Eds.),

Developments in Precambrian Geology 15, 481–526.

Lowe, D.R., Byerly, G.R., Heubeck, C., 1999. Structural divisions and development of the west central part of the Barberton Greenstone Belt. In: Lowe, D.R., Byerly, G.R. (Eds.), Geologic Evolution of the Barberton Greenstone Belt. Geological Society of America, South Africa, pp. 37–82, Special Paper 329.

Ludwig K (2003) Isoplot/Ex version 3: a Geochronological toolkit for Microsoft Excel. Geochronology Center, Berkeley

Martin, H., 1986. Effect of steeper Archean geothermal gradient on geochemistry of subduction-zone magmas. Geology 14, 753–756.

Martin, H., 1987. Petrogenesis of Archaean trondhjemites, tonalites and granodiorites from eastern Finland; major and trace element geochemistry. Journal of Petrology 28 (5), 921–953.

Martin, H., 1994. The Archean grey gneisses and the genesis of the continental crust. In: Condie, K.C. (Ed.), The Archean Crustal Evolution, Developments in Precambrian Geology. Elsevier, Amsterdam, pp. 205–259.

Martin, H., 1999. The adakitic magmas: modern analogues of Archaean granitoids. Lithos 46, 411– 429.

Martin, H., Smithies, R.H., Rapp, R., Moyen, J.F., Champion, D., 2005. An overview of adakite, tonalite–trondhjemite–granodiorite (TTG), and sanukitoid: relationships and some implications for crustal evolution. Lithos 79, 1–24.

Martin, H., Moyen, J.-F., Rapp, R., 2010. Sanukitoids and the Archaean–Proterozoic boundary. In: Clemens, J.D., Frost, C.D., Kisters, A., Moyen, J.-F., Rushmer, T., Stevens, G. (Eds.), Sixth Hutton Symposium on The Origin of Granites and Related Rocks: Proceedings of a Symposium held in Stellenbosch, South Africa, 2–6 July 2007. Geological Society of America, Boulder, pp. 15–33.

Mattey JM (2010) Analysis of the relative decay constants of 235U and 238U by multi-step CA-TIMS measurements of closed-system natural zircon samples. Chem Geol 275: 186–198.

McGregor, A.I., 1951. Some milestones in the Precambrian of southern Rhodesia. Trans. Geol. Soc. S. Afr., 54: 27-68.

McMillan, K., 1986. Spatially varied miaroles in the albite porphyry of Cuchillo Mountain, southwestern New Mexico. American Mineralogist, 71, 625-631.

Moyen, J.-F., 2009. High Sr/Y and La/Yb ratios: the meaning of the "adakitic signature". Lithos 112, 556–574.

Moyen, J.-F., 2011. The composite Archaean grey gneisses: Petrological significance, and evidence for a non-unique tectonic setting for Archaean crustal growth. Lithos 123, 21–36.

Moyen, J.-F., Martin, H., 2012. Forty years of TTG research. Lithos 148, 312-336.

Moyen, J.F., Martin, H., Jayananda, M., 2001. Multi-element geochemical modelling of crust–mantle interactions during late-Archaean crustal growth: the closepet granite (South India). Precambrian Res. 112, 87– 105.

Moyen, J.-F., Stevens, G., Kisters, A.F.M., 2006. Record of mid-Archaean subduction from metamorphism in the Barberton terrain, South Africa. Nature 443, 559–562.

Moyen, J.-F., Stevens, G., 2006. Experimental constraints on TTG petrogenesis: implications for Archean geodynamics. Geophysical Monograph. 164, 149-175.

Moyen J.-F., Stevens, G., Kisters, A.F.M., Belcher, R.W., 2007. TTG plutons oft he Barberton granotoid-greenstone terrain, South Africa. Developments in Precambrian Geology 15, 607-667.

Nagel, T.J., Hoffmann J.E., Münker, C., 2012. Generation of Eoarchean tonalite-trondhjemite granodiorite series from thickened mafic arc crust. Geology 40, 375-378.

Nasdala L, Hofmeister W, Norberg N, Mattinson JM, Corfu F, Dörr W, Kamo SL, Kennedy AK, Kronz A, Reiners PW, Frei D, Košler J, Wan Y, Götze J, Häger T, Kröner A, Valley JW (2008) Zircon M257–a homogeneous natural reference material for the ion microprobe U-Pb analysis of zircon. Geostand Geoanal Res 32: 247–265.

Naslund, H.R., 1986. Disequilibrium partial melting and rheomorphic layer formation in the contact aureole of the Basistoppen sill, East Greenland. Contrib Mineral Petrol. 93, 359-367.

Nédélec, A., Chevrel, M.O., Moyen, J-F., Ganne, J., Fabre S., 2012. TTGs in the making: Natural evidence from Inyoni shear zone (Barberton, South Africa). Lithos, in press.

Nelson, S.T., Montana, A., 1992. Sieve-textured plagioclase in volcanic rocks produced by rapid decompression. American Mineralogist 77, 1242–1249.

O'Connor, J.T., 1965. A classification for quartz-rich igneous rocks based on feldspar ratios. U.S. Geological Survey Professionnal Paper 525, 79–84 (B).

O'Hara, M. J. (1980). Non-linear nature of the unavoidable long-lived isotopic, trace and major element contamination of a developing magma chamber. Philosophical Transactions of the Royal Society of London, Series A 297, 215–227.

Oosthuyzen, E.J., 1970. The geochemistry of a suite of rocks from the granitic terrain surrounding the Barberton Mountain Land. Ph.D. thesis, Uni. Witwaterrand, Johannesburg, 94 pp. (unpubl.).

Patchett, P.J., Kouvo, O., Hedge, C.E., Tatsumoto, M., 1981. Evolution of continental crust and mantle heterogeneity: evidence from Hf isotopes. Contributions to Mineralogy and Petrology 78, 279–297.

Patchett, P.J., 1983. Importance of the Lu–Hf isotopic system in studies of planetary chronology and chemical evolution. Geochimica et Cosmochimica Acta 47, 81–91.

Peacock, S.M., van Keken, P.E., Holloway, S.D., Hacker, B.R., Abers, G.A., Fergason, R.L., 2005. Thermal structure of the Costa Rica–Nicaragua subduction zone. Physics of the Earth and Planetary Interiors 149, 187–200.

Pearce, J.A., 1983, Role of the sub-continental lithosphere in magma genesis at active continental margins. In: Hawkesworth C. J. and Norry M. J. (eds.), Continental basalts and mantle xenoliths, Shiva, Nantwich, 230 – 249.

Petford, N., Atherton, M., 1996. Na-rich partial melts from newly underplated basaltic crust: the Cordillera Blanca Batholith, Peru. J. Petrol., 37, 1491-1521.

Pin, C., Binon, N., Belin, J.M., Barbarin, B., Clemens, J.D., 1990. Origin of microgranular enclaves in granitoids—equivocal Sr– Nd evidence from Hercynian rocks in the Massif Central (France). J. Geophys. Res. 95, 17821– 17828.

Poujol, M., Robb, L.J., Anhaeusser, C.R., Gericke, B., 2003. A review of the geochronological constraints on the evolution of the Kaapvaal Craton, South Africa. Precambrian Research 127, 181–213.

Rapp, R., Shimizu, N., Norman, M.D., Applegate, G.S., 1999. Reaction between slab-derived melts and peridotite in the mantle wedge: experimental constraints at 3.8 GPa. Chemical Geology 160, 335–356.

Rapp, R.P., Shimizu, N., Norman, M.D., 2003. Growth of early continental crust by partial melting of eclogite. Nature 425, 605–609.

Rapp, R.P., Watson, E.B., Miller, C.F., 1991. Partial melting of amphibolite/eclogite and the origin of Archaean trondhjemites and tonalites. Precambrian Research 51, 1–25.

Rapp, R.P., Watson, E.B., 1995. Dehydratation melting of metabasalt at 8-32 kbar : implications for continental growth and crust-mantle recycling. Journal of Petrology 36 (4), 891–931.

Renjith, M.L., in press. Micro-textures in plagioclase from 1994e1995 eruption, Barren Island Volcano: Evidence of dynamic magma plumbing system in the Andaman subduction zone. Geoscience Frontiers.

Reymer, A., Schubert, G., 1984. Phanerozoic additions to the continental crust and crustal growth. Tectonics 3, 63–77.

Robb, L.J., Barton, J.M., Kable, E.J.D., Wallace, R.C., 1986. Geology, geochemistry and isotopic characteristics of the Archaean Kaap Valley pluton, Barberton mountain land, South Africa. Precambrian Research 31, 1-36.

Rollinson, H., 1997. Eclogite xenoliths in west African kimberlites as residues from Archean granitoid crust formation. Nature 389, 173–176.

Rudnick, R.L., 1995. Making continental crust. Nature 378, 571–578.

Rushmer, T., 1991. Partial melting of two amphibolites: contrasting experimental results under fluid-absent conditions. Contribution to Mineralogy and Petrology 107, 41–59.

Sanchez-Garrido, C. J. M. G., 2012. The petrogenesis of the older (> 3.0 Ga) potassic granitoids of eastern Mpumalanga (South Africa) and Swaziland: An investigation of crustal formation processes in the early Earth. PhD thesis, Stellenbosch University, Stellenbosch, South Africa, 222 pp.

Scherer, E., Munker, C., Mezger, K., 2001. Calibration of the lutetium–hafnium clock. Science 293, 683–687.

Schmidt, M.W., 1992. Amphibole composition in tonalite as a function of pressure: an experimental calibration of the Al-in-hornblende barometer Contrib Mineral Petrol 1 t 0, 304-310.

Schmidt M.W., Dardon A., Chazot G. and Vannucci R., 2004. The dependence of Nb and Ta

rutile-melt partitioning on melt composition and Nb/Ta fractionation during subduction processes. Earth Planet. Sci. Lett. 226, 415–432.

Schoene, B., De Wit, M.J., Bowring, S.A., 2008. MesoArchaean assembly and stabilization of the eastern Kaapvaal craton. A structural-thermochronological perspective. Tectonics 27, 1-27.

Sen, C., Dunn, T., 1994. Dehydration melting of a basaltic composition amphibolite at 1.5 and 2.0 GPa: implications for the origin of adakites. Contributions to Mineralogy and Petrology 117, 394–409.

Sisson, T.W., Ratajeski, K., Hankins, W.B., Glazner, A.F., 2005. Voluminous granitic magmas from common basaltic sources. Contributions to Mineralogy and Petrology
148, 635–661.

Smithies, R.H., 2000. The Archaean tonalite–trondhjemite–granodiorite (TTG) series is not an analogue of Cenozoic adakite. Earth Planet. Sci. Lett. 182, 115– 125.

Smithies, R.H. and Champion, D.C., 2000. The Archaean high-Mg diorite suite: link to tonalite-trondhjemite-granodiorite magmatism and implications for Early Archaean. Journal of petrology 41(12), 1653-1671.

Smithies, R.H., Champion, D.C., Cassidy K.F., 2003. Formation of Earth's early Archaean continental crust. Precambrian Research 127, 89–101.

Smithies, R.H., Champion, D.C., Van Kranendonk, M.J., 2009. Formation of Paleoarchean continental crust through infracrustal melting of enriched basalt. Earth Planet. Sci. Lett. 281, 298–306.

Soderlund, U., Patchett, J.P., Vervoort, J.D., Isachsen, C.E., 2004. The 176Lu decay constant determined by Lu–Hf and U–Pb isotope systematics of Precambrian mafic intrusions. Earth and Planetary Science Letters 219, 311–324.

Spera, F.J., Bohrson, W.A., 2001. Energy-constrained open system magmatic processes I: general model and energy-constrained assimilation and fractional crystallization (EC-AFC) formulation. Journal of Petrology 42, 999–1018.

Stevens, G., Droop, G.T.R., Armstrong, R.A., Anhaeusser, C.R., 2002. Amphibolite facies metamorphism in the Schapenburg schist belt: a record of the midcrustal response to 3.23 Ga terrane accretion in the Barberton greenstone belt. South African Journal of Geology 105, 271-284.

Stevens, G., Villaros, A., Moyen, J.F., 2007. Selective peritectic garnet entrainment as the origin of geochemical diversity in S-type granites. Geology 35, 9–12.

Swanson, S. E., 1977. Relation of nucleation and crystal-growth rate to the development of granitic textures. American Mineralogist, 62, 966-978.

Taylor, J., 2012. The anatectic history of Archaean metasedimentary granulites from the Ancient Gneiss Complex, Swaziland. PhD thesis, Stellenbosch University, Stellenbosch, South Africa, 140 pp.

Taylor, S.R., McLennan, S.M., 1985. The Continental Crust: Its Composition and Evolution. Blackwell, Oxford.

Toulkeridis, T., et al., 1998. Sm-Nd, Rb-Sr and Pb-Pb dating of silicic carbonates from the early Archaean Barberton Greenstone Belt, South Africa evidence for post-depositional isotopic resetting at low temperature, Precamb. Res. 92, 129-144.

Tsuchiyama, A., 1985. Dissolution kinetics of plagioclase in the melt of the system diopside-albite-anorthite, and origin of dusty plagioclase in andesites. Contributions to Mineralogy and Petrology 89 (1), 1–16.

Van Keken, P.E., Kiefer, B., Peacock, S.M., 2002. High-resolution models of subduction zones: implications for mineral dehydration reactions and the transport of water into the deep mantle. Geochemistry, Geophysics, Geosystems 3 (10), 1056.

Van Kranendonk, M.J., 2010, Two types of Archean continental crust: Plume and plate tectonics on early Earth. American Journal of Science 310, 1187–1209.

Vernon, R.H., 1990. Crystallization and hybridism in microgranitoid enclave magmas: microstructural evidence. J. Geophys. Res. 95, 17849– 17859.

Vernon, R.H., 1991. Interpretation of microstructures of microgranitoid enclaves. In: Didier, J., Barbarin, B. (Eds.), Enclaves and Granite Petrology. Elsevier, Amsterdam, pp. 277– 291.

Vervoort J. D., Patchett P. J., Gehrels G. E., and Nutman A. P., 1996. Constraints on early Earth differentiation from hafnium and neodymium isotopes. Nature 379, 624–627.

Vervoort J. D., Blichert-Toft J., 1999. Evolution of the depleted mantle: Hf isotope evidence from juvenile rocks through time. Geochimica et Cosmochimica Acta 63, 533–556.

Vielzeuf, D., Schmidt, M.W., 2001. Melting reactions in hydrous systems revisited: application to metapelites, metagreywackes and metabasalts. Contribution to Mineralogy and Petrology 141, 251–267.

Viljoen, M.J., Viljoen, R.P., 1969. An introduction to the geology of the Barberton granite-greenstone terrain. Geological Society of South Africa 2, 9–28, Special Publication.

Waight, T.E., Maas, R., Nicholls, I.A., 2000. Fingerprinting feldspar phenocrysts using crystal isotopic composition stratigraphy: implications for crystal transfer and magma mingling in S-type granites. Contrib. Mineral. Petrol. 139, 227–239.

Wall, V.J., Clemens, J.D., Clarke, D.B., 1987. Models for granitoid evolution and source compositions. J. Geol. 95, 731–749.

Watkins, J. M., Clemens J. D. and Treloar, P. J., 2007. Archaean TTGs as sources of younger granitic magmas: melting of sodic metatonalites at 0.6–1.2 GPa. Contributions to Mineralogy and Petrology 154(1), 91-110.

Wedepohl, K.H., 1995. The compositions of the continental crust. Geochimica et Cosmochimica Acta 59, 1217–1232.

Winther, T.K., 1996. An experimentally based model for the origin of tonalitic and trondhjemitic melts. Chemical Geology 127, 43–59.

Woodhead, J.D., Hergt, J.M., 2005. A preliminary appraisal of seven natural zircon reference materials for in situ Hf isotope determination. Geostandards and Geoanalytical Research 29, 183–195.

Xiong X. L., Adam J. and Green T. H., 2005. Rutile stability and rutile/melt HFSE partitioning during partial melting of hydrous basalt: implications for TTG genesis. Chem. Geol. 218, 339–359.

Xu, W.L., Gao, S., Wang, Q.H., Wang, D.Y., Liu, Y.S., 2006. Mesozoic crustal thickening of the eastern North China craton: evidence from eclogite xenoliths and petrologic implications. Geology 34, 721-724.

Yearron, L.M., 2003. Archaean granite petrogenesis and implications for the evolution of the Barberton Mountain Land, South Africa. Unpub. PhD thesis, Kingston University, Kingtson, UK, 315 pp.

Zeh, A., Gerdes, A., Barton, J.J., Klemd, R., 2010. U–Th–Pb and Lu–Hf systematics of zircon from TTG's, leucosomes, meta-anorthosites and quartzites of the Limpopo Belt (South Africa): Constraints for the formation, recycling and metamorphism of Palaeoarchaean crust. Precambrian Research 179, 50-68.

Zeh, A., Gerdes, A., 2012. U–Pb and Hf isotope record of detrital zircons from gold-bearing sediments of the Pietersburg Greenstone Belt (South Africa)—Is there a common provenance with the Witwatersrand Basin? Precambrian Research 204–205, 46–56.

Appendix

Sample location

Sample	Rock type	Texture	Latitude	Longitude
NLG1R	C-gd trondhjemite	Foliated	S25°53'40.74"	E30°40'5.34"
NLG4R	C-gd granodiorite	Foliated	S25°47'29.04"	E30°45'1.92"
NLG7R	C-gd trondhjemite	Granitic	S25°46'49.50"	E30°43'10.32"
NLG8R	C-gd trondhjemite	Granitic	S25°46'18.54"	E30°43'7.08"
NLG9R	Potassic granite	Granitic	S25°46'19.38"	E30°43'6.48"
NLG10R	M-gd trondhjemite	Granitic	S25°46'1.98"	E30°42'24.18"
NLG11R	C-gd tonalite	Granitic	S25°46'1.98"	E30°42'24.18"
NLG12R	F-gd trondhjemite	Porphyritic	S25°46'4.32"	E30°42'21.30"
NLG13R	C-gd granodiorite	Granitic	S25°46'31.20"	E30°37'36.06"
NLG14R	C-gd granodiorite	Granitic	S25°46'31.20"	E30°37'36.06"
NLG16R	C-gd trondhjemite	Granitic	S25°47'8.82"	E30°38'42.36"
NLG17R	Potassic granite	Granitic	S25°47'24.48"	E30°38'48.48"
NLG18R	C-gd granodiorite	Granitic	S25°47'24.48"	E30°38'48.48"
NLG19R	M-gd trondhjemite	Xenomorphic-granular	S25°46'41.76"	E30°39'32.88"
NLG20R	M-gd trondhjemite	Granitic	S25°46'41.76"	E30°39'32.88"
NLG21R	C-gd trondhjemite	Granitic	S25°46'18.96"	E30°39'37.74"
NLG22R	Potassic granite	Granitic	S25°46'18.96"	E30°39'37.74"
NLG24R	M-gd granite	Granitic	S25°45'46.02"	E30°40'27.78"
NLG26R	C-gd granite	Granitic	S25°45'38.58"	E30°40'30.96"
NLG29R	F-gd trondhjemite	Xenomorphic-granular	S25°51'16.02"	E30°45'6.54"
NLG30R	M-gd granodiorite	Xenomorphic-granular	S25°51'41.34"	E30°45'10.56"
NLG31R	C-gd trondhjemite	Foliated	S25°52'9.24"	E30°43'48.66"
NLG32R	Potassic granite	Porphyritic	S25°52'9.24"	E30°43'48.66"
NLG34R	C-gd granite	Foliated	S25°54'36.18"	E30°41'59.70"
NLG35R	C-gd tonalite	Hypidiomorphic-granular	S25°55'40.92"	E30°41'9.24"
NLG36R	M-gd granite	Foliated	S25°55'46.62"	E30°41'0.72"
NLG38AR	M-gd trondhjemite	Foliated	S25°56'53.44"	E30°38'03.31"
NLG40R	M-gd trondhjemite	Foliated	S25°56'42.03"	E30°38'0.17"
NLG41R	M-gd trondhjemite	Foliated	S25°56'42.03"	E30°38'0.17"
NLG42R	C-gd trondhjemite	Foliated	S25°56'42.03"	E30°38'0.17"

* C-gd, Coarse grained; M-gd, Medium grained; F-gd, Fine grained